Improving the Sustainability of Synthetic Methods for Accessing *d*- and *f*-Block Metal–Organic Frameworks

Amna Muhammad

A Thesis

In

The Department of

Chemistry and Biochemistry

Presented in Partial Fulfilment of the Requirements

For the Degree of Master of Science (Chemistry) at

Concordia University

Montreal, Quebec, Canada

December 2022

CONCORDIA UNIVERSITY

School of Graduate Studies

This is to certify that the thesis prepared

By: Amna Muhammad

Entitled: Improving the Sustainability of Synthetic Methods for Accessing d- and f-Block Metal–Organic Frameworks

and submitted in partial fulfillment of the requirements for the degree of

Master of Science (Chemistry)

complies with the regulations of the University and meets the accepted standards with respect to originality and quality.

Signed by the final examining committee:

_____

Dr. Melissa Passarelli   Chair

_____

Dr. Louis Cuccia   Examiner

_____

Dr. Rafik Naccache   Examiner

_____

Dr. Ashlee Howarth   Thesis Supervisor

    Approved by   _____

                        Paul Joyce, Chair of Chemistry and Biochemistry

                    _____

                        Pascale Sicotte, Dean of Faculty of Arts and Science

    Date   Sunday January 15th 2023
                _____

Abstract

Improving the Sustainability of Synthetic Methods for Accessing *d*- and *f*-Block Metal–Organic Frameworks

Amna Muhammad

The work described herein explores sustainable methods for the synthesis of metal–organic frameworks (MOFs), a subclass of coordination polymers distinguished from other subclasses by their porosity, which engenders MOFs with high surface area and tunability. This thesis explores various synthetic and post-synthetic methods to obtain a variety of *d*- and *f*-block metal MOFs.

Chapter 2 explores the use of rotary-evaporation as a distillation technique for the purification and recycling of two solvents commonly used in MOF synthesis and purification, N,N-dimethylformamide and acetone. Solvents previously used for MOF purification are collected, purified, and re-used for MOF synthesis. The quality of the recycled solvents is confirmed by ^{1}H-NMR before being used in the synthesis of four well-studied, structurally diverse *d*-block metal MOFs, Zr-UiO-66, Zr-MOF-808, ZIF-8(Zn), and HKUST-1(Cu). These MOFs are characterized using a variety of techniques and compared to counterparts synthesized with commercial and as-collected unrecycled solvent in order to confirm viability and efficiency, both in results and environmental impact of the procedure, and to understand the effects of using previously used vs. treated solvents in the synthesis of MOFs.

Chapter 3 explores the impact of performing post-synthetic exchange at the metal node (also known as transmetalation) using microwave-assisted heating with the goal of shortening reaction times compared to transmetalation performed using conventional methods. Samples of Y-UiO-66 are transmetalated to yield a library of RE-UiO-66 analogues with seven lanthanoids, Yb(III), Tm(III), Er(III), Ho(III), Tb(III), Gd(III), and Eu(III) using microwave-assisted heating for one and two rounds of transmetalation. The reactions are performed in under three hours compared to weeks with conventional methods. The samples are analyzed for retention of crystallinity and degree of transmetalation to confirm the efficacy of the process and the ability of the MOF to survive microwave conditions.

Acknowledgements

To Lars, my joy and comfort. Before I started my MSc, I hoped you'd be nice because we were starting at the same time; I had no idea that our friendship would become indescribably precious to me. Thank you for getting me to explore Montreal, for all the onigri runs and café sessions, for teaching me to swim and trying your best to teach me to bike :P . Thank you for teaching me how to find excitement in pretty much anything, who would have thought public transport and urban planning could be so entertaining. Thank you for so much more than I can say in one document.

Here's to the Majewski group; To Linyi with her impressive lego sets and impeccable fashion. To JDC, thanks for the good vibes. To Zujhar, my office buddy; thank you for all the entertaining convos and for the very intriguing vibes, and the reminders to maintain stress.

To Victoria; Times relatable person of the year, thank you for all the homemade cookies and ramblings, you are a gem.

To Will and Caroline; the welcome committee for HOMA. Will, my resident anime enthusiast, who frankly should win an award for the best kindest smile, thank you for your humorous conversations and readiness for adventure ~~thank you for being comically Italian~~. To Caroline, who has a big heart and lots of care to share; thank you for looking out for everyone and hosting the best parties, conferences and basically any event.

To Joey and Jacob; who I am knighting in this thesis. Joey, thank you for all the 'it'll oks', you have an amazing and quick sense of humour and lots of charm, I deem you the universal drinking buddy. To Jacob; dude, you're always willing and able to help with anything, thank you for all the shared commutes and food recs. I deem you the HOMA food critic.

To Rehmat, here goes; thank you for always being patient with me and never making me feel like I'm too much even when I admittedly am being too much. Thank you for always just getting it, for always being open to hearing me out. You deserve a lot more credit and appreciation than I can give here. Thank you for making Concordia home.

To Fran, Jess, and all the other lovely people I met here; Fanks Chem.

To all of my friends who have cheered me on and let me cheer them on; Rabeeya, Amna, Alex, Zahra, Sara, Julia, Clem, Spencer, everyone… Thank you for keeping me grounded and reminding me of where I started and how far I've come.

Dedications

امی اور ابو کے لیے

Contribution of Authors

In all chapters, Dr. Ashlee J. Howarth acted in a supervisory role.

Chapter 2 is an advanced project which will soon be made into a manuscript for submission to a peer-reviewed journal. I am the primary author of this work. Lars Miller performed all N_2 sorption experiments. Chris Copeman performed some PXRD and all DRIFTS analysis. Zoey Davis assisted with solvent purification and optical microscopy. Samantha Prelaz and Victor-Quezada-Novoa obtained SEM micrographs. Pedro Rafael Donnarumma performed TGA analysis on all samples. Dr. Heng Jiang performed ICP-MS analysis that can be found in the appendix in Table A.1

Chapter 3 is an advanced project which will soon be made into a manuscript for submission to a peer-reviewed journal. I am the primary author of this work. Lars Miller performed all N_2 sorption experiments. Dr. Heng Jiang performed all ICP-MS analysis.

Table of Contents

List of Figures

List of Tables

List of Abbreviations

2,6-DFBA	2,6-diflurobenzoic acid
BDC	1,4-benzenedicarboxylic acid
BET	Brunauer-Emmet-Teller
BTC	1,3,5-benzenetricarboxylic acid
CCDC	Cambridge Crystallographic Data Centre
CDCl$_3$	Deuterated chloroform
CN	coordination number
DEF	*N,N*-diethylformamide
DMA	*N,N*-dimethylacetamide
DMF	*N,N*-dimethylformamide
DMSO-d$_6$	Deuterated dimethyl sulfoxide
DRIFTS	Diffuse reflectance infrared Fourier transform spectroscopy
EDS	Energy dispersive X-ray spectroscopy
fcu	Face-centred cubic topology
HCl	Hydrochloric acid
H$_2$O$_2$	Hydrogen peroxide
HNO$_3$	Nitric acid
ICP-MS	Inductively coupled plasma-mass spectrometry
IUPAC	International Union of Pure and Applied Chemistry
KBr	Potassium bromide
MI	Optical microscopy images
mIm	2-methyl imidazole
MOF	Metal–organic framework
NLDFT	Non-local density functional theory
NMR	Nuclear magnetic resonance spectroscopy
PXRD	Powder X-ray diffraction
RCSR	Reticular chemistry structural resource
RE	rare-earth
SBU	Secondary building unit
SCXRD	Single crystal X-ray diffraction
scCO$_2$	Super-critical CO$_2$
SEM	Scanning electron microscopy
sod	sodalite topology
spn	spinel topology
tbo	Twisted boracite topology
TGA	Thermogravimetric analysis
UV-Vis	Ultraviolet-visible spectroscopy

Chapter One

Introduction

1.1. Brief History and Overview of Metal–Organic Frameworks

A large aspect of chemistry involves understanding the nature of bonding and coordination between atoms. The study of reticular chemistry involves comprehending the connections between various atoms or molecules to form extended ordered network structures.[1] This includes materials with open, or porous, frameworks. Various porous materials, such as charcoal, have been used for centuries, with innovations in this realm growing exponentially in the 20th century with increasing chemical knowledge.[2] With this growth came more sophisticated subclasses of materials within reticular chemistry. Early examples of materials made with metal and organic connections can be attributed to works such as the 1965 reporting by Tomic on potentially porous compounds made of naphthalene containing carboxylic acid ligands coordinating with metals such as zinc, nickel, aluminum and iron.[3] It wasn't until the 1990s, after notable works by Yaghi and Kitagawa were published,[4,5] that the field began garnering significant attention. Eventually, the term metal–organic framework, or MOF for short, would be coined by Yaghi in 1995[6] with the subsequent publication of MOF-5, the first reported MOF with permanent porosity.[7]

Inorganic metal node

Organic linker

Metal-organic framework
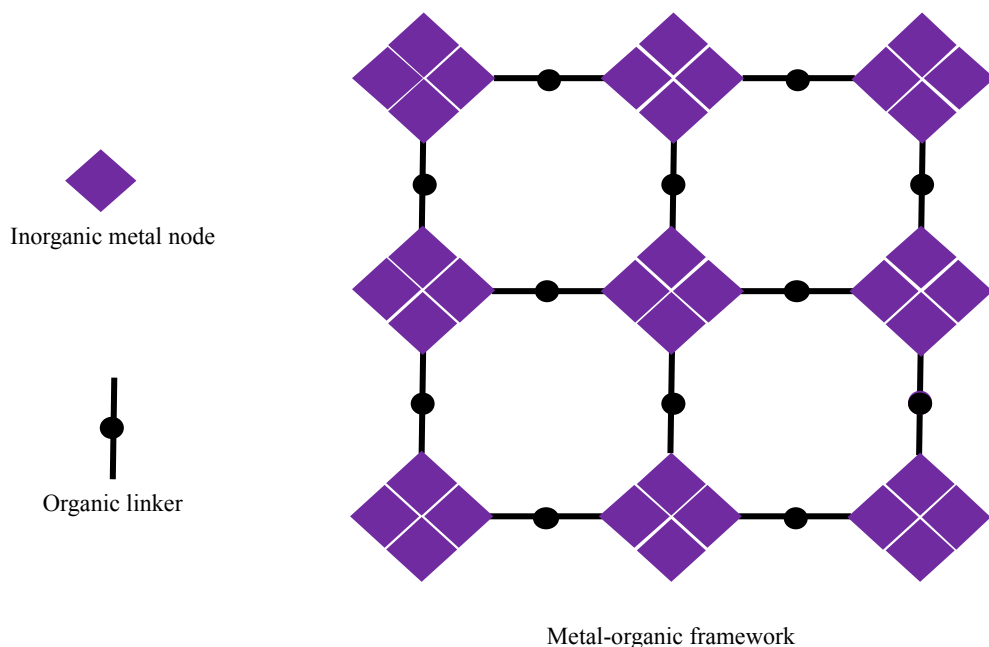
Figure 1.1 Depiction of a 2-D MOF made from a metal cluster node and ditopic inorganic linker

The IUPAC would subsequently define the term MOF as 'a coordination network with organic ligands containing potential voids' in 2013.[8,9] Further IUPAC consensus places MOFs as a subclass of coordination polymers, defined by the IUPAC as 'a coordination compound with repeating coordination entities extending in 1, 2 or 3 dimensions'.[8,10] The frameworks can be crystalline or amorphous, the former being highly arranged with long-range order (over infinite distances) and the latter having short-range order or no order (within an interatomic distance).[11] Amorphous MOFs are far less studied than their crystalline counterparts, primarily due to challenges in characterizing amorphous MOFs.[12] It is thus common practice to primarily study MOFs that are crystalline in order to gain a better understanding of their properties through techniques such as powder and single crystal X-ray diffraction that work only with crystalline compounds.

MOFs are distinguished from other coordination polymers due to their porosity, which arises from their structures made with secondary building units (or SBUs for short). These SBUs includes an inorganic and organic aspect. The inorganic aspect being a metal node, either in the form of ions, clusters or chains,[13] where the metal falls in the s-,[14,15] p-,[16,17] d-,[18,19] or f-[20,21] block. The organic ligand, also known as a linker, can be multitopic, such as a ditopic,[22] tritopic,[23] tetratopic.[24] Carboxylates are one of the most commonly explored linkers, with reports of imidazole,[25] phosphonate,[26] sulfonates,[27] and other anionic organic functional groups that are able to coordinate with metals also being reported for the formation of MOFs.[28]

1.2. Topology and Reticular Chemistry

The meteoric rise in popularity of MOFs has led to the necessity of a classification system and refinement of approaches to the synthesis of well-known and novel MOFs alike.

1.2.1. Topology

In order to further distinguish the identity of MOFs from other porous materials, specific terminology is essential, and several guidelines have been established. Topology and topology descriptors have become a sophisticated tool to describe crystal structures of these ordered frameworks.[8] The topology of a compound is unchanged with bending, stretching and squeezing; only being altered with the breaking of bonds.[29] Topology is dependent entirely on the overall connectivity and symmetry of the metal and organic node. Several synthetic parameters can

influence the overall structure and topology of a compound, including pH, metal and organic reagents, and the choice of solvent amongst others. The number of possible structures and therefore the number of possible topologies is infinite.[30] The most common structures and topologies are deposited in the Reticular Chemistry Structure Resource (RCSR) online database.[31] A three letter code is used to denote the particular topology of a MOF, such as **spn** and other topologies.[30] The isoreticular principle states that MOFs made from organic linkers of different sizes, but with the same geometry, symmetry and connectivity share the same topology.[32] This principle can help guide MOF chemists in designing various MOFs with the same topology, but with potential changes in other properties such as density and surface area. By exploring various changes, such as using linkers with similar structures but additional functional groups to further manipulate properties of a MOF, a new level of tunability is unlocked.
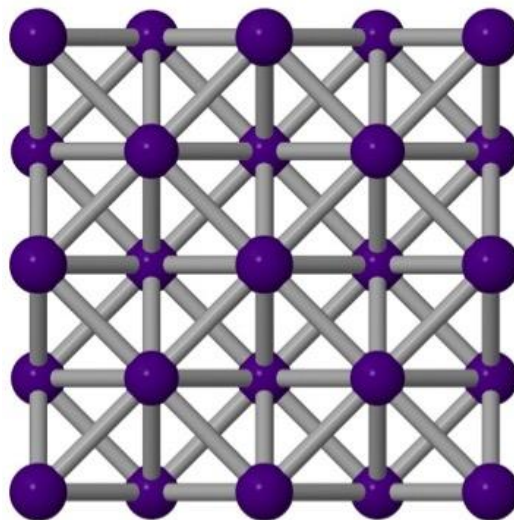
Figure 1.2 Depiction of the **fcu** topology

1.2.2. Reticular Chemistry

Reticular chemistry, which can be defined as the connecting of molecular building blocks through strong connections to make network structures,[33] calls for a different approach than the traditional retrosynthetic routes often used in synthetic chemistry. Where retrosynthesis allows for consecutive expansion of a compound's existing structure, reticular synthesis calls for the completed structure to be formed with no expansion later.[34] For MOFs, the use of building blocks to form parts of the final structure are common, with the inorganic metal node and organic linker forming the SBUs. The final topology a MOF takes on can be determined based on the chemistry

of the components of the so-called 'building-blocks' that are used, this includes the geometry, angles of connection, and symmetry amongst other elements.[35]

1.3. MOF Properties

MOFs have garnered a lot of attention for their tunable design and properties, and research in the field continues for the sake of developing methods of understanding and manipulating these properties.

1.3.1. High Porosity and Surface Area

The publication of MOF-5 detailing its permanent porosity catalysed research into developing MOFs with optimized pores and apertures for various applications.[36,37] MOF pores can take on a variety of shapes and sizes, including spherical,[38] cylindrical,[39] or other shapes.[40] As for the size of MOF pores, they can be diverse with a range of micro (pore diameter < 2 nm), meso (20 to 50 nm) or macropores (> 50 nm),[41] further enhancing possibilities for design. The strategic use of various linkers and metal nodes can aid with designing the size and shape of the pores within a MOF. Further modifications can be made to the material after synthesis, such as removal of 'labile terminal ligands' to create open-metal sites for further coordination points without damaging the crystallinity and structure of the framework.[42] Methods for optimizing access to pore space include strategies such as removing guest solvent molecules from the pores after synthesis, freeing up to 93% of the pore volume in some instances.[43]

As a result of their porosity, MOFs have relatively high surface areas for uptake, storage and release of various compounds. These surface areas range from anywhere between 100 m^2g^{-1} to a record high of 7839 m^2g^{-1} and pore volumes of 5.02 $cm^{-3}g^{-1}$.[44] Reported computational analysis has predicted the possibility of MOFs with surface areas up to 14 600 m^2g^{-1} with permanent porosity.[43] Although this may be hard to achieve experimentally, this showcases the immense potential of MOFs as porous materials, and the recent popularity in MOF research can be majorly attributed to this property.

1.3.2. Low Density

Another result of the porosity of MOFs includes their ability to achieve low densities, with the lowest reported density of a MOF currently standing at 0.124 $\mathrm{gcm^{-3}}$,[45] this density is tunable through strategic choice of metal nodes and organic linkers.

1.4. *d*- and *f*-Block MOFs

The most commonly studied MOFs are composed of *d*-block metal nodes.[46] These include metals such as zinc(II),[47] nickel(II),[48] or copper(II),[49] amongst others, with a large interest in the synthesis and application of zirconium(IV)-based MOFs[50] due to their chemical and thermal stability.[51]

A growing amount of research is being conducted into the synthesis of MOFs with rare-earth metal nodes.[52] Rare-earth ions include yttrium(III), scandium(III) and the fifteen *f*-block lanthanoids, which mostly adopt a Ln(III) oxidation state, but can also adopt a higher or lower valency, such as with cerium(IV) or europium(II). The access to *f*-block MOFs has allowed for tunable metal-based luminescent properties,[53] making RE-MOFs an attractive candidate for applications in chemical sensing and other applications involving luminescence.[54]

This thesis explores four different diverse *d*-block metal MOFs; Zr-UiO-66, Zr-MOF-808, HKUST-1(Cu) and ZIF-8(Zn), along with exploration of a series of seven *f*-block lanthanoid analogues of UiO-66.

Figure 1.3 Periodic table highlighting the d- (purple) and f- block metals (pink)

1.4.1. UiO-66, MOF-808, HKUST-1, ZIF-8

UiO-66, comprised of a hexanuclear zirconium(IV) cluster node and a linear ditopic 1,4-benzenedicarboxylic acid (BDC) linker, has an **fcu** topology (Figure 1.4).[55] The overall framework has a 12- connected net with an octahedral cage of 12 Å internal diameter, a tetrahedral cage with a 7.5 Å internal diameter, and 6 Å pore apertures for both cages.[56,57]

MOF-808, comprised of a hexanuclear zirconium(IV) cluster node and a tritopic 1,3,5-benzentricarboxylic acid (BTC) linker, has an **spn** topology with 18.4 Å spherical apertures (Figure 1.4). The metal node is 6-connnected rather than 12-connected[58] meaning that MOF-808 is commonly explored for its open metal sites.[59]

HKUST-1, comprised of a copper(II) cluster node and the tritopic BTC linker, has a **tbo** topology with 9 x 9 Å square apertures giving a cubic lattice building block (Figure 1.4).[60,61]

ZIF-8, comprised of a zinc(II) ion nodes and a 2-methyl-imidazolate (mIm) linker has an **sod** topology with 11.6 Å pores and 3.4 Å apertures giving a rhombic dodecahedron morphology (Figure 1.4).[62,63]
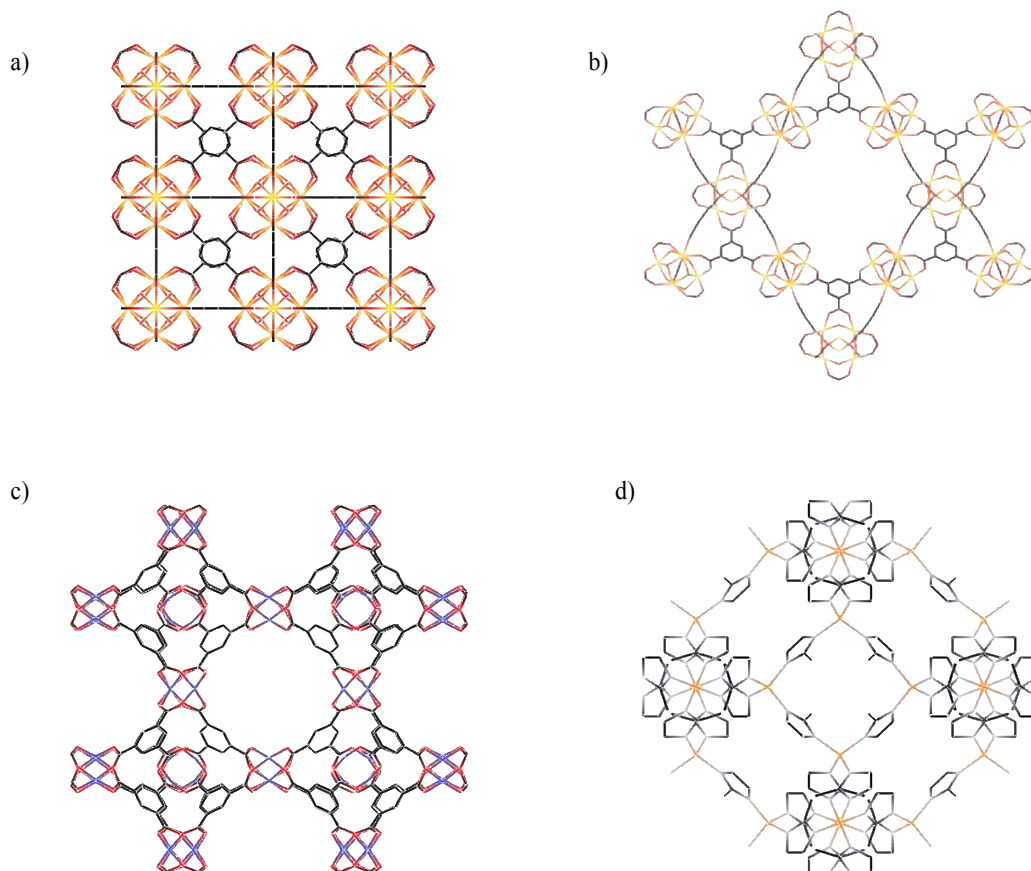
Figure 1.4 Wireframe depictions of a) UiO-66, b) MOF-808, c) HKUST-1, and d) ZIF-8

1.4.2. UiO-66 Analogues

Tetravalent analogues of UiO-66 with hafnium(IV),[64] cerium(IV),[65] and plutonium(IV),[66] have been reported.[67] Recently, a library of trivalent rare-earth analogues of UiO-66 (Figure 1.5) have also been reported by our group.[68]
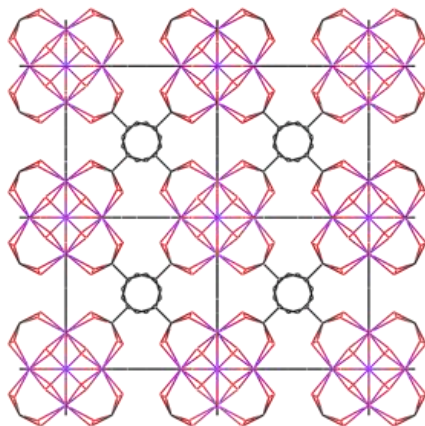
Figure 1.5 Wireframe depiction of RE-UiO-66

1.5. Synthetic and Post-synthetic Methods to Obtain MOFs

The endless possibilities in designing MOFs with various properties can be realized through "new", or *de novo*, synthesis, and can be further tailored through post-synthetic methods.[69,70] The typical reagents used to synthesize a MOF involve a metal salt (i.e., nitrate, acetate, chloride etc.) with a multitopic linker, and a modulator (see below) to control metal-linker bonding. The reaction is typically carried out in a high-boiling point solvent such as N,N-dimethylformamide (DMF), N,N-diethylformamide (DEF), N,N-dimethylacetamide (DMA) and other solvents.[71] Current understanding of MOF formation proposes a four stage process; i) an incubation stage, where the SBU starts to template, typically with the assistance of solvent effects, ii) a nucleation stage, where the framework starts to take form with several small 'seeds' before going through the iii) growth stage, where the material formed during the nucleation stage develops and grows before undergoing a iv) stationary stage where the crystals homogenize depending on the conditions.[72]

MOFs syntheses are often considered to be a self-assembly process, typically initiated by thermal decomposition of a solvent (usually formamide based) to form base allowing for bonding between inorganic metal nodes and organic linkers. To slow down the nucleation and growth process, research has been carried out using monotopic linkers that can mimic the multitopic

linkers being used to potentially exert kinetic control and allow for direction of properties such as particle size, morphology, porosity, and formation of defects.[73] These compounds, called modulators, can either prevent deprotonation of the linker or compete for binding at the metal node with the linker; resulting in a reduction in the rate of nucleation that aims to help promote crystallinity in the material being synthesised.[74] Acids such as acetic and nitric acid are commonly used for this purpose, along with the use of fluorinated carboxylic acids in rare-earth MOF synthesis.

In some cases, MOFs with specific metal nodes or organic linkers can be very difficult or impossible to synthesize *de novo* and thus post-synthetic procedures might be a more convenient, or even the sole, route to producing frameworks with specific properties.[75] Post-synthetic modification (PSM) is defined as 'chemical derivatization of MOFs after their formation'.[76]

1.5.1. Solvothermal Synthesis

The most traditional route to synthesizing MOFs includes solvothermal synthesis, defined as reactions involving heating of a chosen non-aqueous solvent in a closed vessel under autogenous pressure.[77,78] while reactions done with water as the solvent are known as 'hydrothermal' reactions.[79] The conditions for solvothermal synthesis result in a closed environment where the metal and linker are allowed to bond in a dynamic manner, allowing for greater control and more ordered propagation resulting in crystallinity.[71,80]

1.5.2. Microwave-Assisted Synthesis

Microwave radiation can serve as a heating source in MOF synthesis, with a magnetron generating microwaves that then transfer into the sample chamber, where molecules with dielectric moments rotate to be in alignment with the electric field, generating heat.[81] The main difference between microwave heating and conventional heating is how the entire sample is heated from the inside out during microwave irradiation whereas heating by convection results in heating from the outside in.[82] The sample holder often acts a Faraday cage, trapping the heat from the microwave irradiation.[83] This internal mechanism results in faster heating, as the overall vessel gets heated throughout from the start rather than gradually working its way through the outside of the vessel like in conventional heating. Microwave synthesis has become very popular for organic reactions,[84] and only has recently gained momentum for the synthesis of MOFs.[85] Tan δ, which

describes how efficiently microwave energy is converted to thermal energy in specific solvents, should ideally be above 0.1. DMF has a Tan δ between 0.09-0.19 between room temperature at 100 °C with medium absorbance for use in microwave synthesis. [86]
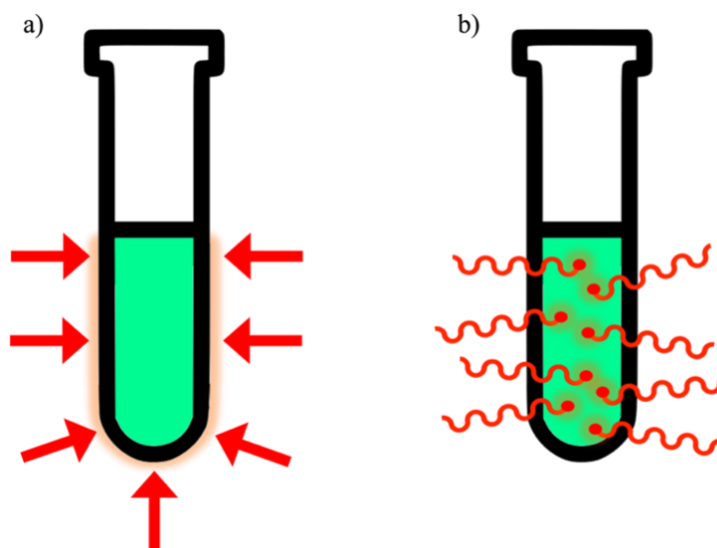
Figure 1.6 Depiction of a) conventional heating and b) microwave-assisted heating

1.5.3. Transmetalation

Post-synthetic modification allows for further tuning of MOFs with final structures that may be too complex to access via *de novo* methods, or as a way of expanding into new frameworks with different properties than the parent framework.[87] While methods are available for post-synthetic linker exchange, complimentary methods exist for post-synthetic changes to the metal node. Atomic layer deposition,[88] solvent-assisted metal insertion,[89] and transmetalation[90] are all options for post-synthetically modifying the metal node. Transmetalation commonly involves immersing a *de novo* synthesised parent MOF sample into a solution of dissolved salt of the target metal while under heat in order to promote complete or partial exchange within the metal node.[91] This results in MOFs with mixed metal nodes with different properties to monometallic MOFs or with completely new metal nodes. The degree of exchange depends on, and can be adjusted by, the conditions of the transmetalation procedure. Factors that need to be considered for transmetalation to occur include similarities in the ionic radii and preferred coordination number and geometry of the incoming and outgoing metal ions, as well as the lability of the metal-ligand bond. More labile

metal-ligand bonds, and closer properties of the metals involved lead to higher levels of transmetalation.[75]
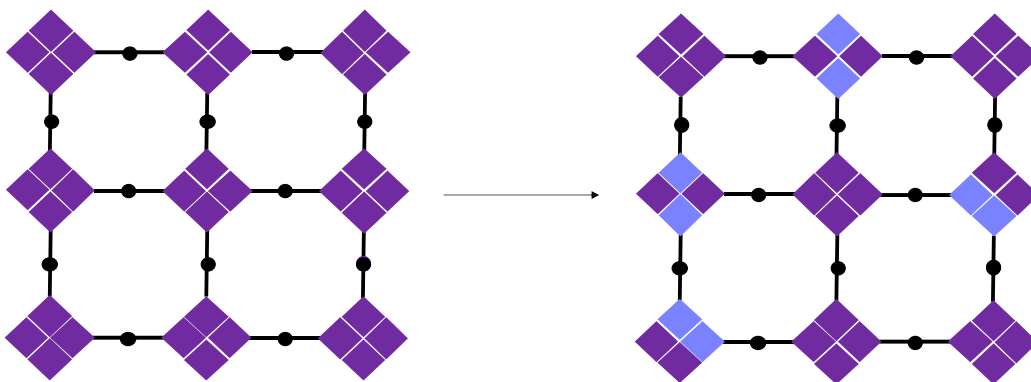
Figure 1.7 Depiction of a transmetalated metal cluster node

1.5.4. MOF Activation

As porous materials, MOFs can retain molecules within their pores during the synthesis and isolation processes. This includes excess linker, solvent and other reagents from the synthesis. The process of removing excess molecules from the pores in order to access a MOFs full porosity is known as 'activation', with several methods being used for activating a MOF, including vacuum-drying and supercritical CO_2 drying (also known as $scCO_2$).[92] Vacuum drying is the most common technique for activating MOFs and involves subjecting the MOF to heat under vacuum with temperature, pressure and time varied depending on the MOF and its condition after synthesis. Relying solely on vacuum drying for activation, however, sometimes results in lower-than-expected surface areas[16,93] as a result of framework collapse caused by high surface tension when liquid solvent molecules are heated to gas phase within the MOF pores.[94] Exchanging the solvent in the MOF for one with a lower boiling point and/or surface tension solvent can help reduce the degree of framework collapse once the MOF begins the activation process.[71,95]
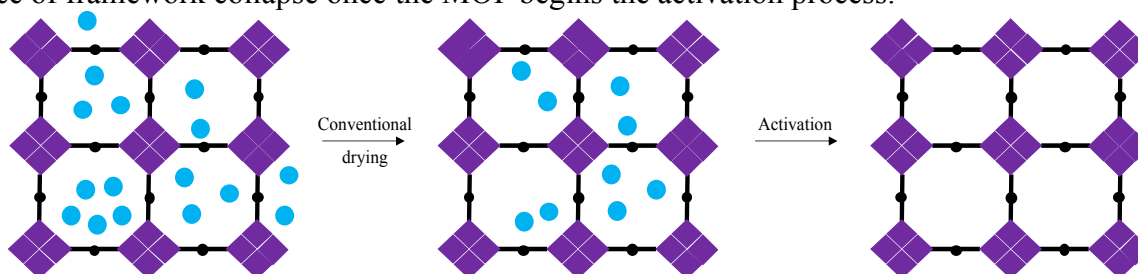
Figure 1.8 Illustration of a MOF before conventional drying in an oven, after conventional drying an oven, and after activation in a vacuum. Blue circles represent solvent molecules

1.6. Sustainable Synthesis of MOFs

The growing urgency for sustainable materials and environmentally friendly chemical processes as a result of climate change and growing awareness of the health risks associated with improper handling of chemicals and chemical waste has led to many initiatives for improving synthetic methods currently used in chemistry.[96,97] The climate crisis has propelled the world to a new era of research, both academically and industrially, in order to address the challenges of devastating environmental events and to maintain the health of populations. The 1990s saw the inception of the field of green chemistry, which IUPAC has defined as the area of research for 'the invention, design, and application of chemical products and processes to reduce or to eliminate the use and generation of hazardous substances'.[98,99]

1.6.1. The Twelve Principles of Green Chemistry

In 1998, Paul Anastas and John Warner developed the 12 principles of green chemistry; serving as a guide for improving the green output of chemical products from manufacturing to disposal.[100] The principles of green chemistry aim to promote processes and materials that are better for the environment and for global health; splitting into categories that can be considered either reducing waste (Principles 1, 2, 6, 7, 8, 9, 10, and 11) or reducing health hazards (Principles 3, 4, 5, and 12).
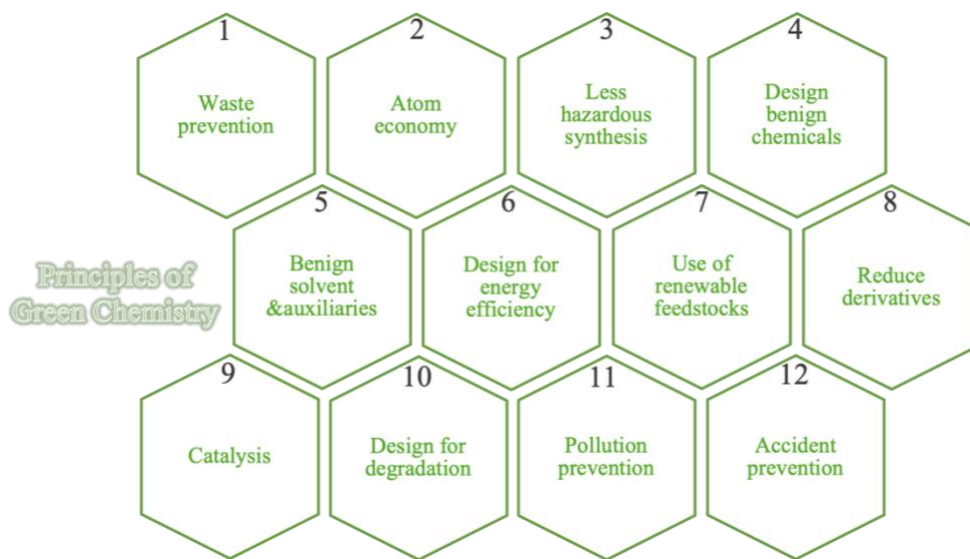
Figure 1.9 The Twelve Principles of Green Chemistry

1.6.2. Green Synthetic Methods

Improving the synthesis of MOFs using the 12 principles of green chemistry involves assessing the impact of traditional solvothermal synthesis that is used to make a vast majority of MOFs. Arguably, the most concerning aspect of MOF synthesis is the copious usage of DMF in both synthesis and washing processes. These processes often result in large amounts of DMF, and other solvents, being wasted, which is not only an environmental issue, but also a very costly process in terms of transporting the solvents for one-time use and disposal afterwards. DMF is also a category 4 toxin for dermal contact and inhalation.[100] Reducing the overall amount of DMF being used could be beneficial in reducing overall exposure through inhalation or skin contact. MOF chemists face a unique challenge in that the use of DMF and similarly toxic high boiling point solvents are currently the staple for progress in discovering new frameworks. With the impending ban on the use of DMF by the EU,[101] a new normal needs to be found, and this new normal should involve a diverse range of options, from the proposal of viable alternatives to DMF, such as STEPOSOL-MET-10U (*N,N*-dimethyl-9-decenamide),[102] or solvent-free methods,[103,104] to options that involve an optimization of current synthetic methods, and also to recycling and reusing the DMF that is used..

Another aspect of MOF synthesis that can be considered for a sustainability assessment includes the energy and time taken for synthesis and post-synthetic modification of MOFs. Most procedures require the use of an oven at high temperatures, requiring a substantial amount of energy and time, often several days.[105,106,107] Other methods, such as the development of room-temperature procedures [108,109,110] and microwave-assisted synthesis,[111,112,113] are being explored as a way to reduce the amount of energy used overall by reducing the need for high levels of heating, or by decreasing the overall time and energy needed for synthesis.

1.7. Characterization of MOFs

Fundamental characterization of MOFs includes powder X-ray diffraction (PXRD) to confirm the phase purity of the compound, as well as gaining insight into the crystallinity of the samples. Nitrogen adsorption/desorption isotherms give critical information into the porosity and calculated surface area of synthesized MOFs. Scanning electron microscopy (SEM) provides valuable imagery of the morphology of the MOF along with details on the size of the crystallites and can

be coupled with energy dispersive X-ray spectroscopy (EDS) for even more information on elemental composition.

Other useful techniques that can be used depend on the MOF property being investigated. Diffuse reflectance infrared Fourier transform spectroscopy (DRIFTS) is used to gain insight into the presence of IR-active functional groups. Single-crystal X-ray diffraction gives intricate details on the structure and bonding of the MOF. Nuclear magnetic resonance (NMR) spectroscopy can be useful in confirming the purity of the organic linker. Inductively coupled plasma-mass spectrometry (ICP-MS) is a highly sensitive technique used to quantify amounts of different elements, typically metals in MOFs. Thermogravimetric analysis (TGA) is used to find information on the thermal decomposition of MOFs.

1.7.1. Powder X-ray Diffraction (PXRD)

PXRD is the first characterization method employed when a MOF is synthesized, as the diffractogram provides essential information on the 'bulk crystallinity' of a MOF. These experimental patterns can be compared to patterns of MOFs from the Cambridge Structural Database (CSD),[114] simulated from single-crystal data or though computational modelling to confirm phase purity.
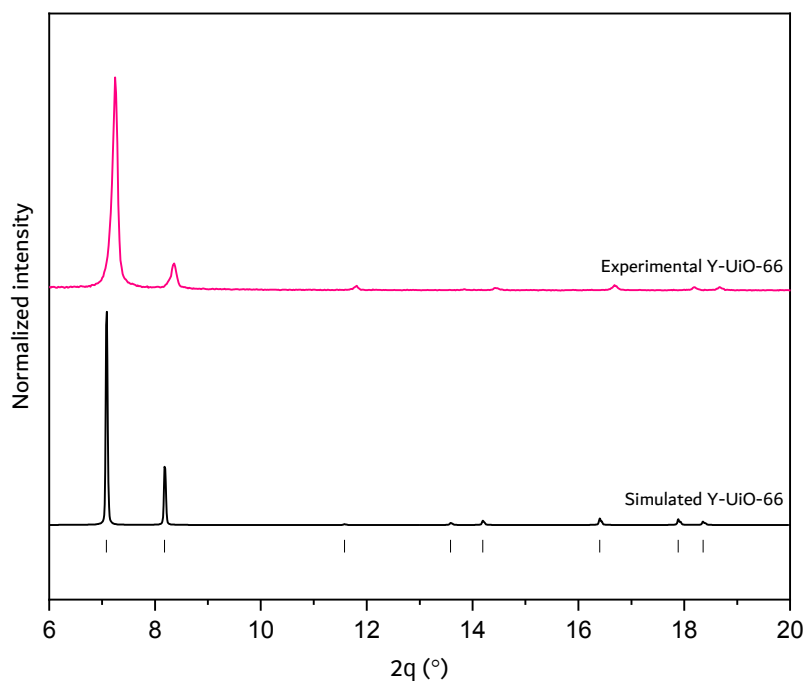
Figure 1.10 Example of a PXRD pattern of Y-UiO-66

13

Phase composition and unit cell dimensions can be determined by analysing the position of the reflections. Reflection intensities are determined by the strength of diffraction and distribution of atoms in the crystal planes. Crystallite size is determined by analysing the width and shape of reflections.[115] Computational modelling methods, such as Rietveld refinement,[116] can be used to gain further information on the crystal structure of the sample.

Crystalline materials are able to diffract X-rays when the spacing between atom layers is close to the radiation wavelength, with the X-rays that pass through striking the additional layers of atoms, creating a diffraction pattern. When diffraction from two different layers, or planes, are in-phase, constructive interference occurs. Braggs law, defined by the equation $2d \sin(\theta) = n\lambda$ (where d is the spacing between atom layers, θ is the incident angle, λ is the wavelength of the X-ray and n is an integer), dictates the condition for this constructive interference to occur. In samples with small crystallite sizes (less than 1 μm), peak broadening is seen in accordance with the Scherrer equation and broadening effect.[117]

To run a PXRD, the sample is loaded onto holder, either as a dry powder or by drop-casting from a volatile solvent where it can dry completely. If the sample is packed in a particular way, especially with needle or plate shaped crystals,[118] they may order themselves in a preferred orientation, and the intensities of the diffraction pattern may be modified.[119] Sample rotation can help with attaining more reliable diffraction patterns when preferred orientation is a concern.

1.7.2. N_2 Adsorption/Desorption

The adsorption of inert gases is important for determining details about the porosity of a MOF. N_2 at 77K tends to be utilized the most for reporting sorption data. N_2 gas adsorption requires the use of liquid N_2, which condenses the N_2 gas, allowing it to stick better to MOF surfaces, providing an accurate analysis of porosity. The N_2 (adsorbate) reversibly sticks to the MOF surface (adsorbent) *via* van-der Waals, long-range London dispersion forces and short-range intermolecular repulsion, caused by repellence from like forces interacting at close ranges, in a phenomenon known as physisorption.[120]

Physisorption takes place in stages, starting with monolayer adsorption, where all the adsorbate molecules are in contact with the adsorbent surface. This is followed by multi-layer adsorption, where the pressure increases and the pores get filled sequentially, with the order of adsorption providing insight into the size and nature of the pores present in the porous material.

In order to obtain an isotherm, an appropriate amount of sample is first activated to ensure no solvent or other molecules are present in the pores, and then weighed accurately in a sealed tube before being placed in the instrument. The sample is then evacuated at room temperature under vacuum before being backfilled with an inert gas such as helium to measure the free space in the tube. Following this measurement, the tube gets evacuated once more to remove all the inert gas in order for liquid nitrogen to cool the sample and be adsorbed in the pores. This step takes place slowly at different pressures in an orderly manner, with the instrument recording how much nitrogen is being taken up as a function of pressure.

Isotherms can be separated into six different categories. Type I isotherms are typically obtained when analyzing microporous solids, with two subtypes: Type I(a) seen in materials with narrow micropores (less than 1 nm), and Type I(b), seen in materials with larger micropores or mesopores. Type II and III isotherms are seen in microporous or non-porous materials (non-porous referring to the external surface of compound), with Type III isotherms forming poorly identifiable monolayers. Type IV isotherms are seen in mesoporous compounds that undergo 'capillary condensation'- a phenomenon where a gas condenses to a liquid-like phase at a certain pressure: Type IV(a) isotherms seen in cylindrical pores larger than 4 nm, and Type IV(b) isotherms seen in mesopores smaller than 4 nm.
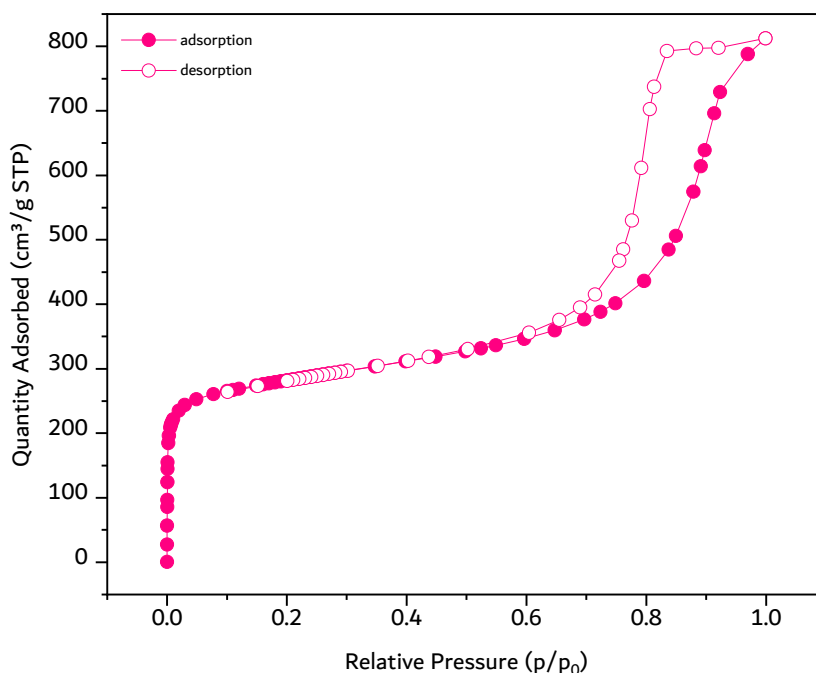
Figure 1.11 Example of an N_2 adsorption -desorption isotherm for Y-UiO-66 showcasing a Type-1a isotherm

Type V isotherms occur under the same conditions as Type III, at higher relative pressures. Type VI isotherms are seen in non-porous materials with uniform layer-by-layer adsorption.[121]
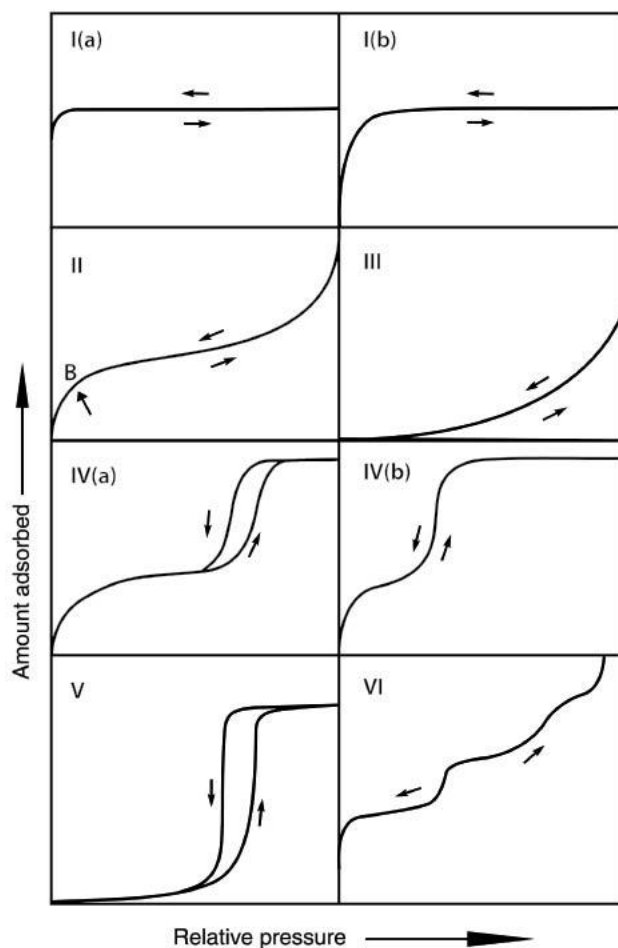
Figure 1.12 Depiction of the various isotherm shapes as reported by Thommes et al.[107]

In order to calculate surface area from a gas adsorption isotherm, analysis is often performed using Brunauer-Emmet-Teller or Langmuir theory, with the former being the more commonly used method due to its inclusion of multi-layer gas adsorption.[122] Langmuir theory only accounts for monolayer gas adsorption[123] leading to the possibility of over-estimating surface areas; it is mostly applicable to Type I isotherms and is rarely used for MOFs.

Gas adsorption isotherms can also be used to calculate pore volume and size distribution of the sample being analyzed. Non-local density functional theory (NLDFT)[124,125,126] is the standard model used to fit the isotherms to determine pore volume and size distribution.

1.7.3. Scanning Electron Microscopy (SEM)

Scanning electron microscopy (SEM) is used to understand crystallite size, morphology and surface topography. Elemental composition data can also be obtained when coupling SEM with energy dispersive X-ray spectroscopy (EDS).[71] While an optical microscope can reliably magnify images by about 1000x, an SEM is able to obtain much higher magnification by about 1 000 000x,[127] by using high energy (between 2 and 100 keV) electron beams.[128] These high energy electrons can cause damage due to their acceleration voltage, and an ultra-thin layer of a conducting material, such as gold, can be added via sputter coating to decrease the damage and sample charging caused by the electron gun.[129]

1.7.4. Diffuse Reflectance Infrared Fourier Transform Spectroscopy (DRIFTS)

Infrared spectroscopy subjects a sample to infrared radiation and detects vibrations of functional groups that occur with a dipole moment change. Each IR functional active group absorbs at different wavelengths and intensities.[130] As MOFs have organic and inorganic components, peaks can arise from the organic linkers, inorganic nodes, and the organic-inorganic bonds connecting the two components.[131] In order to run a DRIFTS spectra, the sample must be thoroughly dried to be able to properly observe all functional groups. Samples often need to be mixed with material such as potassium bromide (KBr) in order to maximize intensities of peaks.
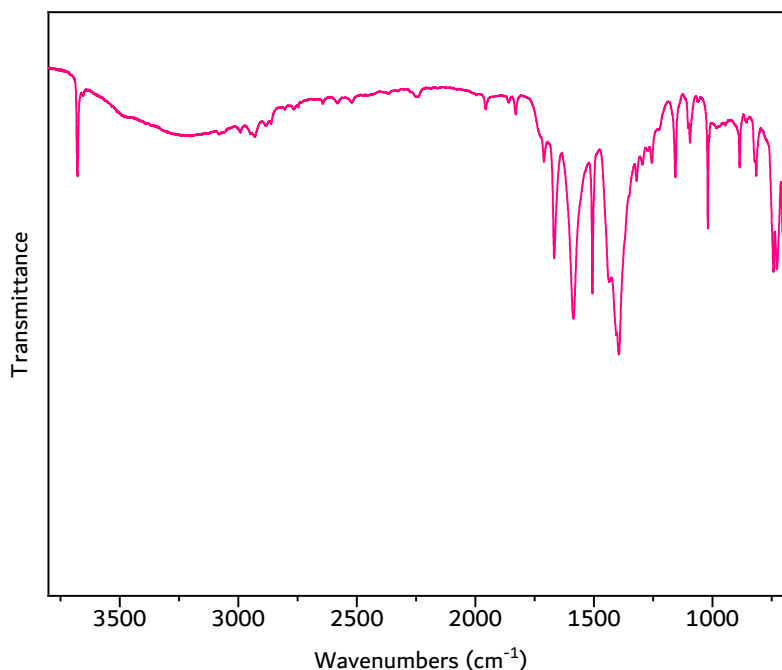
Figure 1.13 Example DRIFTS spectra of Y-UiO-66

1.7.5. Inductively Coupled Plasma-Mass Spectrometry (ICP-MS)

Mass spectrometry is a commonly used analytical tool that allows for the measuring of the mass-to-charge ratio of molecules after they have been ionized, giving an accurate molecular weight of the individual molecules present in a sample.[132] In inductively coupled plasma-mass spectrometry (ICP-MS), the sample is ionized by extremely hot plasma before it is sent through the detector.[133] It is a highly sensitive technique that allows for the quantification of metals and is typically used in MOF chemistry to confirm purity and elemental ratios within a sample. In order to run an ICP-MS analysis, it is important to accurately weigh out and digest samples with no solid particulates. Digestion can be done using an inorganic acid such as nitric (HNO_3) or sulphuric (H_2SO_4) acid, and with hydrogen peroxide (H_2O_2) being added to mineralize any organic compound and heating the sample (around 100 °C). The digested sample is then diluted with deionized water to ensure the sample is within an appropriate concentration for detection.

1.7.6. Thermogravimetric Analysis (TGA)

The use of thermogravimetric analysis (TGA) is common for assessing thermal decomposition of samples by monitoring percent weight change over a range of high temperatures at a controlled rate under a carrier gas such as air, N_2, or O_2.[134] TGA can provide information on the weight loss of guest molecules and components of the MOF, as well determining a MOFs molecular formula.[135] It is best to run TGA analysis on activated MOF samples unless analysis of guest molecules is required. In some cases, a MOF can undergo phase transitions at different temperatures without weight loss that may not be detected by TGA, and another method, such as variable temperature PXRD (VT-PXRD) might be required to monitor phase changes.[136]

1.7.7. Nuclear Magnetic Resonance (NMR) Spectroscopy

Nuclear magnetic resonance (NMR) spectroscopy is used to understand the nature and presence of organic molecules within a compound. In MOF chemistry, NMR spectroscopy is helpful for determining if the linker is present and how pure the linker is, along with information on any organic solvent and guest molecules that may be present within a MOF sample. To prepare a MOF sample for NMR spectroscopy analysis, a small amount (~1-3 mg) of the sample is treated

with 3-10 drops of a deuterated acid (such as D_2SO_4) with sonication and/or heat before the addition of a suitable solvent such as DMSO-d_6. For the analysis of purely organic compounds (such as the organic linker or solvent used for MOF synthesis) the sample can simply be analyzed with deuterated solvent like DMSO-d_6.[137]

1.8. Statement of the Problem and Scope of Thesis

This thesis describes two different sustainable synthetic methods for obtaining a series of *d*- and *f*-block metal MOFs aiming to address issues associated with the use of copious amounts of DMF (chapter 2) and extended reaction times at high temperatures (chapter 3).

Chapter 2 explores the purification of DMF and acetone collected from the solvent exchange stage of MOF synthesis. The collected solvent is recycled and reused for the synthesis and solvent exchange of four diverse MOFs, Zr-UiO-66, Zr-MOF-808, HKUST-1(Cu) and ZIF-8(Zn). The purity of the recycled solvent is confirmed by NMR. The MOFs are characterized by PXRD, BET, DRIFTS, SEM and TGA.

Chapter 3 explores transmetalation, a post-synthetic process, conducted *via* microwave irradiation as opposed to conventional heating. Y-UiO-66 is used as a starting point to create a library of lanthanoid analogues of RE-UiO-66 with europium, gadolinium, terbium, holmium, erbium, thulium, and ytterbium. This library is characterized with PXRD, BET, SEM with EDS, ICP-MS, optical microscopy and other methods.

Chapter Two

Renewal and Reuse of Solvents for the Synthesis and Purification of Metal–Organic Frameworks

2.1. Introduction

Metal–organic frameworks, or MOFs, are crystalline porous materials that are a subclass of coordination polymers.[4,7] MOFs are comprised of inorganic metal nodes that can take on a cluster, chain, or ion formation, bridged by an organic ligand, also known as a linker, that can take on a di-, tri-, tetra- or further multitopic form. The field of reticular chemistry and research into MOFs is relatively young, with the first report of a MOF with permanent porosity in 1995.[4] The field of MOF chemistry has grown exponentially in popularity due to the wide range of potential applications, including many environmentally relevant applications such as gas capture and storage,[138] water treatment,[139] water harvesting,[140] and many others.

To ensure that MOFs are a sustainable solution for specific environmental issues, it is crucial to ensure that the process used to synthesize MOFs is continuously evaluated to improve sustainability. The twelve principles of green chemistry can be used as a tool for this purpose. The principles, introduced in 1998 by Paul Anastas,[99] were developed as a guide for chemists in all sub-disciplines to analyze and improve the sustainability of all stages of the chemical process, from synthesis, to applications and disposal of materials.[99] In the case of MOF synthesis, the principles of waste prevention (principle 1) and pollution prevention (principle 11) brings attention to the volume of solvents used in MOF synthesis and purification, and the amount of waste generated through the synthetic process.

Solvents play a prominent role in MOF synthesis, namely, in deprotonating the organic linker in order to initiate the reaction between the metal node and linker, promoting dynamic bonding.[71] The solvents commonly used for this purpose include N,N-dimethylformamide (DMF), N,N-dimethylacetamide (DMA) and N,N-diethylformamide (DEF), with DMF being the most commonly used solvent. These are high boiling point solvents, which are often left trapped in MOFs pores after synthesis, and can be difficult to remove without disrupting the integrity of the framework. In order to mitigate this issue, a process known as solvent exchange is used, where the MOF sample is washed several times with DMF to remove any leftover metal salt, linker or modulator trapped in the pores, followed by washing several times with a more volatile solvent

such as acetone, methanol, or ethanol, that can be more easily removed without disrupting the framework's integrity.[141]

Examining synthetic and solvent exchange procedures for commonly studied MOFs can put into perspective the large quantity of solvents used. The archetypal MOFs, UiO-66 and UiO-67, as an example, have reported procedures that call for 15 mL of DMF to be used for synthesis and 60 mL of DMF and 60 mL of acetone used for the solvent-exchange and washing process afterwards.[56] This means that 75 mL of DMF (969 mmol) and 60 mL of acetone (816 mmol) are required to yield 95 mg (0.54 mmol) and 57 mg (0.27 mmol) of UiO-66 and UiO-67 respectively.

Although DMF is often recycled through distillation procedures in large-scale industrial processes,[142] it is common for the solvent waste produced by MOF solvent exchange procedures in academic labs to be discarded. Herein, we explore the reuse and renewal of DMF and acetone collected during MOF solvent exchange procedures to reduce the amount of solvent waste generated in academic research labs studying MOFs. The collected and distilled solvents are then used in the synthesis of four structurally diverse MOFs
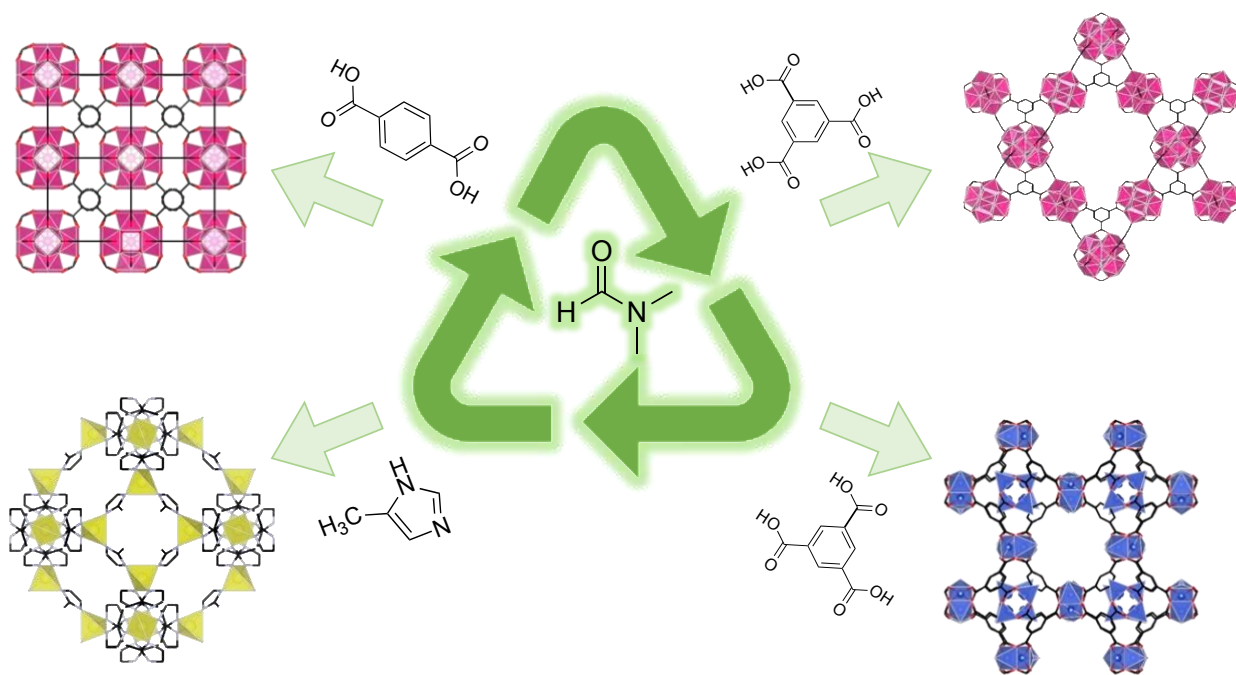
Figure 2.1 Representation of the four MOFs explored in this chapter, including the associated linkers for each framework

2.2. Experimental procedures

2.2.1. Materials and Methods

All reagents and solvents were used without further purification: zirconium dichloride oxide octahydrate ($ZrOCl_2 \cdot 8H_2O$, Alfa Aesar, 98%), copper(II) nitrate trihydrate ($Cu(NO_3)_2 \cdot 3H_2O$, ACROS Organics, 99%), zinc(II) nitrate hexahydrate ($Zn(NO_3)_2 \cdot 6H_2O$, Alfa Aesar, 99%), 1,3,5-benzenetricarboxylic acid (BTC, Alfa Aesar, 98%), 1,4-benzene dicarboxylic acid (BDC, ACROS 98%), 2-methylimidazole (mIm, Sigma Aldrich,99%), formic acid (Alfa Aesar, 97%), nitric acid (Fisher), ethanol (Greenfield Global, 99%), acetone (Fisher Chemicals, 99%), N,N-dimethylformamide (DMF, Fisher Chemicals, 99%).

Inductively coupled plasma–mass spectrometry (ICP-MS) data was measured on an Agilent 7500 Series instrument.

PXRD data was collected on a Bruker D2 Phaser equipped with a Cu$K\alpha$ X-ray source at a wavelength (λ) of 1.54 Å. All samples were drop casted on to the silicon wafer held in a zero-background holder. Scans were run with sample-rotation off at a range of 3-20° 2θ at an increment of 0.2 s for MOF-808, HKUST-1, and ZIF-8 and at an increment of 0.4 s for UiO-66.

Nitrogen adsorption-desorption isotherms were collected at 77 K on a Micromeritics TriStar II Plus surface area and porosity analyzer. All samples were activated (UiO-66, MOF-808, and ZIF-8 at 120 °C for 24 h, HKUST-1 at 150 °C for 24 h) before each isotherm was collected by heating under vacuum using a Micromeritics Smart VacPrep equipped with a hybrid turbo vacuum pump system.

Diffuse reflectance infrared Fourier transform spectroscopy (DRIFTS) spectra were obtained using a Thermo Scientific Nicolet 6700 FT-IR equipped with a MCT detector with a resolution of 1 cm^{-1}.

^{1}H NMR spectroscopy data was collected on a 300 MHz Bruker spectrometer. DMF and acetone were run using 10 drops of d-DMSO$_6$. MOF-808, UiO-66, HKUST-1 and ZIF-8 were first digested in 10 drops of D_2SO_4 with 10 minutes of sonication before being dissolved in d-DMSO$_6$.

Optical microscope images were captured using a Laxco™ LMC-2000 Compound Microscope equipped with a SeBaCam Digital Microscope Camera connected to a computer with SeBaView Software and magnification with a 10X objective lens.

DMF recycling procedure 500 mL of DMF collected from the MOF solvent-exchange process was transferred into a 1000 mL round bottom flask and distilled *via* rotary evaporation on

a Buchi R-300 rotary evaporator equipped with a Buchi V-300 vacuum pump and a Buchi F-305 recirculating chiller. The water bath was set at 65 °C and rotation at 185 rpm. The first ten minutes of rotary evaporation was performed at 200 mbar and the liquid in the collection flask was discarded. Rotary evaporation was continued at 150 mbar for 10 more minutes and the collected liquid was discarded. Finally, rotary evaporation was continued at 0 mbar for 20 minutes until all the solvent was distilled. The liquid in the collection flask was collected and the solid residue left in the round bottom flask was discarded. When noted, a second round of rotary evaporation was performed at 0 mbar for 20 minutes, with the liquid in the collection flask being collected and any remaining residue in the round bottom flask discarded.

Acetone recycling procedure 500 mL of acetone collected from the MOF solvent-exchange process was transferred into a 1000 mL round bottom flask and distilled *via* rotary evaporation on a Buchi R-300 rotary evaporator equipped with a Buchi V-300 vacuum pump and a Buchi F-305 recirculating chiller. The water bath was set at 50 °C and rotation at 185 rpm. The first ten minutes of rotary evaporation was performed at 400 mbar and the liquid in the collection flask discarded. Rotary evaporation was continued at 350 mbar for 15 more minutes until all solvent was distilled, after which the liquid in the collection flask is kept and solid residue left in the round bottom flask is discarded. When noted, a second round of rotary evaporation was performed at 350 mbar for 15 minutes, with the liquid in the collection flask being collected and any remaining residue in the round bottom flask discarded.

The solid residue collected after two rounds of rotary evaporation was digested in 750 µL of H_2SO_4 in a 10 mL microwave vessel by heating in a sand bath at 150 °C for 24 hours before being diluted with MilliQ water in a 10 mL volumetric flask. 1 mL of the sample was then transferred in a microcentrifuge tube for analysis.

2.2.2. Synthesis and Activation of UiO-66, MOF-808, HKUST-1 and ZIF-8

UiO-66, MOF-808, HKUST-1 and ZIF-8 were synthesized using literature procedures using DMF collected from solvent exchange procedures (i.e., collected DMF), distilled DMF, or commercial DMF. All MOFs were washed with commercial DMF and either commercial acetone or distilled acetone.

UiO-66 was synthesized solvothermaly in a 6-dram vial by adding $ZrCl_4$ (31.0 mg, 0.133 mmol) and BDC (31.3 mg, 0.188 mmol) with 7.5 mL of DMF and 750 µL of acetic acid. The

reagents were dissolved by sonication and the sample was heated at 120 °C in an oven for 3 days (72 h). The white precipitate was collected in a 15 mL centrifuge tube and washed with 3 mL of DMF three times and left overnight, followed by washing with 3 mL of acetone three times and left overnight. Samples were air-dried before undergoing activation at 120 °C for 20 hours. Four samples were synthesized including a sample made from distilled DMF and washed with distilled acetone, a sample made from distilled DMF and washed with commercial acetone, and a sample made with collected DMF and washed with commercial acetone, and a sample made with commercial DMF and washed with commercial acetone.

MOF-808 was synthesized solvothermaly in a 6-dram vial by adding $ZrOCl_2 \cdot 8H_2O$ (50.0 mg, 0.154 mmol) and BTC (70.0 mg, 0.333 mmol) with 5 mL of DMF and 5 mL of formic acid. The reagents were dissolved by sonication and the sample was heated at 120 °C for 3 days (72 h). The white precipitate was collected in a 15 mL centrifuge tube and washed with 3 mL of DMF three times and left overnight, followed by washing with 3 mL of acetone three times and left overnight. Samples were air-dried before undergoing activation at 120 °C for 20 hours. Four samples were synthesized including a sample made from distilled DMF and washed with distilled acetone, a sample made from distilled DMF and washed with commercial acetone, and a sample made with collected DMF and washed with commercial acetone, and a sample made with commercial DMF and washed with commercial acetone.

HKUST-1 was synthesized solvothermaly in a 6-dram vial adding $Cu(NO_3)_2 \cdot 3H_2O$ (45.0 mg, 0.186 mmol) and BTC (30.0 mg, 0.143 mmol) with 2 mL of DMF, 2 mL of ethanol 99%, and 2 mL of deionized water. The reagents were dissolved by sonication and the sample was heated at 80 °C for 3 days (72 h). The blue precipitate was collected in a 15 mL centrifuge tube and washed with 3 mL of DMF three times and left overnight, followed by washing with 3 mL of acetone three times and left overnight. Samples were air-dried before undergoing activation at 150 °C for 20 hours. Four samples were synthesized including a sample made from distilled DMF and washed with distilled acetone, a sample made from distilled DMF and washed with commercial acetone, and a sample made with collected DMF and washed with commercial acetone, and a sample made with commercial DMF and washed with commercial acetone.

ZIF-8 was synthesized solvothermaly. For samples made with distilled and commercial DMF, a 25 mL screw-cap reaction jar was used with $Zn(NO_3)_2 \cdot 6H_2O$ (350 mg, 1.18 mmol), 2-mIm (200 mg, 2.44 mmol), 15 mL of DMF, and three drops of HNO_3 added to the mixture with a

Pasteur pipette. Samples made with collected DMF were made in a 50 mL reaction jar at twice the scale adding $Zn(NO_3)_2 \cdot 6H_2O$ (700 mg, 1.18 mmol) and 2-mIm (400 mg, 2.44 mmol), with 30 mL of DMF, and six drops of HNO_3 added to the mixture with a Pasteur pipette After the reagents were dissolved by sonication, the sample was heated in a 120 °C oven for 1 day (24 h). The crystals were collected in 15 mL centrifuge tubes and washed with 3 mL of DMF three times and left overnight, followed by washing with 3 mL of acetone three times and left overnight. Samples were air-dried before undergoing activation at 120 °C for 20 hours. Four samples were synthesized including a sample made from distilled DMF and washed with distilled acetone, a sample made from distilled DMF and washed with commercial acetone, and a sample made with collected DMF and washed with commercial acetone, and a sample made with commercial DMF and washed with commercial acetone.

2.3. Results and Discussion

After evaluating methods to reduce solvent waste in academic research labs studying MOFs, focus was placed on the reuse of solvents collected from the solvent exchange process. In the ideal case, these solvents could be reused as collected, but we also chose to explore the distillation of these solvents and whether distillation is required to reuse the solvents in subsequent MOF synthesis. Distillation by rotary evaporation is an accessible method which is an effective, and relatively energy and time efficient procedure for purifying spent DMF and acetone. Solvent was collected from the solvent exchange procedure performed on various MOFs in our laboratory including zirconium based UiO-66, UiO-67, MOF-808 and NU-1000, along with rare-earth MOFs RE-UiO-66, CU-45, CU-27, and CU-10. Solvent was distilled in 500 mL batches in a 1 L round bottom flask through rotary evaporation with the gradual ramping of pressure as can be seen in Table 2.1 and 2.2. Solvent in the collection flask was discarded until the last stage of the procedure to ensure that low boiling point impurities were removed, and a total two rounds of distillation by rotary evaporation was carried out for both DMF and acetone.

Table 2.1 Procedure for the ramped distillation of DMF

Time	Rotation (RPM)	Water bath temperature (°C)	Pressure (mbar)
First ten minutes	185	65	200
Solvent in collection flask discarded			
Next ten minutes	185	65	150
Solvent in collection flask discarded			
Last twenty minutes	185	65	0

Table 2.2 Procedure for the ramped distillation of acetone

Time	Rotation (RPM)	Water bath temperature (°C)	Pressure (mbar)
First ten minutes	185	50	400
Solvent in collection flask discarded			
Last fifteen minutes	185	50	350

A ramped procedure was found to be most efficient for removing impurities of different volatilities. As expected, due to its high boiling point, DMF distillation required the water bath to be set at a higher temperature with a higher initial pressure when compared to the procedure used for the distillation of acetone. Recovery of solvent was found to be approximately 80-85%

The composition of the various samples of DMF and acetone before and after distillation were analyzed through ^{1}H NMR spectroscopy in order to identify the impurities present. Figures 2.2 to 2.4 summarize the state of DMF as it goes through the distillation process, from collection to the first and second round of distillation. ^{1}H NMR and ICP-MS analysis was also carried out for the remnants of two rounds of distillation (Figure A.1 and Table A.1 respectively)
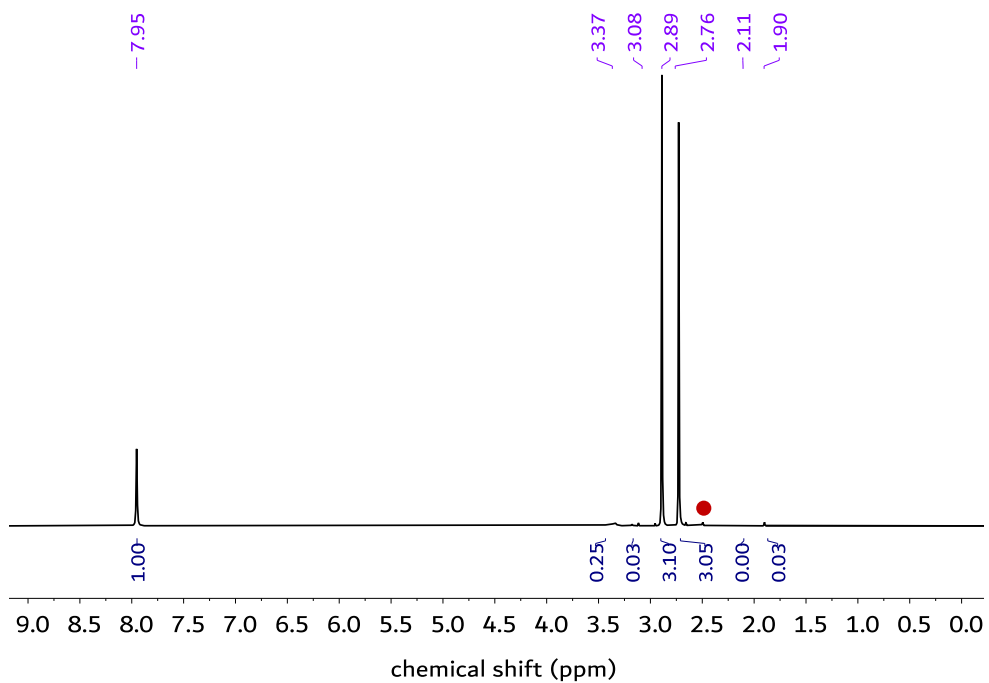
Figure 2.2 ^{1}H NMR spectrum of collected DMF with DMSO-d$_6$ highlighted with a red circle
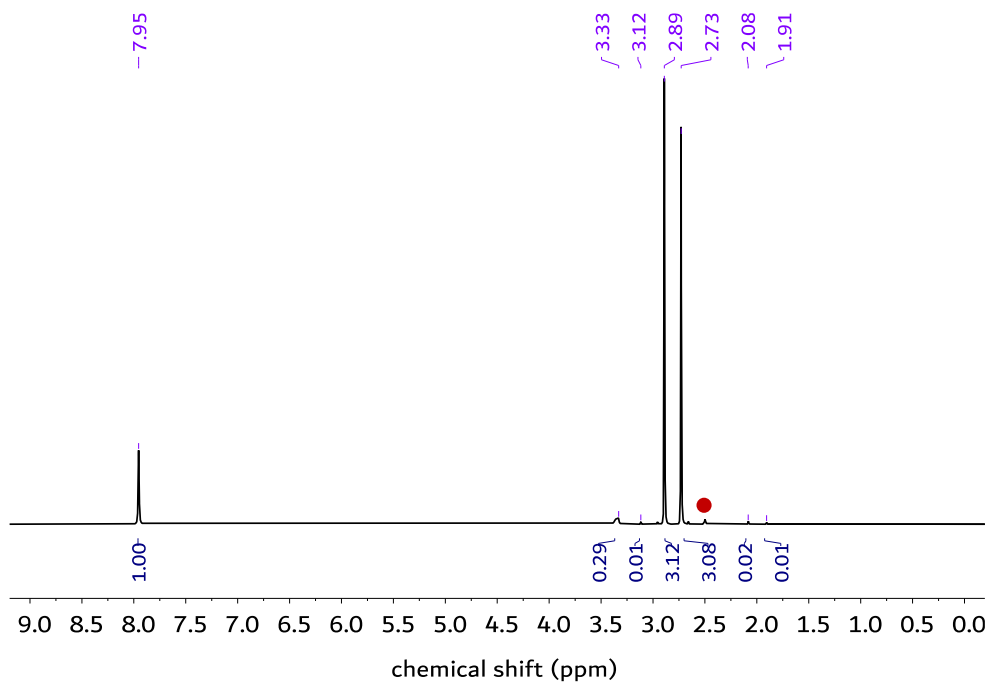
Figure 2.3 ^{1}H NMR spectrum of DMF after one round of distillation with DMSO-d$_6$ highlighted with a red circle
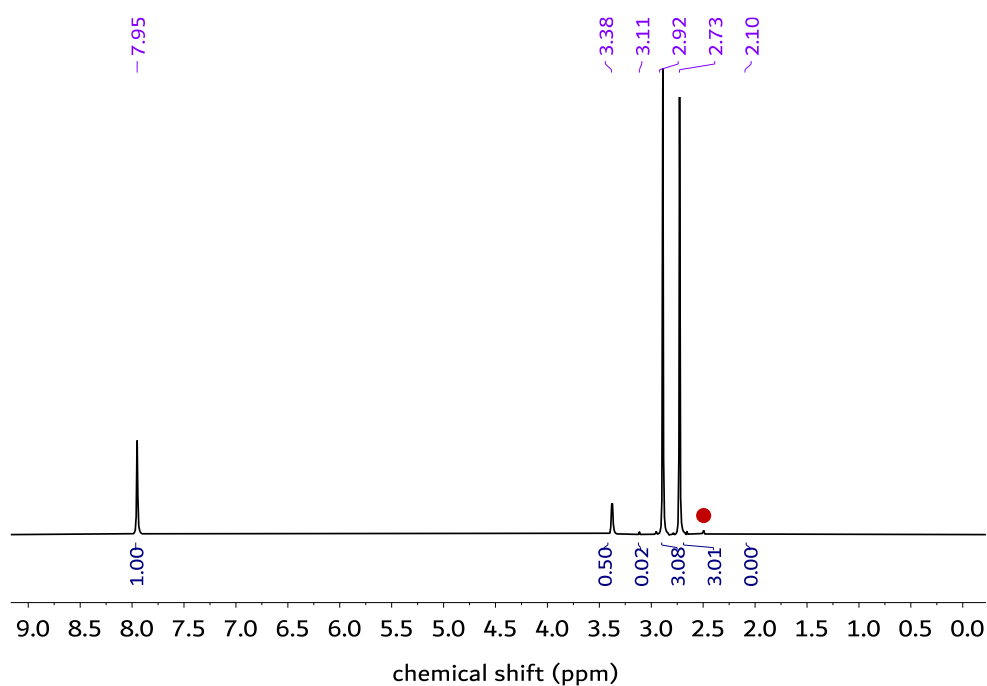
Figure 2.4 ^{1}H NMR spectrum of DMF after two rounds of distillation with DMSO-d$_6$ highlighted with a red circle

Impurities present in the DMF collected from solvent exchange that are visible by ^{1}H-NMR spectroscopy include; acetic acid at 1.90 ppm, methanol at 3.08 ppm and 4.08 ppm, and water at 3.37 pm. The presence of acetic acid can be attributed to its use as a modulator in the synthesis of some MOFs, the presence of water can be attributed to the introduction from the environment, and the presence of methanol can be attributed to its use in MOF solvent exchange procedures and glassware cleaning. Table 2.3 showcases the change in concentration of impurities relative to 1 mole of DMF for the samples as they undergo the distillation process.

Table 2.3 Concentration of contaminants in moles in relation to 1 mole of DMF

Compound	Collected DMF (moles)	Distilled DMF (moles)	Twice distilled DMF (moles)
Acetic acid 1.91 ppm	0.010	0.003	Not detected

Acetone 2.09 ppm	Not detected	0.003	Not detected
Methanol 3.09, 4.08 ppm	0.013	0.010	0.007
Water 3.37 ppm	0.100	0.145	0.250

The introduction of acetone during the first stage of distillation can be attributed to the rotary evaporator glassware cleaning process. With two rounds of distillation, the concentrations of acetic acid and acetone are reduced to below the detection limit, indicating the removal of these impurities. The increase in the concentration of water can be attributed to the hygroscopic nature of DMF[142] and the introduction of water from the environment. This increase in water concentration further explains the reduction in the concentration of methanol by only a half, rather than removal below the detection limit as seen with acetone and acetic acid. This may be attributed to methanol also having hygroscopic properties,[144] leading to some retention with the increasing levels of water as the distillation process continues. An interesting observation is the lack of dimethylamine in the distilled DMF; dimethylamine is a natural decomposition product of DMF that accumulates over time. The lack of dimethylamine in the distilled DMF suggests that the conditions used for distillation, including reduced pressure and heat, does not increase the rates of decomposition of DMF.

Analysis of acetone samples by ^{1}H NMR spectroscopy shows no acetic acid impurity within the solvent collected from solvent exchange processes (Figure 2.5). This is expected as solvent exchange with acetone is typically carried out after solvent exchange with DMF, where the majority of modulators like acetic acid have already been removed. Figures 2.5 to 2.7 and Table 2.4 document the impurities in the acetone sample as observed by ^{1}H NMR spectroscopy as it is collected and distilled for one and two rounds.

29
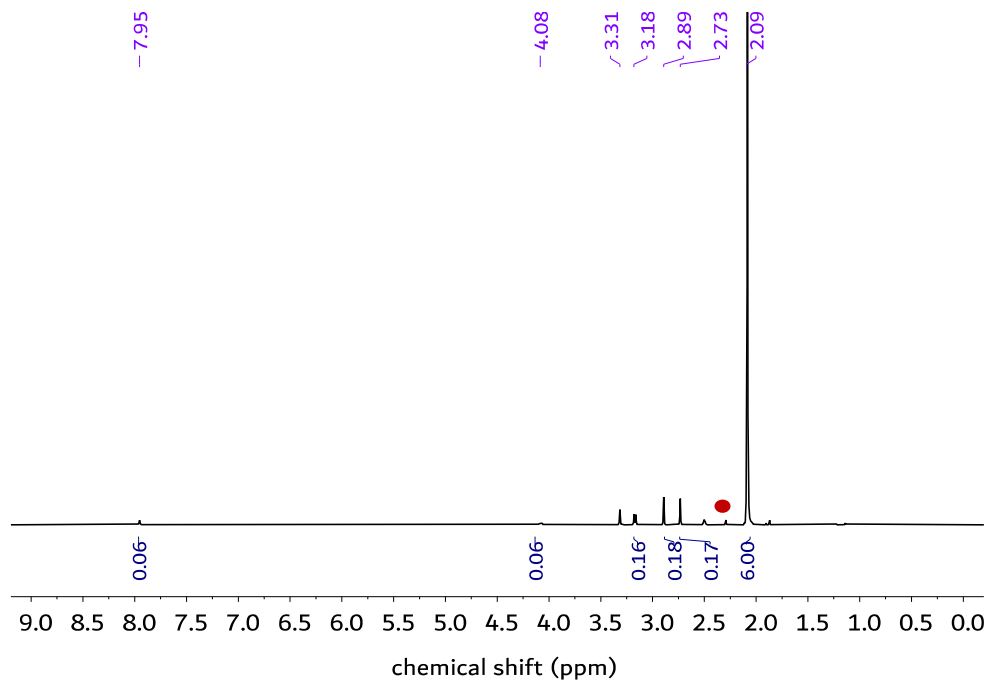
Figure 2.5 ¹H NMR spectrum of collected acetone with DMSO-d₆ highlighted with a red circle
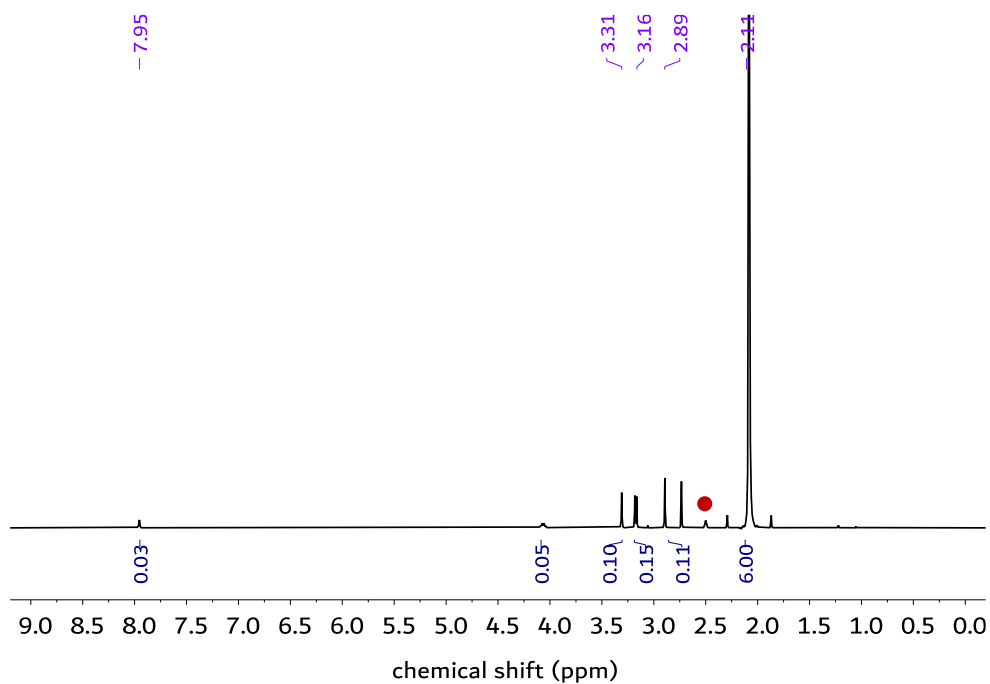
Figure 2.6 ¹H NMR spectrum of acetone after one round of distillation with DMSO-d₆ highlighted with a red circle
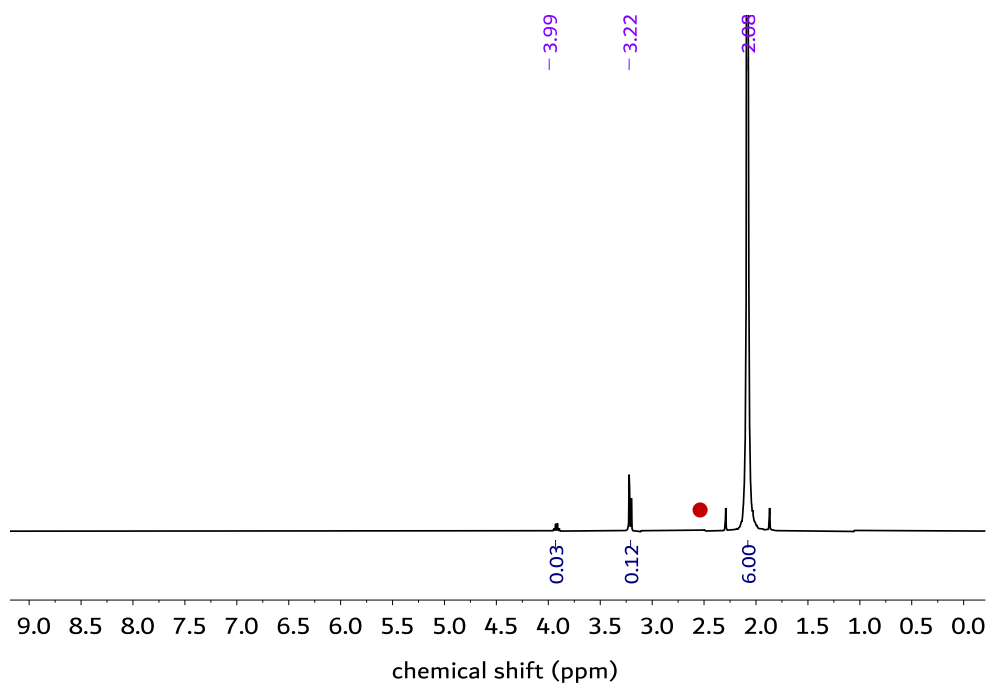
Figure 2.7 ^{1}H NMR spectrum of acetone after two rounds of distillation with DMSO-d$_6$ highlighted with a red circle

Table 2.4 Concentration of contaminants in acetone in moles relative to 1 mole of acetone

Compound	Collected acetone (moles)	Distilled acetone (moles)	Twice distilled acetone (moles)
DMF 2.73, 2.89, 7.95 ppm	0.060	0.030	Not detected
Methanol 3.18, 4.08ppm	0.060	0.050	0.040
Water 3.31 ppm	0.080	0.050	Not detected

The presence of DMF and methanol in the collected acetone can be attributed to retention of these solvents in the MOF pores from the first stage of the solvent exchange process. The

presence of water can be attributed to introduction from the environment. A removal of DMF and water below the detection limit is seen after two rounds of distillation with rotary evaporation, with trace levels of methanol present. The distillation procedures for both DMF and acetone can be considered an effective and accessible way to recycle the respective solvents. As the presence of water does not negatively impact the synthesis of some MOFs, further treatment is optional, such as the use of sieves, in cases where dry DMF is necessary.

The collected and distilled solvents were used for the synthesis of a series of four diverse MOFs. These include well-studied MOFs with known robust synthetic methods. Four samples of each MOF are synthesized; (1) a sample synthesized with commercial DMF from a supplier and washed with commercial acetone, (2) a sample synthesized with collected DMF from solvent exchange procedures and washed with commercial acetone, (3) a sample synthesized with twice distilled DMF and washed with commercial acetone and (4) a sample synthesized with twice distilled DMF and washed with twice distilled acetone.

The structure, bulk crystallinity and phase purity of the synthesized MOFs is confirmed through PXRD. Figures 2.8 to 2.11 below show the PXRD patterns obtained for the synthesized samples. Morphology was also confirmed for the samples (Figures A.2-A.13)
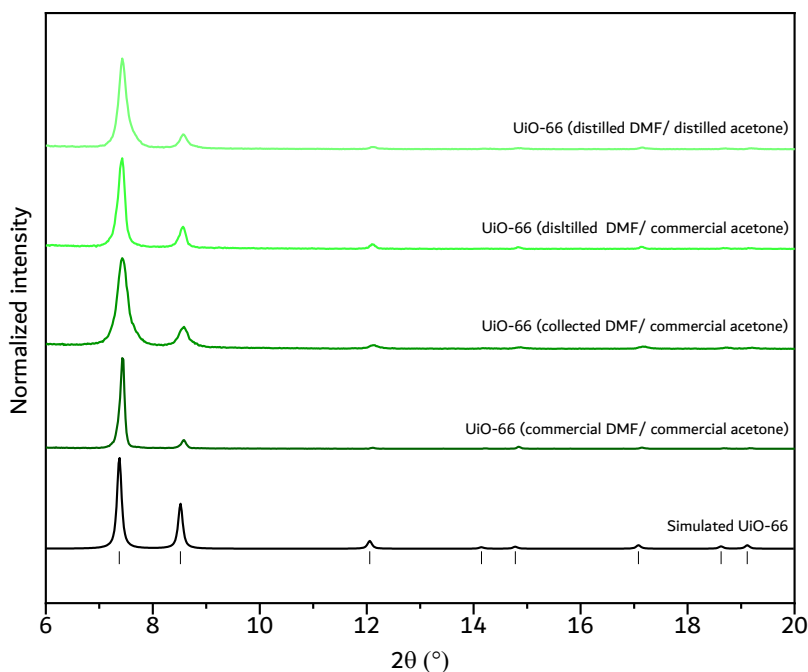
Figure 2.8 PXRD patterns for UiO-66 samples
synthesized using DMF from different sources as noted.
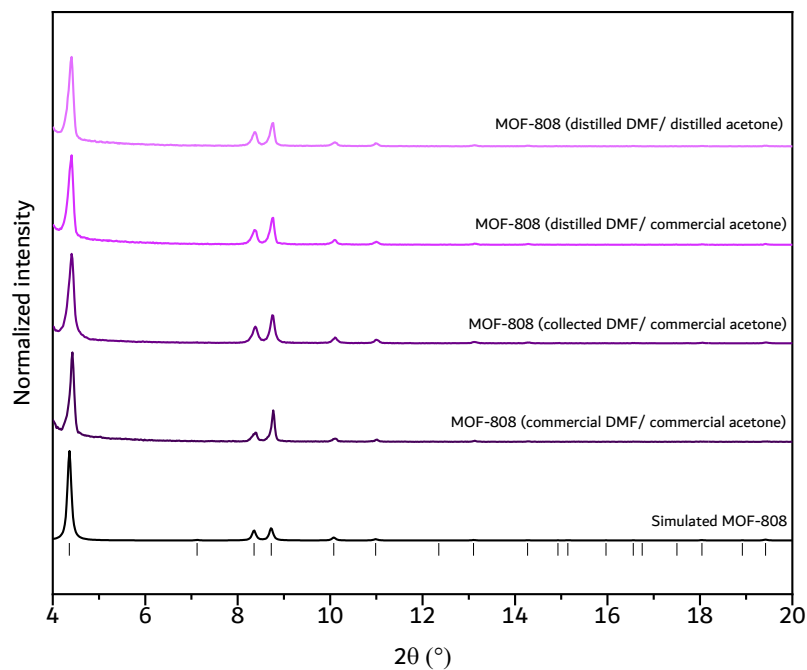
Figure 2.9 PXRD patterns for MOF-808 samples synthesized using DMF from different sources as noted.
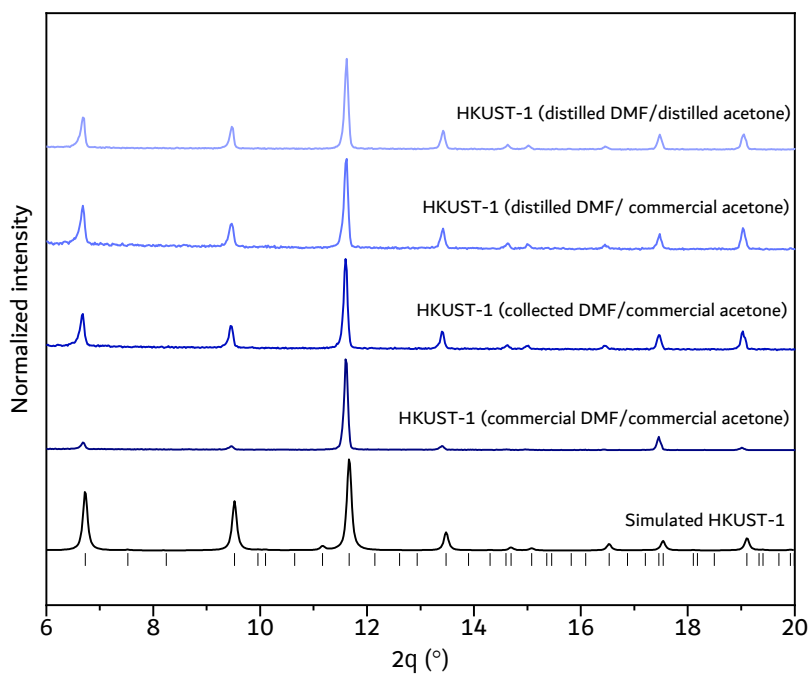
Figure 2.10 PXRD patterns for HKUST-1 samples synthesized using DMF from different sources as noted.
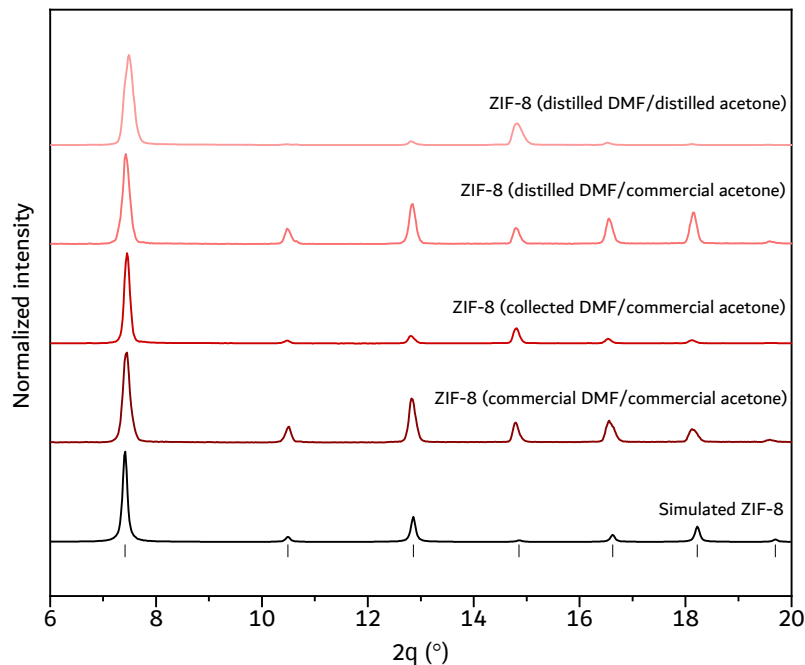
Figure 2.11 PXRD patterns for ZIF-8 samples synthesized using DMF from different sources as noted.

PXRD confirms that UiO-66, MOF-808, HKUST-1, and ZIF-8 were successfully synthesized using collected, distilled, and commercial solvent. In all cases the materials are crystalline and phase pure. This suggests that the low concentration of contaminants present in the collected solvent do not interfere with the formation of dynamic bonds between the metal and linker during the synthesis. This also indicates that the solvent-exchange process is not hindered by the low concentration of contaminants in the distilled acetone used to wash the MOFs.

In order to assess the effect of distilled and collected synthesis solvents on the resulting porosity of the MOFs, N_2 adsorption isotherms were collected and BET areas calculated. Figures 2.12 to 2.15 show the N_2 adsorption-desorption isotherms for all synthesized samples, with Tables 2.5 to 2.8 summarizing the calculated BET area with comparison to expected values.
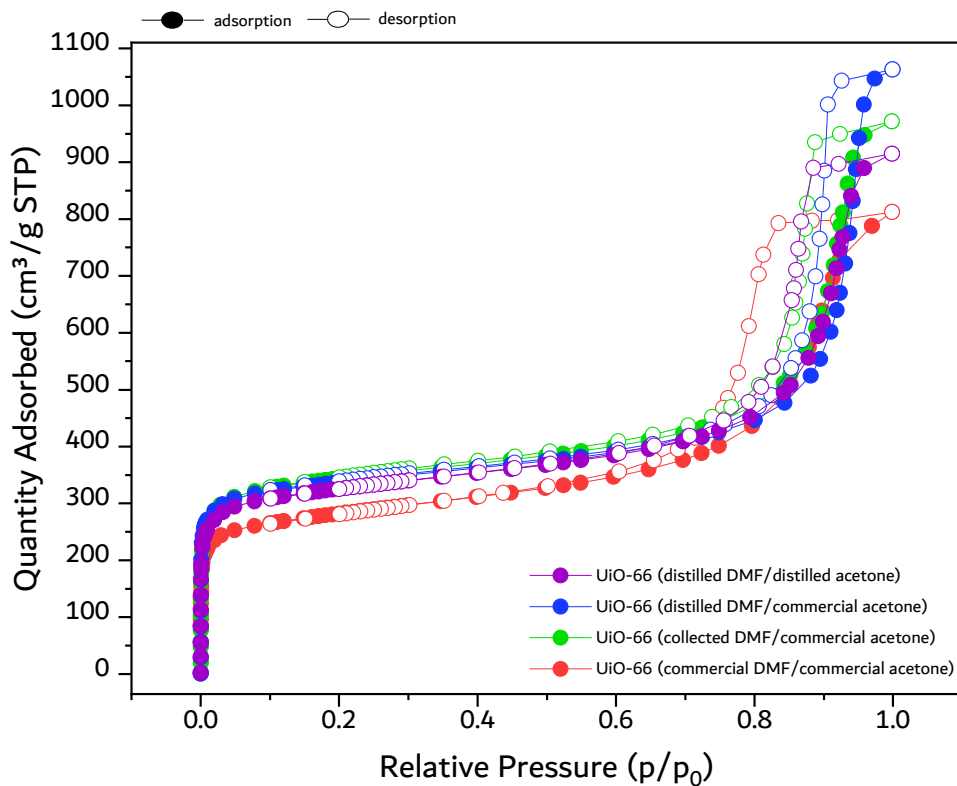
Figure 2.12 N_2 adsorption-desorption isotherms for UiO-66 synthesized using DMF from different sources as noted.

Table 2.5 BET areas of UiO-66 samples

UiO-66 from distilled DMF/ distilled acetone	1240 m^2 g^{-1}
UiO-66 from distilled DMF/ commercial acetone	1300 m^2 g^{-1}
UiO-66 from collected DMF/ commercial acetone	1320 m^2 g^{-1}
UiO-66 from commercial DMF/ commercial acetone	1100 m^2 g^{-1}
Expected BET Area[110]	1000-1200 m^2 g^{-1}
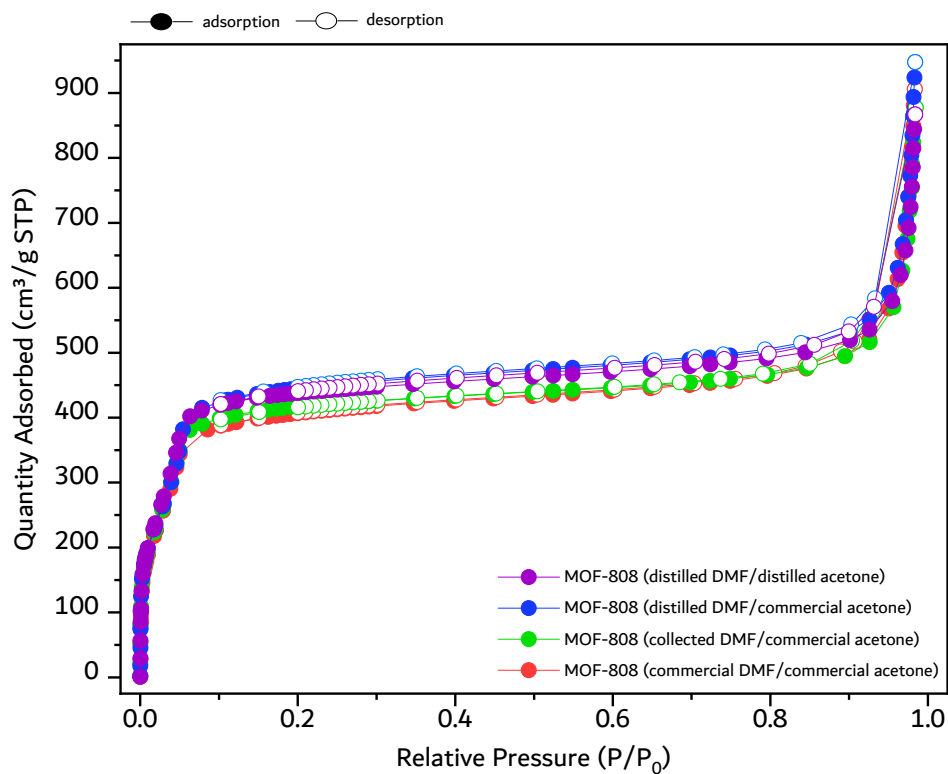
Figure 2.13 N$_2$ adsorption-desorption isotherms for MOF-808 synthesized using DMF from different sources as noted.

Table 2.6 BET areas for MOF-808 samples

MOF-808 from distilled DMF/ distilled acetone	1650 m^2 g^{-1}
MOF-808 from distilled DMF/ commercial acetone	1640 m^2 g^{-1}
MOF-808 from collected DMF/ commercial acetone	1660 m^2 g^{-1}
MOF-808 from commercial DMF/ commercial acetone	1540 m^2 g^{-1}
Expected BET Area[59]	1500-2000 m^2 g^{-1}
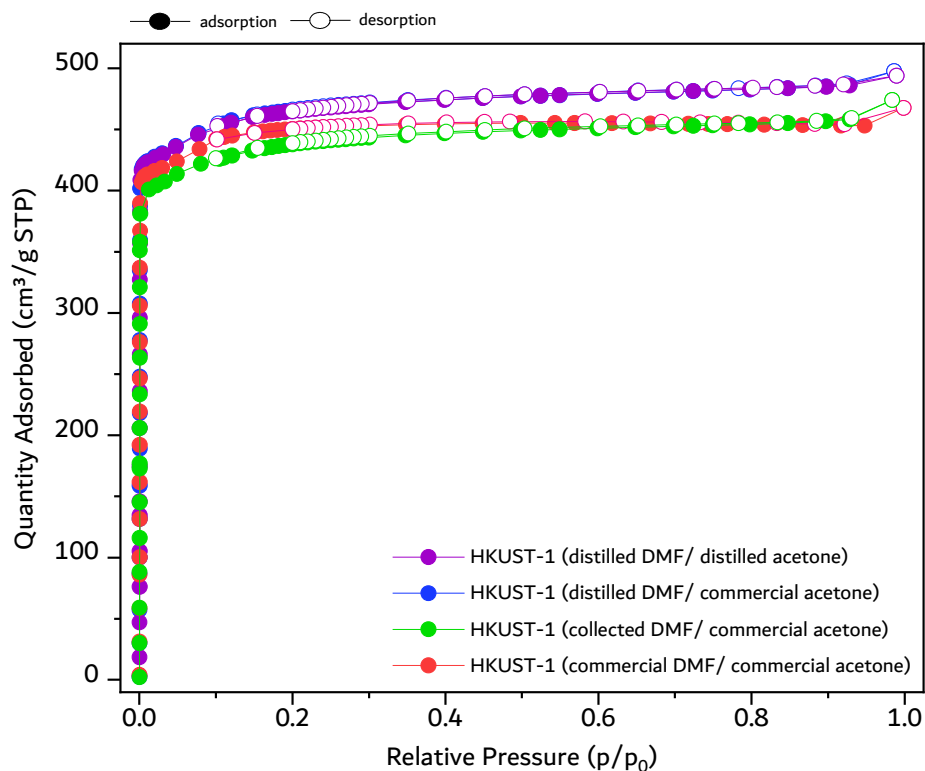
Figure 2.14 N$_2$ adsorption-desorption isotherms for HKUST-1 synthesized using DMF from different sources as noted.

Table 2.7 BET areas of HKUST-1 samples

HKUST-1 from distilled DMF/ distilled acetone	1810 m^2 g^{-1}
HKUST-1 from distilled DMF/ commercial acetone	1810 m^2 g^{-1}
HKUST-1 from collected DMF/ commercial acetone	1710 m^2 g^{-1}
HKUST-1 from commercial DMF/ commercial acetone	1750 m^2 g^{-1}
Expected BET Area[145]	1700-1900 m^2 g^{-1}
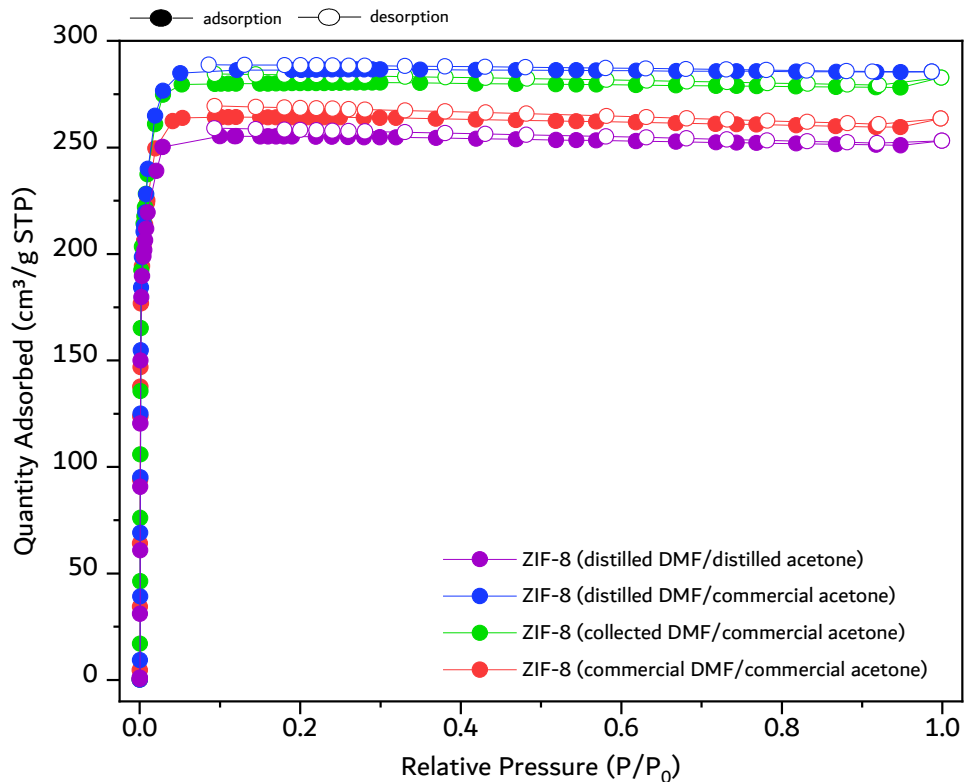
Figure 2.15 N_2 adsorption-desorption isotherms for ZIF-8 synthesized using DMF from different sources as noted.

Table 2.8 BET areas of ZIF-8 samples

ZIF-8 from distilled DMF/ distilled acetone	1110 m^2 g^{-1}
ZIF-8 from distilled DMF/ commercial acetone	1220 m^2 g^{-1}
ZIF-8 from collected DMF/ commercial acetone	1190 m^2 g^{-1}
ZIF-8 from commercial DMF/ commercial acetone	1110 m^2 g^{-1}
Expected BET Area[146]	1400 m^2 g^{-1}

Calculated BET areas are consistent among samples of UiO-66, MOF-808, HKUST-1 and ZIF-8 synthesized and washed with various combinations of commercial, collected, and distilled solvents. Expected Type 1a isotherms are observed for all samples of UiO-66, HKUST-1, and ZIF-

8, indicating the presence of micropores, while expected Type 1b isotherms are observed for all samples of MOF-808, indicating the presence of larger micropores.

DRIFTS spectra were collected to analyze IR active functional groups present in each MOF and can be seen in Figures 2.16 to 2.19
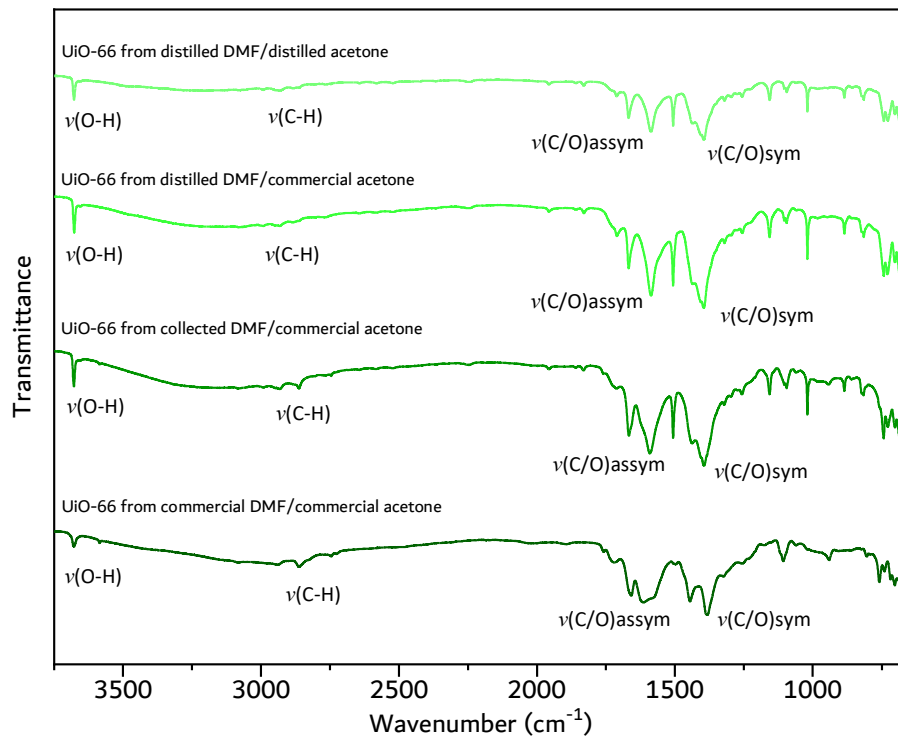
Figure 2.16 DRIFTS spectra for UiO-66 synthesized with DMF from different sources as noted.
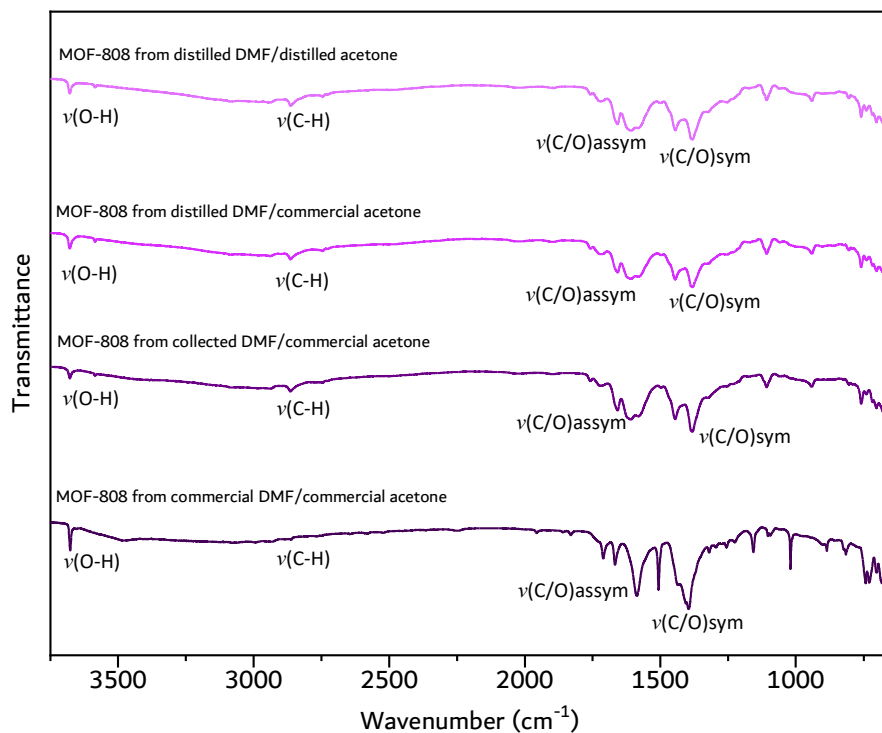
Figure 2.17 DRIFTS spectra for MOF-808 synthesized with DMF from different sources as noted.
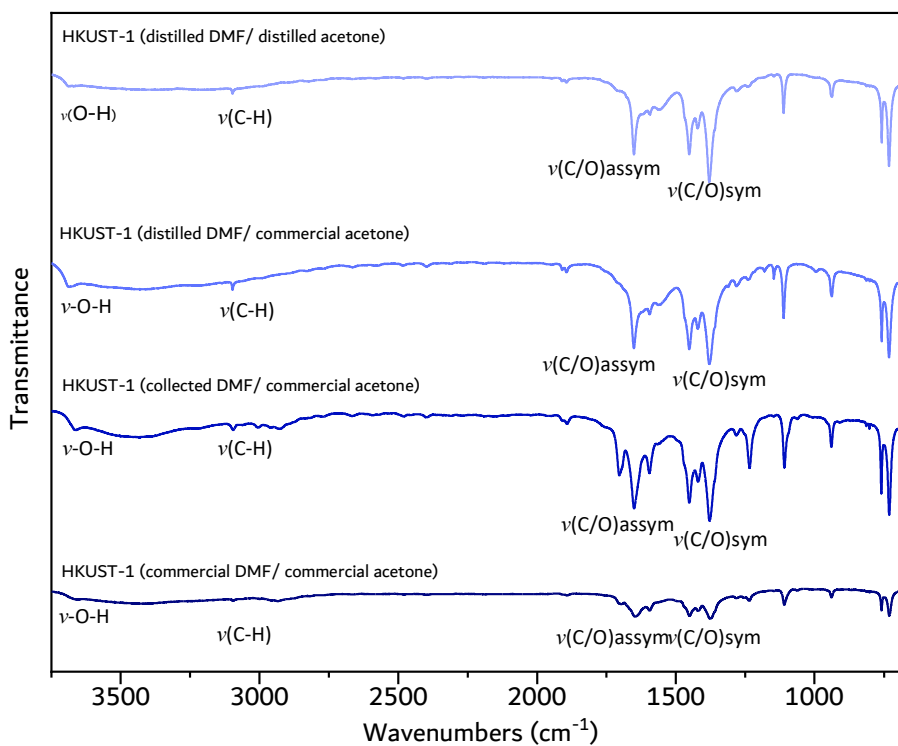
Figure 2.18 DRIFTS spectra for HKUST-1 synthesized with DMF from different sources as noted.
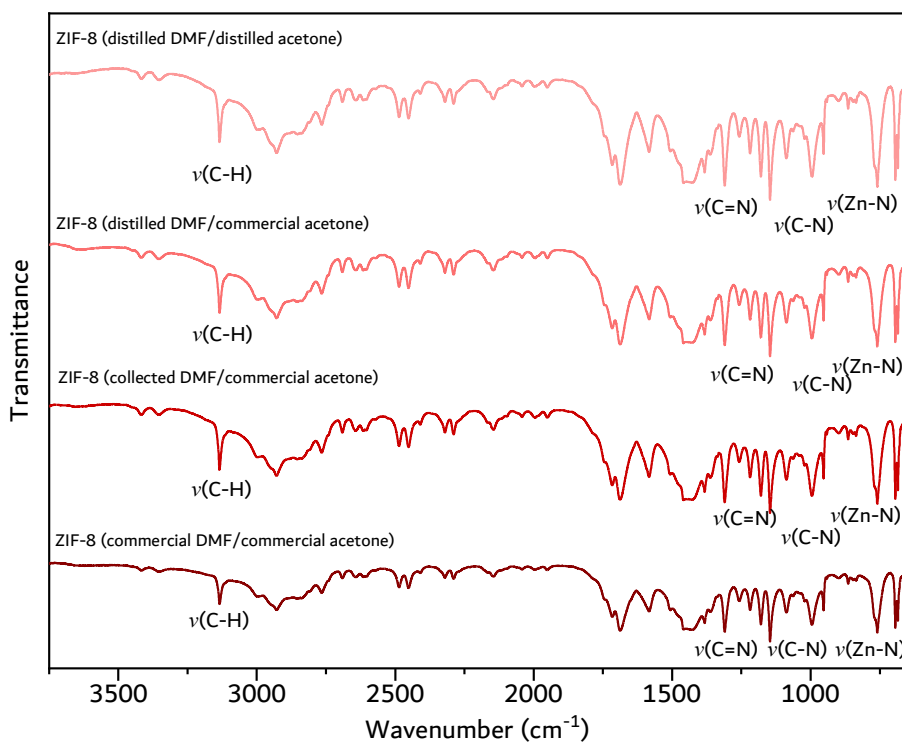
Figure 2.19 DRIFTS spectra for ZIF-8 synthesized with DMF from different sources as noted.

The expected -C–H stretches at 2600 cm^{-1} and -C=O stretches at 1500 cm^{-1} can be seen in all samples of UiO-66, MOF-808, and HKUST-1. A terminal and bridging -OH peak is observed for all the UiO-66 and MOF-808 samples. The terminal -OH peak in UiO-66 indicates the presence of defects in the UiO-66 samples, but as it can also be seen in the control sample, the defects can be attributed to the procedure used rather than the solvents acting as a defect engineering tool. The terminal and bridging -OH stretches are expected in MOF-808 as the structure includes both terminal and bridging -OH ligands due to the 6-connected Zr$_6$-cluster node of this MOF. A terminal -OH peak is also observed in the HKUST-1 samples and suggests hydration of the MOF node, which is expected in samples post-activation that have been exposed to moisture in air. As ZIF-8 is made from 2-mIM and a Zn(II) ion node, the expected stretches are different. Apart from the -CH stretch at 3250 cm^{-1}, a -C=N stretch at 1500 cm^{-1}, a -CN stretch at 1250 cm^{-1} and a -Zn-N cm^{-1} at 800 cm^{-1} stretch is observed.

^{1}H-NMR spectroscopy is used to confirm the presence of the organic linker in each MOF as well as the presence or absence of leftover modulator or solvents. Figures 2.20 and 2.23 show the obtained spectra.
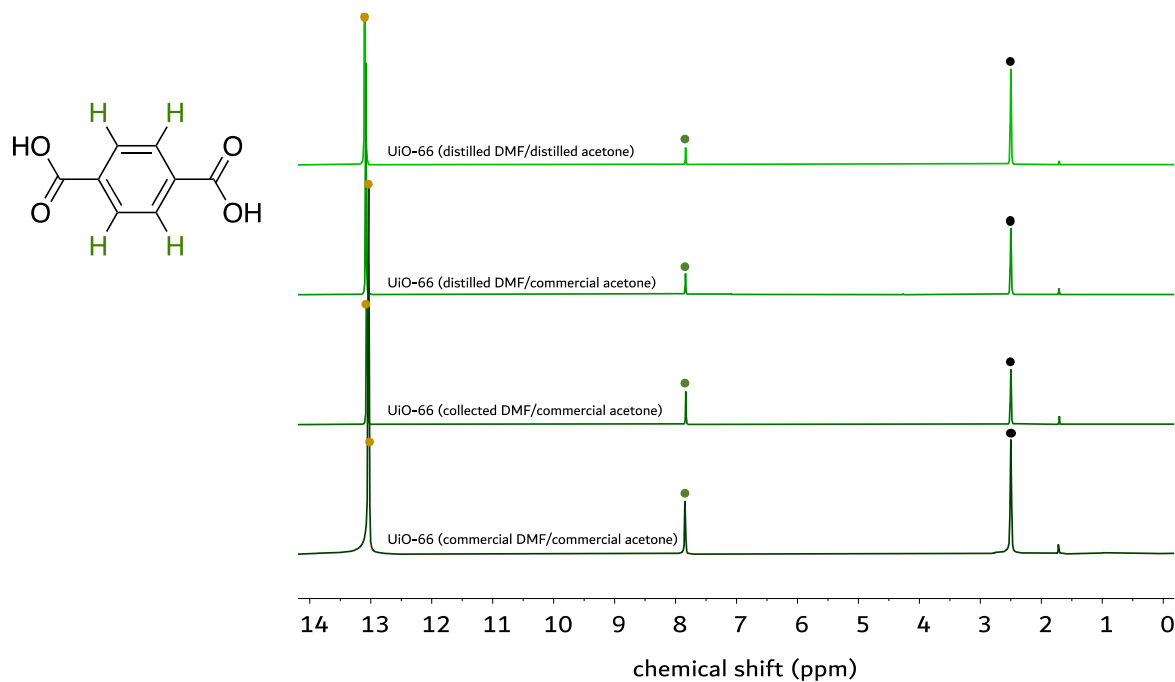
Figure 2.20 ^{1}H NMR spectra of UiO-66 synthesized using DMF from different sources as noted. Samples are digested in DMSO-d$_6$ and D$_2$SO$_4$ which are designated by black and gold circles respectively
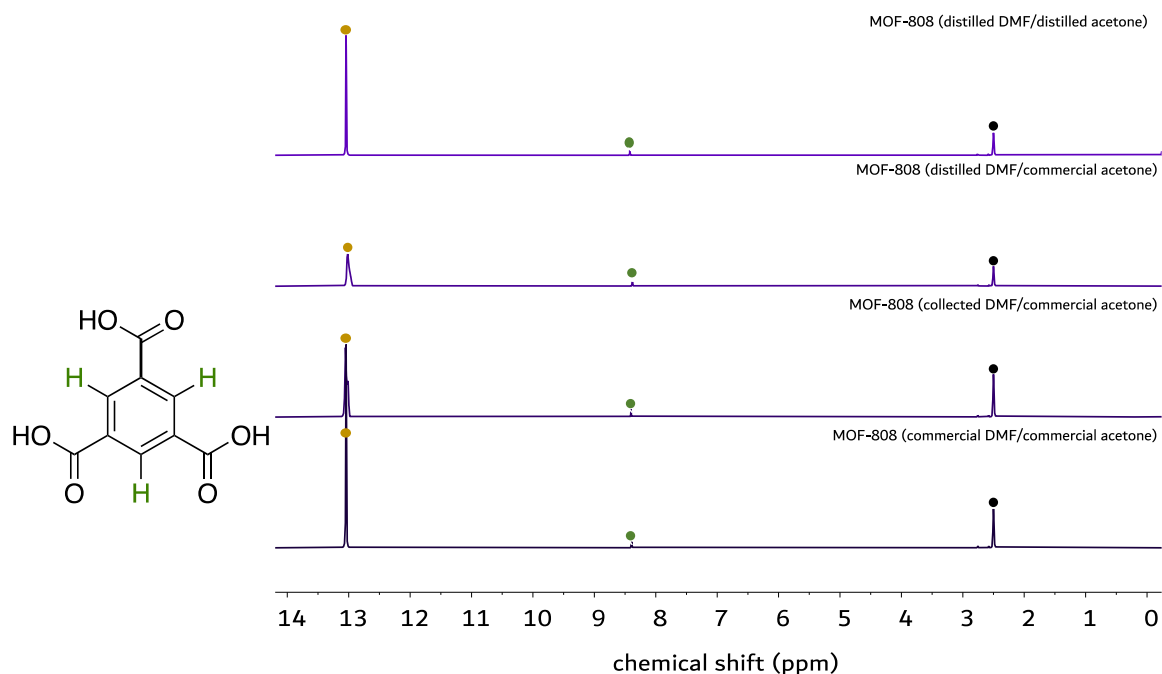
Figure 2.21 ^{1}H NMR spectra of MOF-808 synthesized using DMF from different sources as noted. Samples are digested in DMSO-d$_6$ and D$_2$SO$_4$ which are designated by black and gold circles respectively
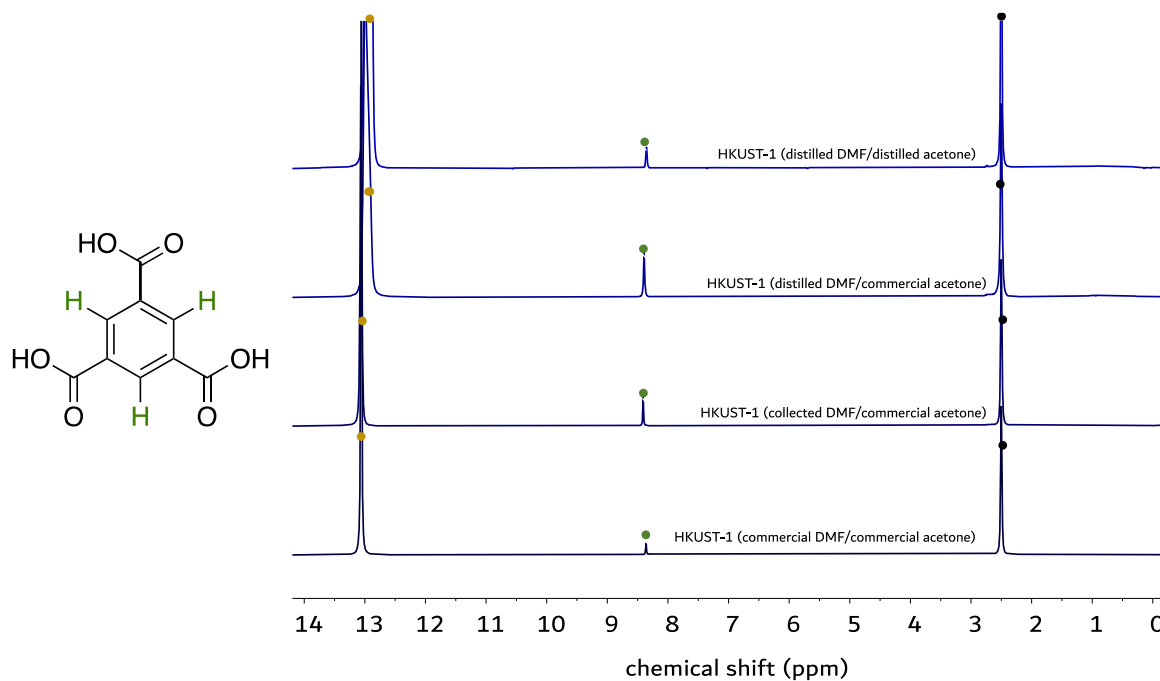
Figure 2.22 ^{1}H NMR spectra of HKUST-1 synthesized using DMF from different sources as noted. Samples are digested in DMSO-d$_6$ and D$_2$SO$_4$ which are designated by black and gold circles respectively
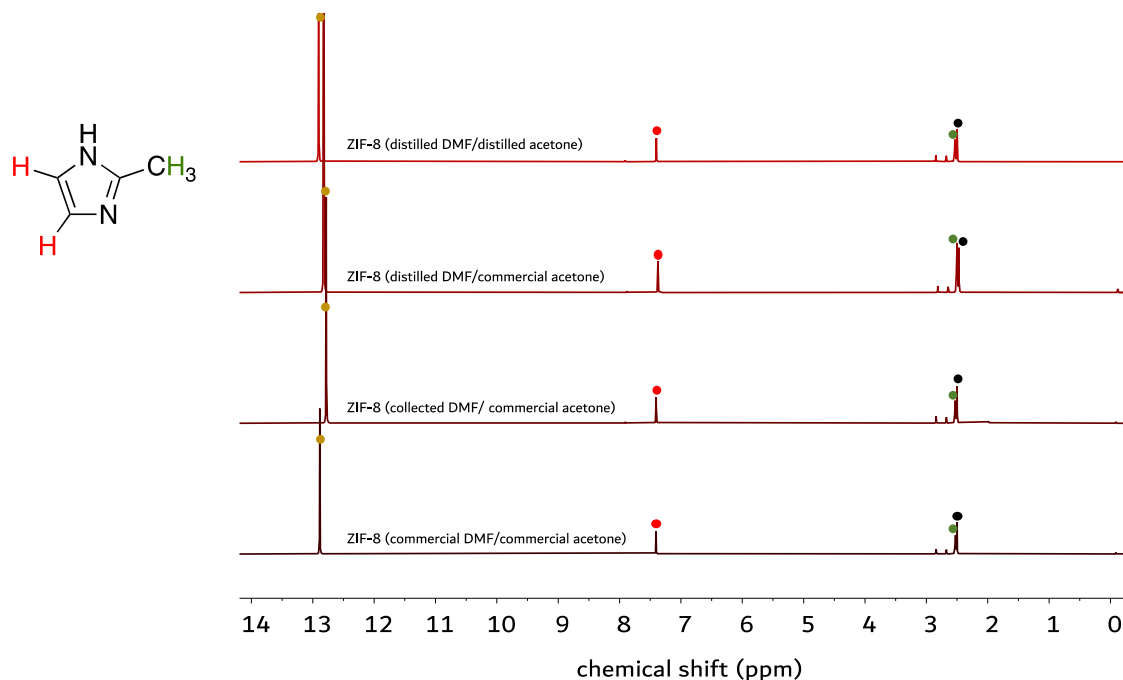
Figure 2.23 ^{1}H NMR spectra of ZIF-8 synthesized using DMF from different sources as noted. Samples are digested in DMSO-d$_6$ and D$_2$SO$_4$ which are designated by black and gold circles respectively

The expected peaks are observed in the ^{1}H-NMR spectra of all digested MOFs. No unexpected impurities are observed when using collected or distilled solvents to synthesize the MOFs.

With confirmation of the successful synthesis of the various MOFs using the various types of solvent, the obtained yields can help further establish if the use of collected vs. distilled vs. commercial solvents has any impact on the resulting synthesis. Table 2.9 shows the yields obtained for all samples.

Table 2.9 Table of experimental and percent yields for synthesized samples

Sample	Experimental yield (mg)	Percent yield (%)
UiO-66 (commercial DMF/commercial acetone)	20.7	88.8
UiO-66	22.1	94.8

(collected DMF/commercial acetone)		
UiO-66 (distilled DMF/commercial acetone)	31.5	92.3
UiO-66 (distilled DMF/distilled acetone)	20.0	85.8
MOF-808 (commercial DMF/commercial acetone)	29.3	76.5
MOF-808 (collected DMF/commercial acetone)	25.5	66.6
MOF-808 (distilled DMF/commercial acetone)	32.1	83.8
MOF-808 (distilled DMF/distilled acetone)	30.1	78.6
HKUST-1 (commercial DMF/commercial acetone)	30.8	35.1
HKUST-1 (collected DMF/commercial acetone)	36.5	42.3
HKUST-1 (distilled DMF/commercial acetone)	32.4	37.5
HKUST-1 (distilled DMF/distilled acetone)	30.3	35.1
ZIF-8 (commercial DMF/commercial acetone)	119.4	44.6
ZIF-8 (collected DMF/commercial acetone)	106.0	39.6
ZIF-8 (distilled DMF/commercial acetone)	211.6	79.0
ZIF-8 (distilled DMF/distilled acetone)	186.6	69.7

The obtained yields are relatively consistent regardless of the source of DMF or acetone used in the synthesis and solvent exchange of for all samples of UiO-66, MOF-808, HKUST-1, with higher yields when using collected or distilled solvents for ZIF-8, suggesting that the low level of impurities in the collected and distilled solvents do not have a large or negative impact on the resulting synthesis.

Thermal stability of sample synthesized in collected DMF and distilled DMF was analyzed through thermogravimetric analysis (A.14 to A.17).

2.4. Conclusions

The results herein demonstrate that the solvent collected from the washing and solvent exchange process during MOF synthesis, which is normally discarded, can be reused to synthesize MOFs. In fact, the collected solvent was as effective as the distilled, or even commercial solvent for MOF synthesis, which brings new opportunities for waste and energy reduction by removing the need for any distillation or other treatment prior to reusing this solvent. Distillation of DMF and acetone was also found to be effective for removing trace impurities in the collected solvents, with rotary evaporation being an accessible tool for this purpose. In cases where small impurities can affect the resulting MOF synthesis, distillation can thus be used. Overall, the ability to reuse and recycle the solvents that are used during the washing and solvent exchange process during MOF synthesis will help to significantly decrease the amount of solvent waste generated in academic labs studying MOFs, improving the sustainability of the process.

Chapter Three

Accessing a Library of Rare-Earth Cluster Based Metal–Organic Frameworks through Microwave-Assisted Transmetalation

3.1. Introduction

Metal–organic frameworks, or MOFs, are porous materials with high surface areas.[4,7] The inorganic component, also known as the metal node, can take on a cluster, chain, or ion formation, and the organic component, also known as the organic linker, connects the metal nodes to form the porous network. In addition to *de novo* synthesis, MOFs can be functionalized or modified post-synthetically, in a process often referred to as post-synthetic modification (PSM).[87] These modifications can be made either through changes to or on the organic linker or changes to or on the inorganic metal node.[88]

Methods for the PSM of MOF metal nodes include solvent-assisted ligand incorporation (SALI),[147] atomic layer deposition (AIM),[148] solvent-assisted metal-insertion (SAMI),[149] and transmetalation,[150] while a method for the PSM of MOF linkers includes solvent-assisted linker exchange (SALE).[151] Transmetalation, in particular, involves the exchange of metal ions in a *de novo* synthesized MOF with a different target metal ion of similar coordination number, ionic radius, and oxidation state. Transmetalation, along with other post-synthetic techniques, can be a useful tool to access isostructures that are difficult or not possible at all to access *de novo*.

Reported methods for transmetalation include immersing a sample of *de novo* synthesized MOF in a solution of a target metal salt in a solvent, typically DMF. The solution is then heated using conventional methods (e.g., an oven or hot plate) to promote exchange at the metal node. Existing transmetalation procedures are quite effective, however, the procedures often call for reactions to be heated for several days, and in some cases weeks to months, depending on the starting MOF. This not only has implications for the amount of time required to obtain transmetalated MOFs, but also brings attention to the large amount of energy required to heat the reaction for the time required.

Existing transmetalation procedures primarily rely on the use of conventional heating, which works through an external method where the sample is heated from the outside in. We hypothesize that an internal heating mechanism, such as microwave irradiation, should help in

reducing the time required to heat a sample and thus the amount of energy utilized in the process. Heating by microwave irradiation occurs through dipole interactions within the sample, essentially acting as an internal heating mechanism.[82]

Herein, we explore microwave-assisted transmetalation to obtain a series of seven mixed metal rare-earth MOF analogues. Starting with Y-UiO-66 as the parent MOF, transmetalation of Y(III) with Eu(III), Gd(III), Tb(III), Ho(III), Er(III), Tm(III), and Yb(III) is presented.
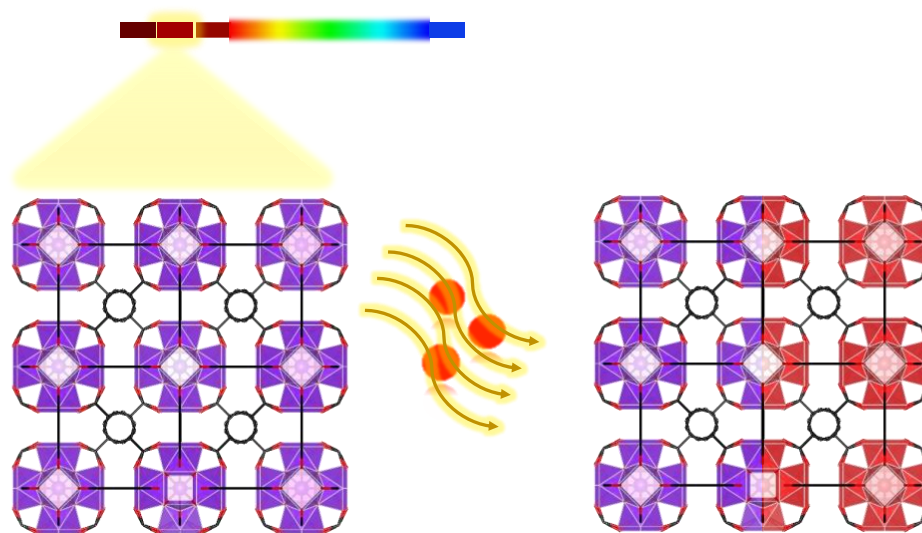
Figure 3.1 Microwave-assisted transmetalation of Y-UiO-66 yields mixed metal RE-UiO-66 analogues.

3.2. Experimental Procedures

3.2.1. Materials and Methods

All reagents were used without further purification. This includes: $Y(NO_3)_3 \cdot 6H_2O$, $Eu(NO_3)_3 \cdot 6H_2O$, $Gd(NO_3)_3 \cdot 6H_2O$, $Tb(NO_3)_3 \cdot 6H_2O$, $Ho(NO_3)_3 \cdot 6H_2O$, $Er(NO_3)_3 \cdot 6H_2O$, $Tm(NO_3)_3 \cdot 6H2O$, and $Yb(NO_3)_3 \cdot 6H_2O$ (Alfa Aesar), 2,6-difluorobenzoic acid (2,6-DFBA) (Combi-Blocks), 1,4-benzene dicarboxylic acid (BDC, ACROS 98%), nitric acid (Fisher), acetone (Fisher Chemicals, 99%), N,N-dimethylformamide (DMF, Fisher Chemicals, 99%), N,N-dimethylacetamide (DMA, Fisher Chemicals, 99%).

Microwave reactions were performed in a CEM Discover 2.0 microwave equipped with an iWave sensor.

PXRD data were collected on a Bruker D2 Phaser equipped with a CuKα X-ray source at a wavelength (λ) of 1.54 Å. All samples were drop casted on to the silicon wafer held in a zero-background holder. Scans were run with sample-rotation off at a range of 3-20° 2θ at an increment of 0.2 s.

Nitrogen adsorption-desorption isotherm data were collected at 77K on a Micromeritics TriStar II Plus surface area and porosity analyzer. All samples were activated at 80 °C for 20 h before each isotherm was collected by heating under vacuum using a Micromeritics Smart VacPrep equipped with a hybrid turbo vacuum pump system.

Inductively coupled plasma–mass spectrometry (ICP-MS) data was measured on an Agilent 7500 Series instrument.

Diffuse reflectance infrared Fourier transform spectroscopy (DRIFTS) spectra were obtained using a Thermo Scientific Nicolet 6700 FT-IR equipped with an MCT detector with a resolution of 1 cm^{-1}

^{1}H NMR spectroscopy data were collected on a 300 MHz Bruker spectrometer with the residual solvent peaks referenced to the residual solvent peaks. DMF and acetone were characterized in d-DMSO6. Samples were first digested in 10 drops of D_2SO_4 with 10 minutes of sonication before being prepared in 0.7 mL of DMSO-d_6.

3.2.2. Synthesis and Activation of Y-UiO-66

Y-UiO-66 was synthesized solvothermaly following a previously reported method.[68] In a 6-dram vial, Y(NO$_3$)$_3$.6H$_2$O (66.6 mg, 0.174 mmol), BDC (28.5 mg, 0.171 mmol), and 2,6-DFBA (440.0 mg, 2.780 mmol) and 8 mL of DMA were added. The reagents were dissolved by sonication and the sample was heated at 120 °C in an oven for 2 days (48 hrs). The pale-yellow precipitate was collected in a 15 mL centrifuge tube and washed with 3 mL of DMF three times and left overnight, followed by washing with 3 mL of acetone three times and left overnight. Samples were air-dried before undergoing activation at 80 °C for 20 hours.

3.2.3. Microwave-assisted transmetalation of Y-UiO-66 with Eu-, Gd-, Tb-, Ho-, Er-, Tm-, and Yb.

Transmetalation of Y-UiO-66 with Eu(III), Gd(III), Tb(III), Ho(III), Er(III), Tm(III) and Yb(III) was conducted in a 35 mL microwave reaction vessel by adding *de* novo synthesized Y-

UiO-66 (10 mg, 21.55μmols), and the target metal salt (nitrate salts of Eu, Gd, Tb, Ho, Er, Tm, Yb = 19.43, 15.82, 15.60, 18.34, 17.83, 19.70, 17.20 mg respectively, 47.62 μmols) with 5 mL of DMF and a stir bar. The reaction mixture was then heated in the microwave at 200 °C for 1 hour and 7 minutes at 200 W on low stir. For samples undergoing two rounds of transmetalation, the DMF-metal salt solution was replaced after the first round with a fresh solution of the metal salt before being reacted under the same conditions as the first round. The sample was collected in a 15 mL centrifuge tube and washed with 3 mL of DMF three times and left for 24 hours, followed by washing with 3 mL of acetone three times and left for 24 hours

3.1. Results and Discussion

Zr-UiO-66 is a well-studied archetypal MOF,[67] and the synthesis of eight rare-earth analogues of UiO-66 was reported by our group in 2021.[68] Y-UiO-66 was chosen as the starting MOF for microwave-assisted transmetalation experiments, with seven lanthanoid ions chosen for transmetalation based on previous success when using these ions for the *de novo* synthesis of RE-UiO-66 (RE = Eu(III), Gd(III), Tb(III), Ho(III), Er(III), Tm(III), Yb(III)). These lanthanoids were chosen as they all have similar properties to yttrium, such as a +3 oxidation state, accessible coordination number of 8, coordination geometry, and similar ionic radii.
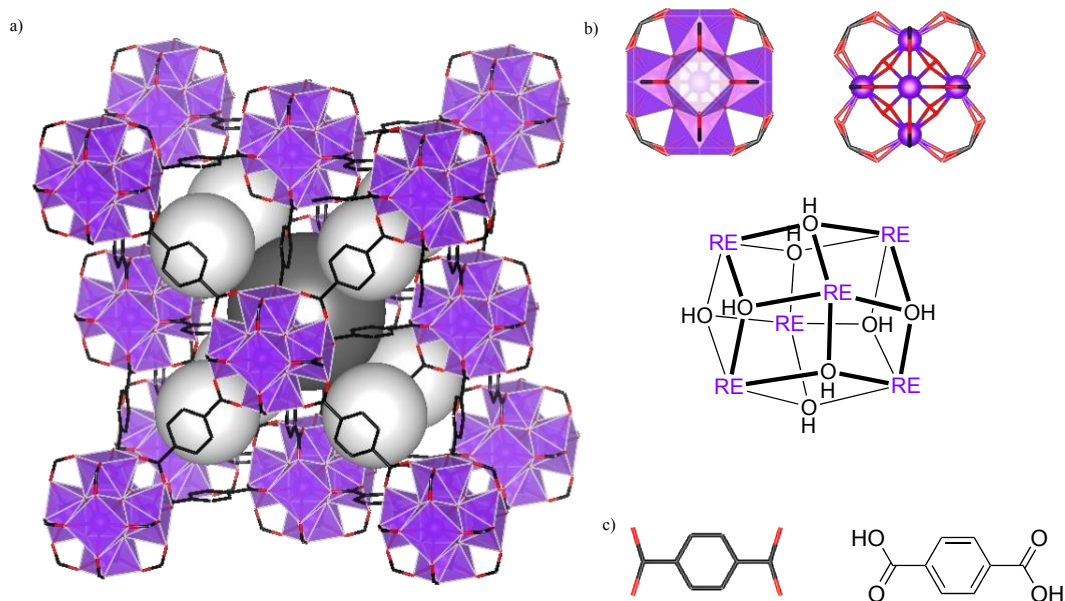
Figure 3.2 Schematic representation of RE-UiO-66 with a) angled view showcasing tetrahedral cages (white spheres) and an octahedral cage (black sphere), b) representation of the cluster, and c) representation of the linker

Transmetalation procedures involving conventional heating have been reported,[150] with a method for the transmetalation of a nonanuclear cluster-based rare-earth MOF published by our group in 2021.[90] This procedure involves the immersion of a *de novo* synthesized MOF, Y-CU-10, in a DMF solution of the target rare-earth metal salt, specifically a rare-earth nitrate salt. The rare-earth metal salt solution is exchanged and replaced with a fresh solution 3 times over the course of 14 days. This conventional heating method was converted to parameters for microwave-irradiation via the following equation establishing the relationship between conventional heating and microwave irradiation.

$$T = T_0 + (10°C)x, \qquad t \approx \frac{t_0}{2^x}$$

Where T is the microwave heating temperature, T_0 is the conventional temperature, t is the microwave heating time, t_0 is the conventional heating time and x is the temperature increase coefficient.

Initial tests show that Y-UiO-66 is stable under microwave-irradiation in DMF (Figure 3.3), but that the MOF degrades with the addition of 5 equivalents of metal nitrate salt under the same conditions (Figure 3.3). As such, lower concentrations of the metal nitrate salt solution (e.g., 1 equivalent) were determined to be ideal for maintaining the integrity of the MOF (Figure 3.3).
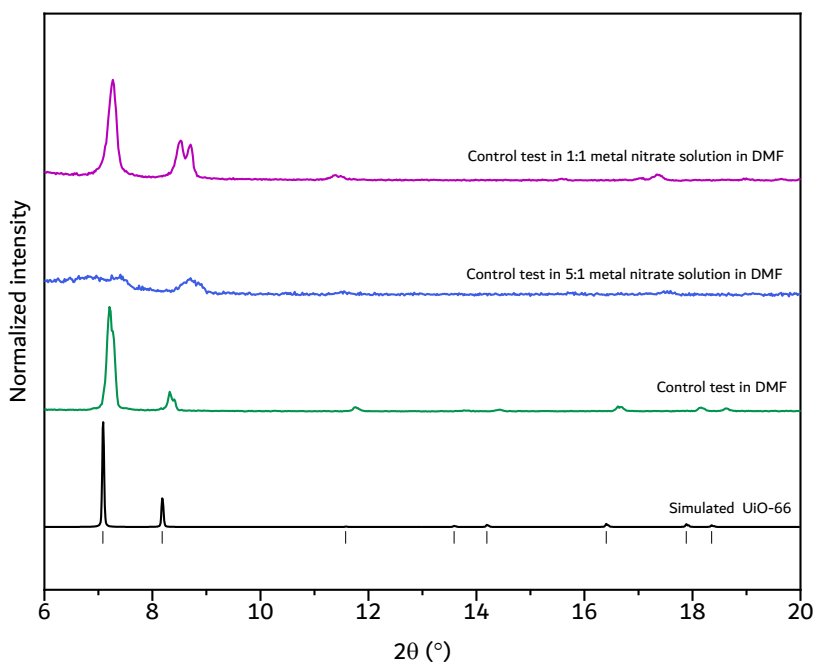
Figure 3.3 PXRD patterns showcasing control tests of Y-UiO-66 under microwave irradiation in DMF, 5:1 metal nitrate solution, and 1:1 metal nitrate solution

Table 3.1 Table sumarizing reported parameters and converted parameters

Conditions	Conventional-heating parameters	Microwave-assisted heating parameters
Amount of metal in *de novo* synthesized MOF (μmols)	24.8	21.55
Amount of target metal salt (μmols)	123.8	31.26
Ratio of metal in MOF to metal salt	1:5	1:2.2
Amount of DMF (mL)	5	5
Temperature (ºC)	140	200
Time for one round of transmetalation	3 days	1 hour 7 minutes

Following the control experiments with Y-UiO-66 and optimization of transmetalation conditions with $Yb(NO_3)_3.6.H_2O$, seven transmetalated mixed metal RE-UiO-66 analogues were synthesized, and their structure and crystallinity was analyzed through PXRD, as seen in Figures 3.4 and 3.5.
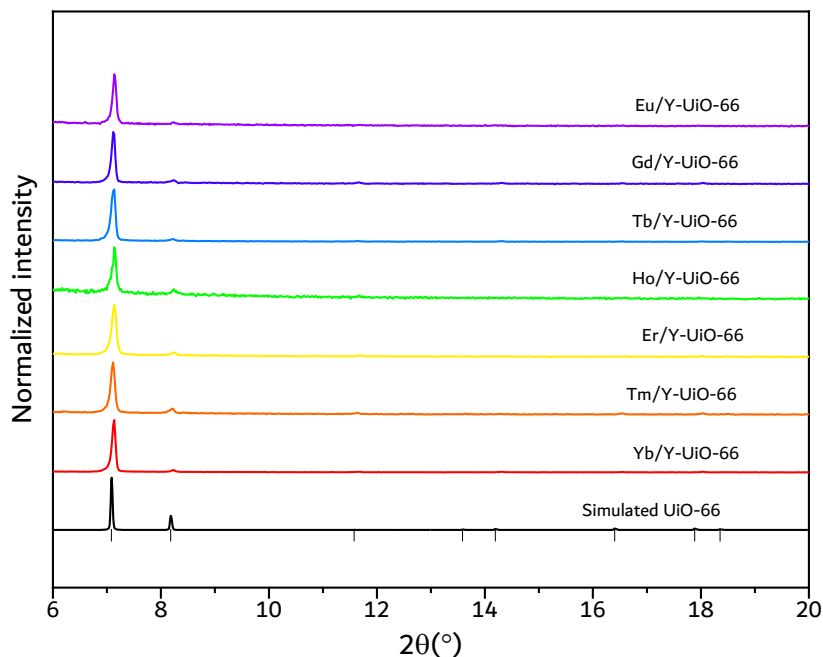
Figure 3.4 PXRD patterns of Y-UiO-66 after one round of transmetalation

The structure and bulk crystallinity of RE-UiO-66 is retained after one round of transmetalation (Figure 3.3), which is determined by comparison of the experimental diffraction patterns with the simulated pattern of Y-UiO-66. The retention of crystallinity after transmetalation can be attributed to the similarity in accessible coordination number going from yttrium to the heavier lanthanoids, with a coordination number of 8 being preferred for Y(III) in the parent Y-UiO-66 and the heavier rare-earth ions.[152] PXRD also indicates that Y-UiO-66 is stable under the microwave-irradiation conditions used for transmetalation with the internal heating mechanism having no effect on the integrity of the *de novo* synthesized MOF.

With confirmation of the stability of Y-UiO-66 to microwave-assisted transmetalation, a second round of transmetalation was performed by isolating the solid through centrifugation and immersing the MOF in a fresh solution of rare-earth metal nitrate precursor. The PXRD patterns for the mixed metal RE-UiO-66 analogues obtained after two rounds of transmetalation are shown in Figure 3.5. PXRD were plotted with the square root of the intensities can also be seen (Figure A.18 and A.19).
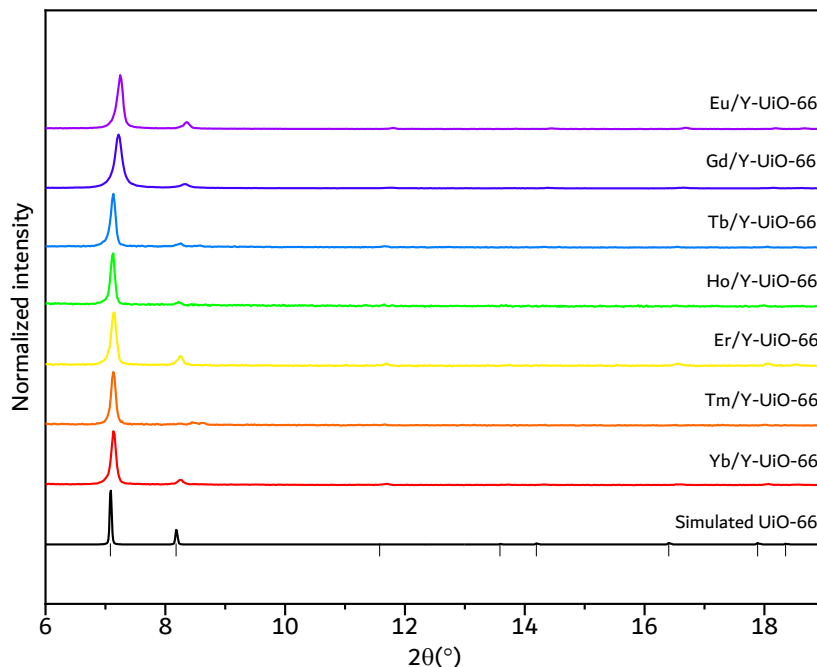
Figure 3.5 PXRD patterns of mixed metal RE-UiO-66
analogues after two rounds of transmetalation

PXRD patterns collected for the mixed metal RE-UiO-66 analogues obtained after two rounds of transmetalation showcase continued retention of structure and crystallinity (Figure 3.4). Slight broadening is observed for the transmetalated europium and gadolinium samples suggesting a decrease in crystallite size. An additional reflection at 8.6º 2θ is observed for the transmetalated europium analogue. This reflection has been observed in other RE-MOFs when a change in carboxylate coordination mechanism results in chelation change, going from bridging two Eu(III) ions to chelating one Eu(III) ion in the hexanuclear cluster node.[152] The broadening and change in carboxylate coordination is likely due to the larger radius of the earlier lanthanoids (i.e., Eu(III), Gd(III)) that prefer a coordination of 9 rather than 8.[152]

Following analysis of crystallinity, the degree of transmetalation in the hexanuclear cluster node of Y-UiO-66 was analyzed through ICP-MS after one and two rounds of transmetalation. The summary of the ICP-MS results is presented in Figure 3.5.
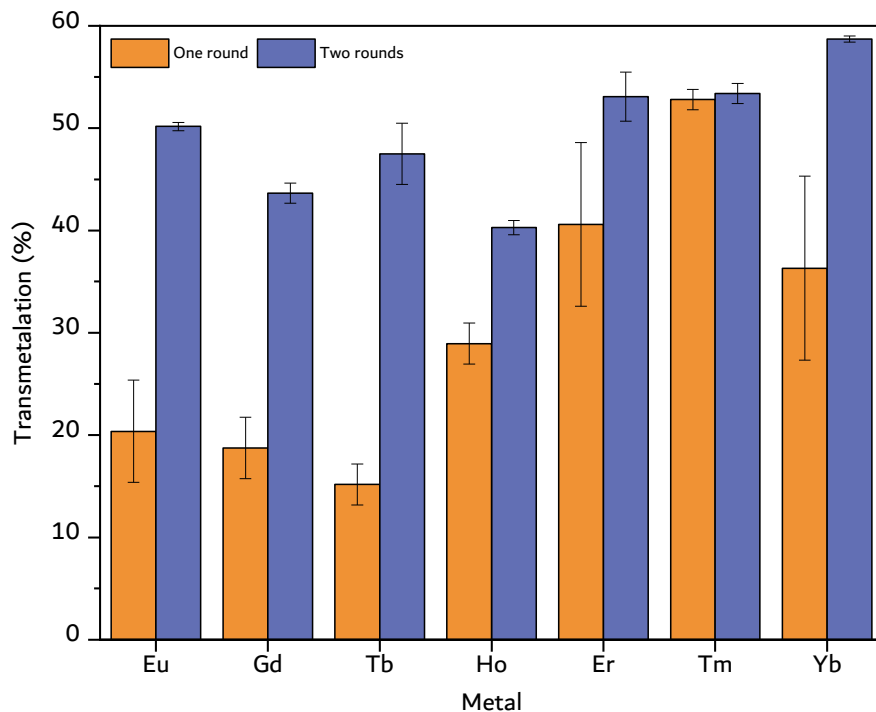
Figure 3.6 Bar chart summarizing of the average percent of transmetalation in the hexanuclear cluster node of Y-UiO-66 with other RE(III) ions. Data is an average of triplicates

In all cases, transmetalation of Y(III) in Y-UiO-66 is higher after two rounds. The corresponding ratio of target RE ion to yttrium within the hexanuclear cluster can be seen in Table 3.2. Table of results for each triplicate can also be seen (Table A.2 and A.3)

Table 3.2 Table summarizing the average percentage of transmetalation within the hexanuclear cluster of Y-UiO-66, and the resulting ratio of RE:Y rounded to the nearest whole number.

Metal	Average percent transmetalation (%)	Target metal to yttrium in hexanuclear cluster
Eu one round	20	1:5
Eu two rounds	50	3:3
Gd one round	19	1:5
Gd two rounds	44	3:3
Tb one round	15	1:5
Tb two rounds	47	3:3
Ho one round	29	2:4

Ho two rounds	40	2:4
Er one round	41	2:4
Er two rounds	53	3:3
Tm one round	53	3:3
Tm two rounds	53	3:3
Yb one round	36	1:5
Yb two rounds	60	4:2

Overall, transmetalation of Y-UiO-66 with ytterbium appears to be the most successful, nearing 60% after two rounds, followed by thulium and erbium, which can be attributed to their smaller ionic radii and preferred coordination number of 8.[152] Transmetalated holmium samples appear to have the lowest success rate after two rounds of transmetalation, followed by gadolinium and terbium respectively. This may be attributed to the larger ionic radii of holmium, gadolinium and terbium and preferred coordination number of 9.[153] With the degree of transmetalation in Y-UiO-66 plateauing at ~50-60%, it is unclear if transmetalation beyond 60% can be achieved in Y-UiO-66. Further evidence for this plateau is observed with the thulium samples, which have an initially high transmetalation of 52.8% after one round, which only increases by 1.41% to 53.39% after two rounds of transmetalation. Partial metal-exchange may occur as a result of various factors.[154] The first reported example of partial metal exchange in a MOF was observed when a 1:1 molar ratio of MOF to target metal was used.[155] The lower ratio of metal in MOF to target metal may lead to an equilibrium between the outgoing and incoming metals, preventing full exchange.

N_2 adsorption-desorption isotherms were obtained to confirm the porosity and BET area of the mixed metal RE-UiO-66 analogues after two rounds of transmetalation, and the results are shown in Figures 3.7.
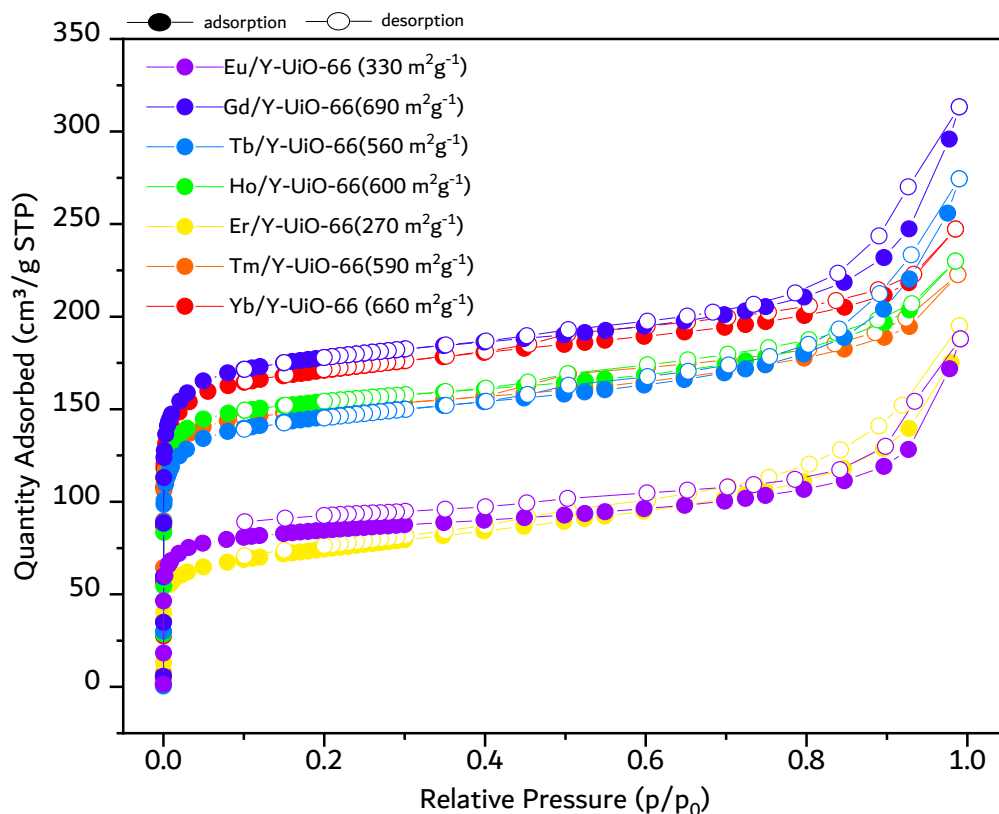
Figure 3.7 N$_2$ adsorption-desorption isotherms of transmetalated samples of Y-UiO-66

The expected BET area of RE-UiO-66 analogues ranges from 900-1200 m^2 g^{-1} depending on the identity of the RE(III) used, with the BET area of the *de novo* Y-UiO-66 samples used herein ranging from 900-950 m^2 g^{-1}. The average BET area for the transmetalated RE-UiO-66 analogues is 500-700 m^2 g^{-1} demonstrating that the BET area decreases after transmetalation. This decrease in BET area is expected since it is a gravimetric measurement that takes into account surface area per mass rather than per volume, and therefore would decrease with heavier metals. In two cases (Eu(III), Er(III)) the BET area drops more significantly, which may be due to poor activation or partial amorphization of the samples. In all cases the samples remain porous after transmetalation, and all present with the expected Type 1a isotherm.

Analysis of IR-active functional groups in the transmetalated RE-UiO-66 analogues was carried out via DRIFTS and the data is presented in Figures 3.8.
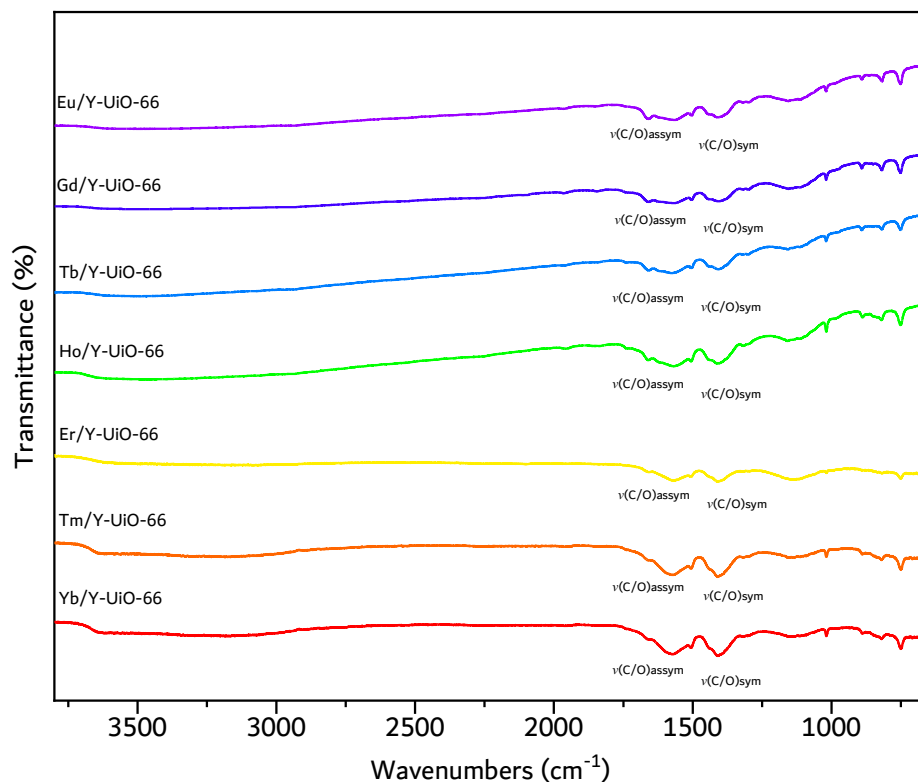
Figure 3.8 DRIFTS spectra of transmetalated RE-UiO-66 samples

The spectra showcase the expected -C=O stretch at around 1600-1400 cm^{-1}. The expected -CH and bridging -OH stretches that typically appear at around 3600 cm^{-1} and 2700-2550 cm^{-1} are difficult to see as not enough sample was used when collecting the data. As such, the DRIFTS analysis remains inconclusive due to the poor resolution of the data.

The organic component of the MOF samples was analyzed by ^{1}H NMR spectroscopy. ^{1}H NMR spectroscopy data was collected for all samples after digestion in deuterated sulphuric acid and dissolution in DMSO-d$_6$. The ^{1}H NMR spectra of the samples can be seen in Figures 3.9.

58
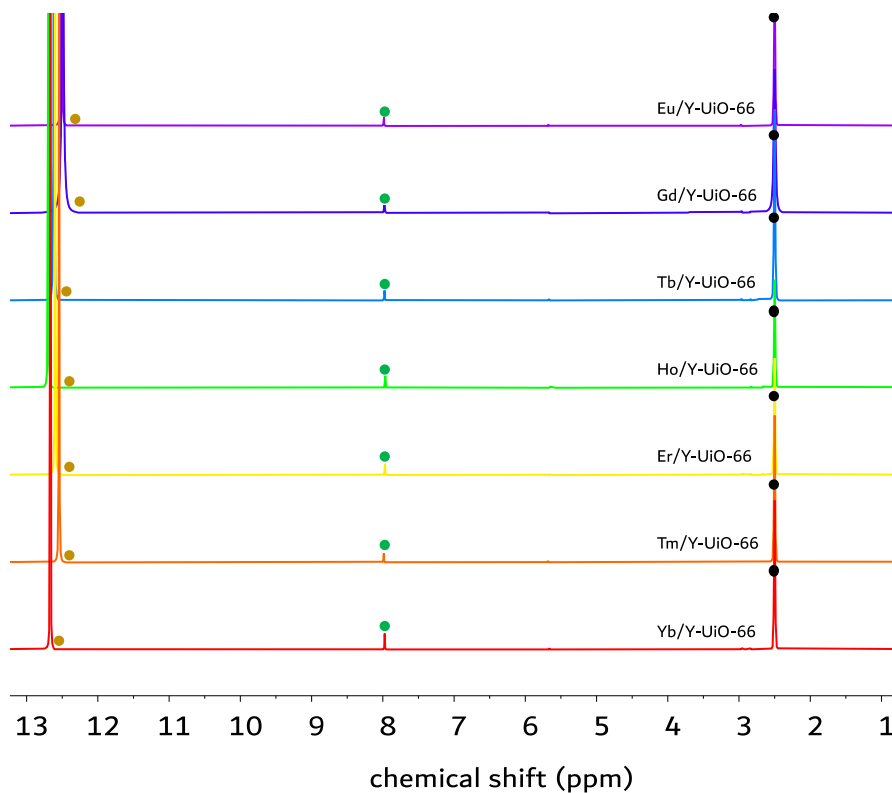
Figure 3.9 ^{1}H NMR spectra of transmetalated samples of Y-UiO-66 after activation

As the samples were prepared by digestion in deuterated sulphuric acid followed by addition of DMSO-d$_6$, peaks for the protons on the carboxylic acid groups of the linker are not observed. The remaining expected peaks include the identical protons on the benzene ring of the linker. All the samples have the expected peak at 8.02 ppm, indicating no degradation of the organic linker during the transmetalation process. In addition, no DMF or acetone is observed in the ^{1}H NMR spectra of the transmetalated samples, suggesting that removal of these solvents occurred during solvent exchange and activation.

3.2. Conclusions

The use of microwave-assisted irradiation for transmetalation was shown to be a successful method to obtain mixed-metal analogues of RE-UiO-66. By translating conventional heating methods to microwave-assisted heating methods, a faster and more energy-efficient alternative for transmetalation is realized. As with transmetalation procedures carried out under conventional heating, the success of post-synthetic exchange at the metal node depends heavily on the nature of

the *de novo* synthesized MOFs and the incoming metal ions including their preferred coordination number, geometry, and oxidation state. Microwave-assisted transmetalation also relies heavily on the conditions of the transmetalation itself, including the choice and amount of solvent and the concentration of the incoming metal ions. When excluding these factors in order to compare the use of conventional methods and microwave-irradiation for transmetalation, not only are the two comparable, the transmetalation procedures carried out with microwave-irradiation are drastically shorter and more energy efficient, reducing the time required from weeks to a less than a day.

Chapter Four

Conclusions and Future work

4.1. Conclusions

The field of MOF chemistry is relatively young, and research ensues to access new structures for various applications. It is crucial to evaluate the sustainability of the synthetic and post-synthetic processes used to obtain MOFs, which was the main goal of this work.

The waste generated in MOF synthetic processes is evaluated in Chapter 2, which details a simple and accessible way to recycle the commonly used solvents, DMF and acetone, in MOF synthesis. In academic labs it is common to discard the solvent used in the washing and purification stage of MOFs, but in this work it is shown that the solvent can be reused. Furthermore, in cases where trace impurities might affect MOF formation, distillation through rotary evaporation using a ramped procedure is shown to be effective to remove impurities of different volatilities. The collected and distilled solvents can be used to synthesize four structurally diverse MOFs; Zr based UiO-66 made from the ditopic terephthalic acid linker with **fcu** topology, Zr based MOF-808 made from the tritopic trimesic acid linker with **spn** topology, Cu based HKUST-1 made from the tritopic trimesic acid linker with the **tbo** topology, and the Zn based ZIF-8 made from the 2-methyl imidazole linker with **sod** topology. We demonstrate the viability of synthesizing MOFs using these collected and distilled solvents compared to commercial solvents with high levels of congruency between bulk crystallinity, porosity, morphology, and nature of the functional groups within the MOF.

The synthetic procedures used for post-synthetic modification to access structures difficult to obtain *de novo* also require evaluation. Post-synthetic modification at the metal node often requires the use of conventional heating for long periods. Chapter 3 details the use of microwave-irradiation to transmetalate MOFs at rates much faster than those observed using conventional heating, serving as an energy efficient alternative. Y-UiO-66, isoreticular to Zr-UiO-66 with the **fcu** topology, was synthesized *de novo* using a reported literature procedure and transmetalated with microwave assisted heating to obtain seven mixed metal rare-earth analogues containing Y(III) as well as Eu(III), Gd(III), Tb(III), Ho(III), Er(III), Tm(III), or Yb(III). One and two rounds of transmetalation were performed to determine how the degree of transmetalation varies after one round (1.5 hours) in the microwave compared to two rounds (3 hours total). Overall, the retention

of crystallinity and porosity demonstrated through PXRD analysis and N_2 adsorption studies demonstrates that the MOF structure remains intact throughout the microwave-assisted transmetalation process. The degree of transmetalation in Y-UiO-66 is observed through ICP-MS analysis, showcasing the effectiveness of the procedure, especially with two rounds of transmetalation.

4.2. Future work

In order to further expand on the promising findings regarding the reuse of solvents, synthesis of an even greater range of MOFs can be explored, such as *p*- or *f*- block metal MOFs and MOFs made from tetratopic linkers, in order to confirm that the findings are able to be extrapolated to a broader range of MOFs. Focus could be placed on luminescent MOFs comprised of metals such as Tb, Gd and Eu, that endow the MOF with these properties, in order to analyze how and if the use of collected or distilled solvents affects the photoluminescence properties of these MOFs. Analysis could also be carried out to investigate the number of times collected solvent can be collected and reused or distilled to establish a truly circular process.

As for microwave-assisted transmetalation of Y-UiO-66, immediate expansions that can be undertaken include investigations into obtaining an even larger, if not the full, series of lanthanoid analogues, with particular focus on isostructures that are difficult to obtain and not yet reported, such as Pr, and Sm analogues. Exploration of three or even four rounds of transmetalation could be carried out to gain an understanding of how MOF crystallinity is impacted and how effective more rounds of transmetalation can be. Long-term expansions could include transmetalation of a diverse range of MOFs using microwave irradiation to confirm the ability of various frameworks and the success of transmetalation in diverse structures.

References

(1)   Yaghi, O. M. Reticular Chemistry—Construction, Properties, and Precision Reactions of Frameworks. *J. Am. Chem. Soc.* **2016**, *138* (48), 15507–15509.

(2)   Day, G. S.; Drake, H. F.; Zhou, H.-C.; Ryder, M. R. *Commun Chem* **2021**, *4* (1), 114.

(3)   Tomic, E. A. *J. Appl. Polym. Sci.* **1965**, *9* (11), 3745–3752.

(4)   Yaghi, O. M.; Li, G.; Li, H. *Nature.* **1995**, *378* (6558), 703–706.

(5)   Kondo, M.; Yoshitomi, T.; Matsuzaka, H.; Kitagawa, S.; Seki, K. *Angew. Chem. Int. Ed.***1997**, *36* (16), 1725–1727.

(6)   Yaghi, O. M.; Li, H. *J. Am. Chem. Soc.* **1995**, *117* (41), 10401–10402.

(7)   Li, H.; Eddaoudi, M.; O'Keeffe, M.; Yaghi, O. M. *Nature.* **1999**, *402* (6759), 276–279.

(8)   Batten, S. R.; Champness, N. R.; Chen, X.-M.; Garcia-Martinez, J.; Kitagawa, S.; Öhrström, L.; O'Keeffe, M.; Paik Suh, M.; Reedijk, J. *Pure Appl Chem.* **2013**, *85* (8), 1715–1724.

(9)   Batten, S. R.; Champness, N. R.; Chen, X.-M.; Garcia-Martinez, J.; Kitagawa, S.; Öhrström, L.; O'Keeffe, M.; Suh, M. P.; Reedijk, J. *CrystEngComm* **2012**, *14* (9), 3001–3004.

(10) Öhrström, L. *Crystals.* **2015**, *5* (1), 154–162.

(11) Bennett, T. D.; Cheetham, A. K. *Acc. Chem. Res.* **2014**, *47* (5), 1555–1562.

(12) Fonseca, J.; Gong, T.; Jiao, L.; Jiang, H.-L. *J. Mater. Chem. A* **2021**, *9* (17), 10562–10611.

(13) Saraci, F.; Quezada-Novoa, V.; Rafael Donnarumma, P.; J. Howarth, A. *Chem Soc Rev.* **2020**, *49* (22), 7949–7977.

(14) Rosi, N. L.; Kim, J.; Eddaoudi, M.; Chen, B.; O'Keeffe, M.; Yaghi, O. M. *J. Am. Chem. Soc.* **2005**, *127* (5), 1504–1518.

(15) Joseph, N.; Lawson, H. D.; Overholt, K. J.; Damodaran, K.; Gottardi, R.; Acharya, A. P.; Little, S. R. *Sci Rep.* **2019**, *9* (1), 13024.

(16) Robison, L.; Zhang, L.; Drout, R. J.; Li, P.; Haney, C. R.; Brikha, A.; Noh, H.; Mehdi, B. L.; Browning, N. D.; Dravid, V. P.; Cui, Q.; Islamoglu, T.; Farha, O. K. *ACS Appl. Bio Mater.* **2019**, *2* (3), 1197–1203.

(17) Férey, G.; Latroche, M.; Serre, C.; Millange, F.; Loiseau, T.; Percheron-Guégan, A. *Chem. Commun.* **2003**, 24, 2976–2977.

(18) Feng, D.; Gu, Z.-Y.; Li, J.-R.; Jiang, H.-L.; Wei, Z.; Zhou, H.-C. *Angew. Chem., Int. Ed.* **2012**, *51* (41), 10307–10310.

(19) Feng, D., Wang, K., Wei, Z. et al. *Nat Commun*, **2014**, 5, 5723

(20) Xue, D.-X.; Cairns, A. J.; Belmabkhout, Y.; Wojtas, L.; Liu, Y.; Alkordi, M. H.; Eddaoudi, M. *J. Am. Chem. Soc.* **2013**, *135* (20), 7660–7667.

(21) Dolgopolova, E. A.; Rice, A. M.; Shustova, N. B. *Chem. Commun.* **2018**, *54* (50), 6472–6483.

(22) Burrows, A. D.; Chan, S.; Gee, W. J.; Mahon, M. F.; Richardson, C.; Sebestyen, V. M.; Turski, D.; Warren, M. R. *CrystEngComm.* **2017**, *19* (37), 5549–5557.

(23) Alkaş, A.; Cornelio, J.; Telfer, S. G. *Chem. Asian J.* **2019**, *14* (8), 1167–1174.

(24) Frahm, D.; Hoffmann, F.; Fröba, M. *Cryst. Growth Des.* **2014**, *14* (4), 1719–1725.

(25)   Haihuan Yu, Mingyue Fan, Qun Liu, Zhongmin Su, Xiao Li, Qingqing Pan, and Xiaoli Hu, *Inorg. Chem.* **2020** *59* (3), 2005-2010

(26) Siemensmeyer, K.; Peeples, C. A.; Tholen, P.; Schmitt, F.-J.; Çoşut, B.; Hanna, G.; Yücesan, G. *Adv. Mater.* **2020**, *32* (24), 2000474.

(27) Guiyang Zhang, Guangfeng Wei, Zhipan Liu, Scott R. J. Oliver, and Honghan Fei *Chem. Mat.* **2016**, 28 (17), 6276-6281

(28) Lu, W.; Wei, Z.; Gu, Z.-Y.; Liu, T.-F.; Park, J.; Park, J.; Tian, J.; Zhang, M.; Zhang, Q.; Iii, T. G.; Bosch, M.; Zhou, H.-C. *Chem. Soc. Rev.* **2014**, *43* (16), 5561–5593.

(29) Öhrström, L. *Crystals.* **2015**, *5* (1), 154–162.

(30) Kim, D.; Liu, X.; Lah, M. S. *Inorg. Chem. Front.* **2015**, *2* (4), 336–360.

(31) O'Keeffe, M.; Peskov, M. A.; Ramsden, S. J.; Yaghi, O. M. *Acc. Chem. Res.* **2008**, *41* (12), 1782–1789.

(32) Schukraft, G. E. M.; Ayala, S.; Dick, B. L.; Cohen, S. M. *Chem. Commun.* **2017**, *53* (77), 10684–10687.

(33) Freund, R.; Canossa, S.; Cohen, S. M.; Yan, W.; Deng, H.; Guillerm, V.; Eddaoudi, M. et al. *Angew. Chem. Int. Ed*. **2021**, *60* (45), 23946–23974.

(34) Ockwig, N. W.; Delgado-Friedrichs, O.; O'Keeffe, M.; Yaghi, O. M. *Acc. Chem. Res.* **2005**, *38* (3), 176–182.

(35) Kalmutzki, M. J.; Hanikel, N.; Yaghi, O. M. *Sci. Adv.* **2018**, *4* (10)

(36) Deng, H.; Grunder, S.; Cordova, K. E.; Valente, C.; Furukawa, H.; Hmadeh, M.; Gándara, F.; Whalley, A. C.; Liu, Z.; Asahina, S.; Kazumori, H.; O'Keeffe, M.; Terasaki, O.; Stoddart, J. F.; Yaghi, O. M. *Science.* **2012**, *336* (6084), 1018–1023.

(37) Idrees, K. B.; Chen, Z.; Zhang, X.; Mian, M. R.; Drout, R. J.; Islamoglu, T.; Farha, O. K. *Chem. Mater.* **2020**, *32* (9), 3776–3782.

(38) Zheng, H.-Q.; Liu, C.-Y.; Zeng, X.-Y.; Chen, J.; Lü, J.; Lin, R.-G.; Cao, R.; Lin, Z.-J.; Su, J.-W. *Inorg. Chem.* **2018**, *57* (15), 9096–9104.

(39) Caskey, S. R.; Wong-Foy, A. G.; Matzger, A. J. *J. Am. Chem. Soc.* **2008**, *130* (33), 10870–10871.

(40) Lin, R.-B.; Xiang, S.; Zhou, W.; Chen, B. *Chem* **2020**, *6* (2), 337–363.

(41) Yuan, S.; Zou, L.; Qin, J.-S.; Li, J.; Huang, L.; Feng, L.; Wang, X.; Bosch, M.; Alsalme, A.; Cagin, T.; Zhou, H.-C. *Nat Commun* **2017**, *8* (1), 15356.

(42) Kökçam-Demir, Ü.; Goldman, A.; Esrafili, L.; Gharib, M.; Morsali, A.; Weingart, O.; Janiak, C. *Chem. Soc. Rev.* **2020**, *49* (9), 2751–2798.

(43) Farha, O. K.; Eryazici, I.; Jeong, N. C.; Hauser, B. G.; Wilmer, C. E.; Sarjeant, A. A.; Snurr, R. Q.; Nguyen, S. T.; Yazaydın, A. Ö.; Hupp, J. T. *J. Am. Chem. Soc.* **2012**, *134* (36), 15016–15021.

(44) Hönicke, I. M.; Senkovska, I.; Bon, V.; Baburin, I. A.; Bönisch, N.; Raschke, S.; Evans, J. D.; Kaskel, S. *Angew. Chem., Int. Ed.* **2018**, *57* (42), 13780–13783.

(45) Li, P.; Vermeulen, N. A.; Malliakas, C. D.; Gómez-Gualdrón, D. A.; Howarth, A. J.; Mehdi, B. L.; Dohnalkova, A.; Browning, N. D.; O'Keeffe, M.; Farha, O. K. *Science* **2017**, *356* (6338), 624–627.

(46) Devic, T.; Serre, C.. *Chem. Soc. Rev.* **2014**, *43* (16), 6097–6115.

(47) Zhi-Qiang Shi, Ning-Ning Ji, Ming-Hao Wang, and Gang Li. *Inorg. Chem.* **2020,** *59* (7), 4781-4789

(48) Yan, J.; Huang, Y.; Yan, Y.; Ding, L.; Liu, P. *ACS Appl. Mater. Interfaces* **2019**, *11* (43), 40781–40792.

(49) Ahamad, M. N.; Shahid, M.; Ahmad, M.; Sama, F. *ACS Omega* **2019**, *4* (4), 7738–7749.

(50) Gándara, F.; Furukawa, H.; Lee, S.; Yaghi, O, M.; *J. Am. Chem. Soc.* **2014**, *136* (14), 5271-5274

(51) Redfern, L. R.; Farha, O. K. *Chem. Sci.* **2019**, *10* (46), 10666–10679.

(52) Saraci, F.; Quezada-Novoa, V.; Donnarumma, P. R.; Howarth, A, J. *Chem. Soc. Rev.*, **2020**,49, 7949-7977

(53) Ajoyan, Z.; Mandl, G.; Donnarumma, R, P.; Quezada-Novoa, V et al. *ACS Materials Lett.* **2022** *4* (6), 1025-1031

(54) Zhang, Y.; Liu, S.; Zhao, Z.-S.; Wang, Z.; Zhang, R.; Liu, L.; Han, Z.-B. *Inorg. Chem. Front.* **2021**, *8* (3), 590–619.

(55) Cavka, J. H.; Jakobsen, S.; Olsbye, U.; Guillou, N.; Lamberti, C.; Bordiga, S.; Lillerud, K. P. *J. Am. Chem. Soc.* **2008**, *130* (42), 13850–13851.

(56) Katz, M. J.; Brown, Z. J.; Colón, Y. J.; Siu, P. W.; Scheidt, K. A.; Snurr, R. Q.; Hupp, J. T.; Farha, O. K. *Chem. Commun.* **2013**, *49* (82), 9449–9451.

(57) Valenzano, L.; Civalleri, B.; Chavan, S.; Bordiga, S.; Nilsen, M. H.; Jakobsen, S.; Lillerud, K. P.; Lamberti, C.. *Chem. Mater.* **2011**, *23* (7), 1700–1718.

(58) Ly, H. G. T.; Fu, G.; Kondinski, A.; Bueken, B.; Vos, D. D.; Parac-Vogt, T. N. *J. Am. Chem. Soc.* **2018**. 140, 20, 6325–6335.

(59) Hardian, R.; Dissegna, S.; Ullrich, A.; Llewellyn, P. L.; Coulet, M.-V.; Fischer, R. A. *Eur. J. Chem.* **2021**, *27* (22), 6804–6814.

(60) Chui, S. S.-Y.; Lo, S. M.-F.; Charmant, J. P. H.; Orpen, A. G.; Williams, I. D. *Science* **1999**, *283* (5405), 1148–1150.

(61) Lin, K.-S.; Adhikari, A. K.; Ku, C.-N.; Chiang, C.-L.; Kuo, H. *Int. J. Hydrog. Energy* **2012**, *37* (18), 13865–13871.

(62) Karagiaridi, O.; Lalonde, M. B.; Bury, W.; Sarjeant, A. A.; Farha, O. K.; Hupp, J. T. *J. Am. Chem. Soc.* **2012**, *134* (45), 18790–18796.

(63) Kida, K.; Okita, M.; Fujita, K.; Tanaka, S.; Miyake, Y. *CrystEngComm* **2013**, *15* (9), 1794–1801.

(64) Jakobsen, S.; Gianolio, D.; Wragg, D. S.; Nilsen, M. H.; Emerich, H.; Bordiga, S.; Lamberti, C.; Olsbye, U.; Tilset, M.; Lillerud, K. P. *Phys. Rev. B* **2012**, *86* (12), 125429.

(65) Lammert, M.; T. Wharmby, M.; Smolders, S.; Bueken, B.; Lieb, A.; A. Lomachenko, K.; De Vos, D.; Stock, N. *Chem. Commun.* **2015**, *51* (63), 12578–12581.

(66) Hastings, A. M.; Ray, D.; Jeong, W.; Gagliardi, L.; Farha, O. K.; Hixon, A. E. *J. Am. Chem. Soc.* **2020**, *142* (20), 9363–9371.

(67) Winarta, J.; Shan, B.; Mcintyre, S. M.; Ye, L.; Wang, C.; Liu, J.; Mu, B. *Cryst. Growth Des.* **2020**, 20, 2, 1347–1362

(68) Donnarumma, P. R.; Frojmovic, S.; Marino, P.; Bicalho, H. A.; Titi, H. M.; Howarth, A. J. *Chem. Commun.* **2021**, *57* (50), 6121–6124.

(69) Kim, M.; Cahill, J. F.; Su, Y.; Prather, K. A.; Cohen, S. M. *Chem. Sci.* **2011**, *3* (1), 126–130.

(70) Dincă, M.; Long, J, R.; *J. Am. Chem. Soc.* **2007** 129 (36), 11172-11176

(71) Howarth, A. J.; Peters, A. W.; Vermeulen, N. A.; Wang, T. C.; Hupp, J. T.; Farha, O. K. *Chem. Mater.* **2017**, *29* (1), 26–39.

(72) Usman, K. A. S.; Maina, J. W.; Seyedin, S.; Conato, M. T.; Payawan, L. M.; Dumée, L. F.; Razal, J. M. *NPG Asia Mater* **2020**, *12* (1), 58.

(73) Forgan, R. S. *Chem. Sci.* **2020**, *11* (18), 4546–4562.

(74) Yuan, S.; Feng, L.; Wang, K.; Pang, J.; Bosch, M.; Lollar, C.; Sun, Y.; Qin, J.; Yang, X.; Zhang, P.; Wang, Q.; Zou, L.; Zhang, Y.; Zhang, L.; Fang, Y.; Li, J.; Zhou, H.-C. *Adv. Mater.* **2018**, *30* (37), 1704303.

(75) Mandal, S.; Natarajan, S.; Mani, P.; Pankajakshan, A. Post-Synthetic Modification of Metal–Organic Frameworks Toward Applications. *Adv. Funct. Mater.* **2021**, *31* (4), 2006291.

(76) Wang, Z.; Cohen, S. M. *Chem. Soc. Rev.* **2009**, *38* (5), 1315.

(77) Sun, Y.; Zhou, H.-C. *Sci. Technol. Adv. Mater.* **2015**, *16* (5), 054202.

(78) Stock, N.; Biswas, S. *Chem. Rev.* **2012**, 112, 2, 933–969

(79) Hu, Z.; Kundu, T.; Wang, Y.; Sun, Y.; Zeng, K.; Zhao, D. *ACS Sustainable Chem. Eng.* **2020**, *8* (46), 17042–17053.

(80) González, C. M. O.; Morales, E. M. C.; Tellez, A. de M. N.; Quezada, T. E. S.; Kharissova, O. V.; Méndez-Rojas, M. A. Chapter 18 - CO2 Capture by MOFs. In *Handbook of Greener Synthesis of Nanomaterials and Compounds*; Kharisov, B., Kharissova, O., Eds.; Elsevier, 2021; pp 407–448.

(81) Wang, H.; Xu, J.-Z.; Zhu, J.-J.; Chen, H.-Y. *J. Crys. Growth.* **2002**, *244* (1), 88–94.

(82) Langa, F.; de la Cruz, P.; de la Hoz, A.; Díaz-Ortiz, A.; Díez-Barra, E. *Contemp. Org. Synth.* **1997**, *4* (5), 373–386.

(83) Klinowski, J.; Paz, F. A. A.; Silva, P.; Rocha, J. *Dalton Trans.* **2010**, *40* (2), 321–330.

(84) Martina, K.; Cravotto, G.; Varma, R. S. *J. Org. Chem.* **2021**, *86* (20), 13857–13872.

(85) Nguyen, L. H. T.; Nguyen, H. T. T.; Le, B. Q. G.; Dang, M.-H. D.; Nguyen, T. T. T.; Mai, N. X. D.; Doan, T. L. H. *Colloids Interface Sci. Commun.* **2022**, *46*, 100511.

(86) Solvent Choice for Microwave Synthesis. https://cem.com/cn/microwave-chemistry/solvent-choice (accessed Jan 5, 2023).

(87) K. Tanabe, K.; M. Cohen, S. *Chem Soc Rev.* **2011**, *40* (2), 498–519.

(88) Islamoglu, T.; Goswami, S.; Li, Z.; Howarth, A. J.; Farha, O. K.; Hupp, J. T. *Acc. Chem. Res.* **2017**, *50* (4), 805–813.

(89) Liu, T.-F.; Vermeulen, N. A.; Howarth, A. J.; Li, P.; Sarjeant, A. A.; Hupp, J. T.; Farha, O. K. *Eur. J. Inorg. Chem.* **2016**, *2016* (27), 4349–4352.

(90) Bicalho, H. A.; Donnarumma, P. R.; Quezada-Novoa, V.; Titi, H. M.; Howarth, A. J. *Inorg. Chem.* **2021**, *60* (16), 11795–11802.

(91) Mondloch, J. E.; Karagiaridi, O.; Farha, O. K.; Hupp, J. T. *CrystEngComm* **2013**, *15* (45), 9258–9264.

(92) Wilmer, C. E.; Leaf, M.; Lee, C. Y.; Farha, O. K.; Hauser, B. G.; Hupp, J. T.; Snurr, R. Q. *Nature Chem* **2012**, *4* (2), 83–89.

(93) Ma, J.; Kalenak, A. P.; Wong-Foy, A. G.; Matzger, A. J. *Angew. Chem.* **2017**, *129* (46), 14810–14813.

(94) Mondloch, J. E.; Katz, M. J.; Planas, N.; Semrouni, D.; Gagliardi, L.; Hupp, J. T.; Farha, O. K. *Chem. Commun.* **2014**, *50* (64), 8944–8946.

(95) Sobus, J. R.; Wambaugh, J. F.; Isaacs, K. K.; Williams, A. J.; McEachran, A. D.; Richard, A. M.; Grulke, C. M.; Ulrich, E. M.; Rager, J. E.; Strynar, M. J.; Newton, S. R. *J Expo Sci Environ Epidemiol* **2018**, *28* (5), 411–426.

(96) de Marco, B. A.; Rechelo, B. S.; Tótoli, E. G.; Kogawa, A. C.; Salgado, H. R. N. *Saudi Pharm. J.* **2019**, *27* (1), 1–8.

(97) *Sustainable Chemistry*. IUPAC | International Union of Pure and Applied Chemistry. https://iupac.org/who-we-are/committees/sustainable-chemistry/ (accessed 2022-07-26).

(98) Tundo, P.; Anastas, P.; Black, D. S.; Breen, J.; Collins, T. J.; Memoli, S.; Miyamoto, J.; Polyakoff, M.; Tumas, W. *Pure Appl. Chem.* **2000**, *72* (7), 1207–1228.

(99) *12 Principles of Green Chemistry*. American Chemical Society. https://www.acs.org/content/acs/en/greenchemistry/principles/12-principles-of-green-chemistry.html (accessed 2022-07-24).

(100) Request for Assistance in Preventing Adverse Health Effects from Exposure to Dimethylformamide (DMF). **2020**.

(101) *European Commission adopts REACH DMF restriction*. https://chemicalwatch.com/377082/european-commission-adopts-reach-dmf-restriction (accessed 2022-07-29).

(102) Marino, P.; Donnarumma, P. R.; Bicalho, H. A.; Quezada-Novoa, V.; Titi, H. M.; Howarth, A. J. *ACS Sustainable Chem. Eng.* **2021**, *9* (48), 16356–16362.

(103) Pichon, A.; Lazuen-Garay, A.; James, S. L. Solvent-Free Synthesis of a Microporous Metal–Organic Framework. *CrystEngComm* **2006**, *8* (3), 211.

(104) Beamish-Cook, J.; Shankland, K.; Murray, A, C.; Vaqueiro, P.; *Cryst. Growth Des.* **2021** *21* (5), 3047-3055

(105) Dietzel, P. D.; Morita, Y.; Blom, R.; Fjellvåg, H. *Angew Chem.* **2005**, *117* (39), 6512–6516.

(106) Dietzel, P. D. C.; Panella, B.; Hirscher, M.; Blom, R.; Fjellvåg, H. *Chem. Commun.* **2006**, 9, 959–961.

(107) Zhou, W.; Wu, H.; Yildirim, T.; *J. Am. Chem. Soc.* **2008** *130* (46), 15268-15269

(108) Tranchemontagne, D. J.; Hunt, J. R.; Yaghi, O. M. *Tetrahedron* **2008**, *64* (36), 8553–8557.

(109) Sánchez-Sánchez, M.; Getachew, N.; Díaz, K.; Díaz-García, M.; Chebude, Y.; Díaz, I. *Green Chem.* **2015**, *17* (3), 1500–1509.

(110) DeStefano, M. R.; Islamoglu, T.; Garibay, S. J.; Hupp, J. T.; Farha, O. K. *Chem. Mater.* **2017**, *29* (3), 1357–1361.

(111) Albuquerque, G. H.; Herman, G. S. *Cryst. Growth Des.* **2017**, *17* (1), 156–162.

(112) Wu, X.; Bao, Z.; Yuan, B.; Wang, J.; Sun, Y.; Luo, H.; Deng, S. *Micropor Mesopor Mat.* **2013**, *180*, 114–122.

(113) Taddei, M.; Steitz, D. A.; van Bokhoven, J. A.; Ranocchiari, M. *Eur. J. Chem.* **2016**, *22* (10), 3245–3249.

(114) *The Cambridge Structural Database (CSD) - The Cambridge Crystallographic Data Centre (CCDC)*. https://www.ccdc.cam.ac.uk/solutions/csd-core/components/csd/ (accessed 2022-10-25).

(115) *X-ray Powder Diffraction (XRD)*. Techniques. https://serc.carleton.edu/research_education/geochemsheets/techniques/XRD.html (accessed 2022-10-25).

(116) Evans, J. S. O.; Evans, I. R. *J. Chem. Educ.* **2021**, *98* (2), 495–505.

(117) Martí-Rujas, J. *Dalton Trans.* **2020**, *49* (40), 13897–13916.

(118) *Sample Preparation – EAS X-Ray Diffraction Laboratory – University of Alberta*. https://cms.eas.ualberta.ca/xrd/sample-preparation/ (accessed 2022-10-26).

(119) Holder, C. F.; Schaak, R. E. *ACS Nano* **2019**, *13* (7), 7359–7365.

(120) Thommes, M. *Chemie Ingenieur Technik* **2010**, *82* (7), 1059–1073.

(121) Thommes, M.; Kaneko, K.; Neimark, A. V.; Olivier, J. P.; Rodriguez-Reinoso, F.; Rouquerol, J.; Sing, K. S. W. *Pur Appl. Chem.* **2015**, *87* (9–10), 1051–1069.

(122) Brunauer, S.; Emmett, P. H.; Teller, E. *J. Am. Chem. Soc.* **1938**, *60* (2), 309–319.

(123) Langmuir, I. *J. Am. Chem. Soc.* **1918**, *40* (9), 1361–1403.

(124) Olivier, J. P. *Carbon* **1998**, *36* (10), 1469–1472.

(125) Occelli, M. L.; Olivier, J. P.; Petre, A.; Auroux, A. *J. Phys. Chem. B* **2003**, *107* (17), 4128–4136.

(126) Lastoskie, C.; Gubbins, K. E.; Quirke, N. *J. Phys. Chem.* **1993**, *97* (18), 4786–4796.

(127) *Electron microscopes*. https://oumnh.ox.ac.uk/learn-electron-microscopes (accessed 2022-11-08).

(128) Vernon-Parry, K. D. III-Vs *Rev.* **2000**, *13* (4), 40–44.

(129) *"Charging" effects in the scanning electron microscope - IOPscience*. https://iopscience.iop.org/article/10.1088/0022-3735/4/9/002 (accessed 2022-08-13).

(130) *Reflectance Spectroscopy | SpringerLink*. https://link.springer.com/book/10.1007/978-3-642-88071-1 (accessed 2022-10-26).

(131) Hadjiivanov, K. I.; Panayotov, D. A.; Mihaylov, M. Y.; Ivanova, E. Z.; Chakarova, K. K.; Andonova, S. M.; Drenchev, N. L. *Chem. Rev.* **2021**, *121* (3), 1286–1424.

(132) *Review of inductively coupled plasmas: Nano-applications and bistable hysteresis physics: Applied Physics Reviews: Vol 5, No 1.*

(133) Beauchemin, D. *Anal. Chem.* **2006**, *78* (12), 4111–4136.

(134) Borrachero, M. V.; Payá, J.; Bonilla, M.; Monzó, J. *J Therm Anal Calorim* **2008**, *91* (2), 503–509.

(135) Lázaro, I. A. *Eur. J. Chem.* **2020**, *2020* (45), 4284–4294.

(136) Wharmby, M. T.; Henke, S.; Bennett, T. D.; Bajpe, S. R.; Schwedler, I.; Thompson, S. P.; Gozzo, F.; Simoncic, P.; Mellot-Draznieks, C.; Tao, H.; Yue, Y.; Cheetham, A. K. *Angew. Chem.* **2015**, *127* (22), 6547–6551.

(137) Wang, T. C.; Vermeulen, N. A.; Kim, I. S.; Martinson, A. B. F.; Stoddart, J. F.; Hupp, J. T.; Farha, O. K. *Nat Protoc* **2016**, *11* (1), 149–162.

(138) Emam, H. E.; Abdelhameed, R. M.; Ahmed, H. B. *J. Environ. Chem. Eng.* **2020**, *8* (5), 104386.

(139) Ahmadijokani, F.; Molavi, H.; Rezakazemi, M.; Tajahmadi, S.; Bahi, A.; Ko, F.; Aminabhavi, T. M.; Li, J.-R.; Arjmand, M. *Prog. Mater. Sci.* **2022**, *125*, 100904.

(140) H. Kim, S. Yang, S. R. Rao, S. Narayanan, E. A. Kapustin, H. Furukawa, A. S. Umans, O. M. Yaghi, E. N. Wang.; *Science,* **2017***, 356, 430–434.

(141) Ma, J.; Kalenak, A. P.; Wong-Foy, A. G.; Matzger, A. J. *Angew. Chem.* **2017**, *129* (46), 14810–14813.

(142) Ferrari, H. J.; Heider, J. G. *Microchem. J.* **1963**, *7* (2), 194–202.

(143) *Dimethylformamide (DMF)*. Eastman. https://www.eastman.com/en/products/product-detail?product=71103587&pn=dimethylformamide+(dmf) (accessed 2022-11-09).

(144) Primorac, T.; Požar, M.; Sokolić, F.; Zoranić, L.; Urbic, T. *J. Mol. Liq.* **2018**, *262*, 46–57.

(145) Zhuang, J.-L.; Ceglarek, D.; Pethuraj, S.; Terfort, A. *Adv. Funct. Mater.* **2011**, *21* (8), 1442–1447.

(146) Lee, Y.-R.; Jang, M.-S.; Cho, H.-Y.; Kwon, H.-J.; Kim, S.; Ahn, W.-S. *J. Chem. Eng.* **2015**, *271*, 276–280.

(147) Grancha, T.; Ferrando-Soria, J.; Zhou, H.-C.; Gascon, J.; Seoane, B.; Pasán, J.; Fabelo, O.; Julve, M.; Pardo, E. *Angew. Chem.* **2015**, *54* (22), 6521–6525.

(148) Mondloch, J. E.; Bury, W.; Fairen-Jimenez, D.; Kwon, S.; DeMarco, E. J.; Weston, M. H.; Sarjeant, A. A.; Nguyen, S. T.; Stair, P. C.; Snurr, R. Q.; Farha, O. K.; Hupp, J. T. *J. Am. Chem. Soc.* **2013**, *135* (28), 10294–10297.

(149) Yuan, S.; Chen, Y. P.; Qin, J.; Lu, W.; Wang, X.; Zhang, Q.; Bosch, M.; Liu, T. F.; Lian, X.; Zhou, H. C. *Angew. Chem.* **2015**, *127* (49), 14909–14913.

(150) Lalonde, M.; Bury, W.; Karagiaridi, O.; Brown, Z.; Hupp, J. T.; Farha, O. K. *J. Mater. Chem. A.* **2013**, *1* (18), 5453.

(151) Karagiaridi, O.; Bury, W.; Mondloch, J. E.; Hupp, J. T.; Farha, O. K. *Angew. Chem., Int. Ed.* **2014**, *53* (18), 4530–4540.

(152) Martinez-Gomez, N, C.; Vu, H.; Skovran, E.; *Inorg. Chem.* **2016** *55* (20), 10083-10089

(153) Henkelis, S. E.; Vogel, D. J.; Metz, P. C.; Valdez, N. R.; Rodriguez, M. A.; Rademacher, D. X.; Purdy, S.; Percival, S. J.; Rimsza, J. M.; Page, K.; Nenoff, T. M. *ACS Appl. Mater. Interfaces.* **2021**, *13* (47), 56337–56347.

(154) Rice, A. M.; Leith, G. A.; Ejegbavwo, O. A.; Dolgopolova, E. A.; Shustova, N. B. *ACS Energy Lett.* **2019**, *4* (8), 1938–1946.

(155) Li, J.; Li, L.; Hou, H.; Fan, Y. *Cryst. Growth Des.* **2009**, *9* (10), 4504–4513.

Appendix
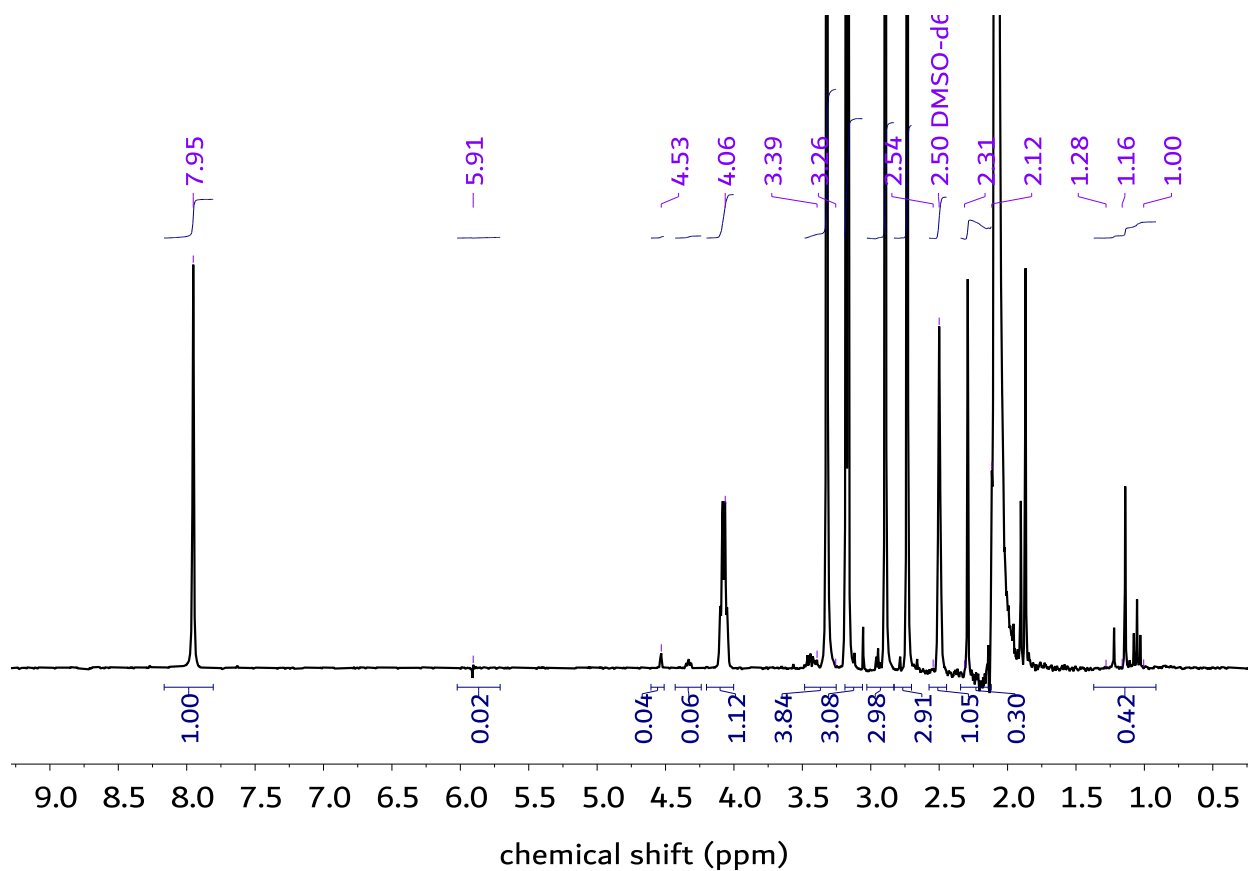
Figure A.1 ^{1}H NMR spectra of remnants from two rounds of distillation

Table A.1 ICP-MS data analyzing remnants from two rounds of distillation

Metal	Concentration (ppm)	Counts
Y	2.570×10^{-3}	44 210.22
Zr	2.869×10^{-2}	275 096.40
Ce	8.483×10^{-4}	24 272.60
Tb	1.416×10^{-3}	60 890.24
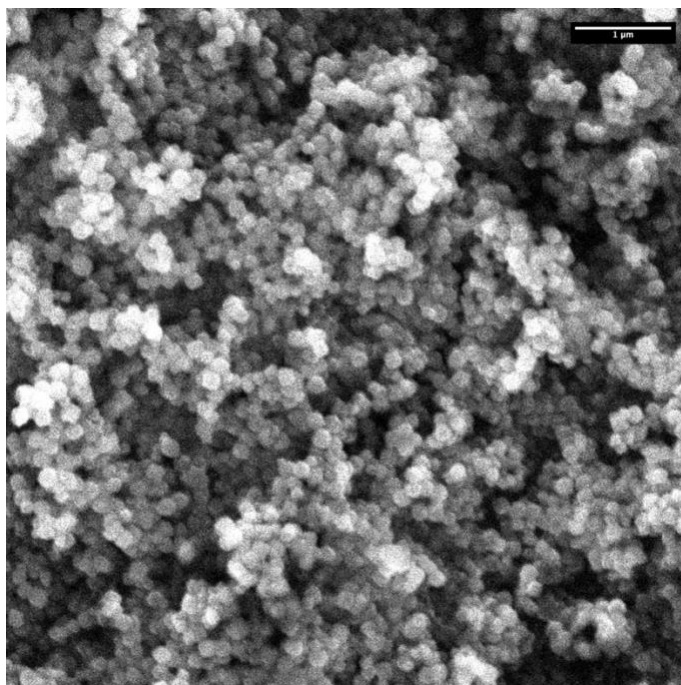
Figure A.2 SEM micrograph of UiO-66 (distilled DMF/ distilled acetone)
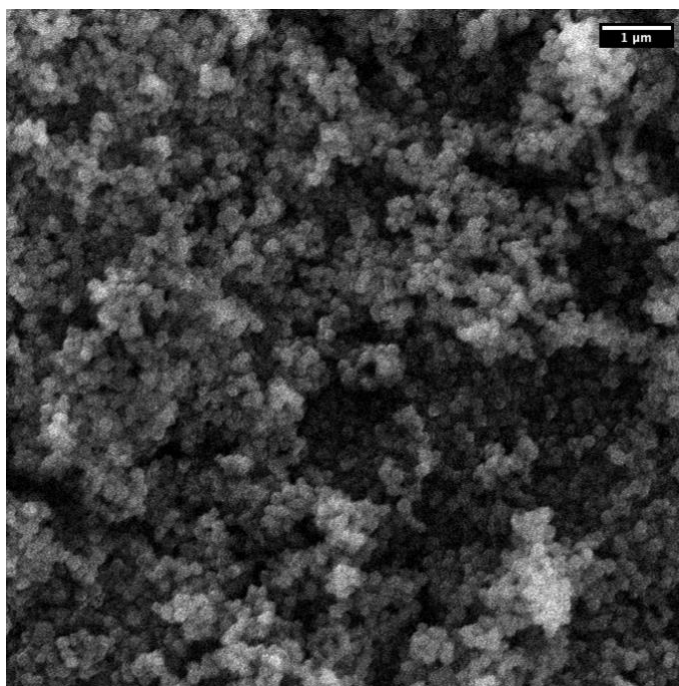
Figure A.3 SEM micrograph of UiO-66 (distilled DMF/ commercial acetone)
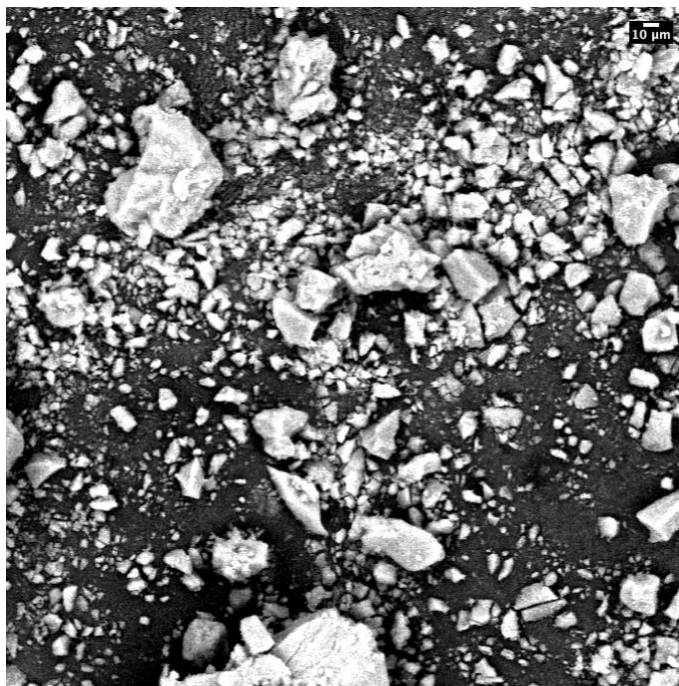
Figure A.4 SEM micrograph of UiO-66 (collected DMF/ commercial acetone)
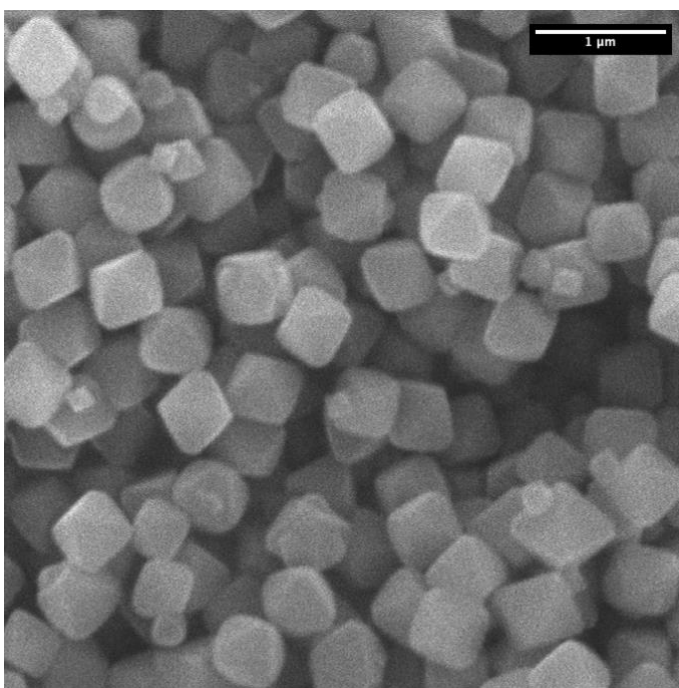
Figure A.5 SEM micrograph of UiO-66 (commercial DMF/ commercial acetone)
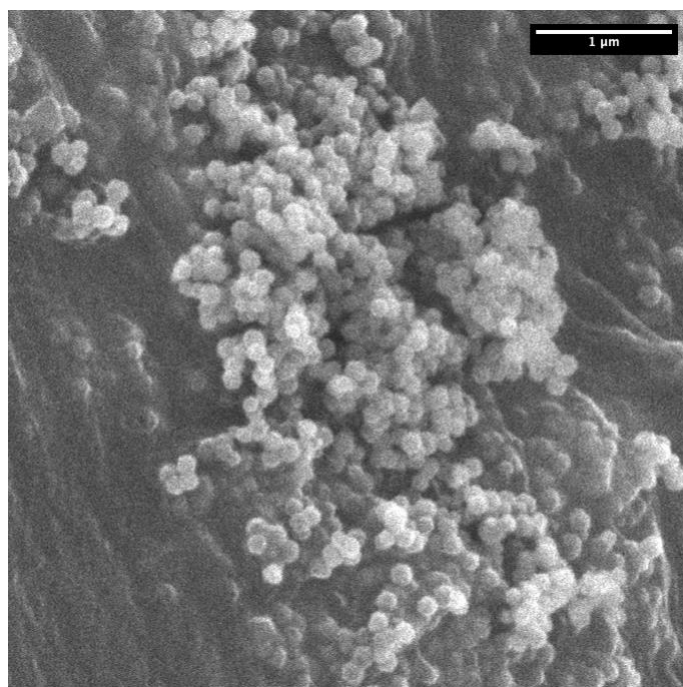
Figure A.7 SEM micrograph of MOF-808 (distilled DMF/ distilled acetone)
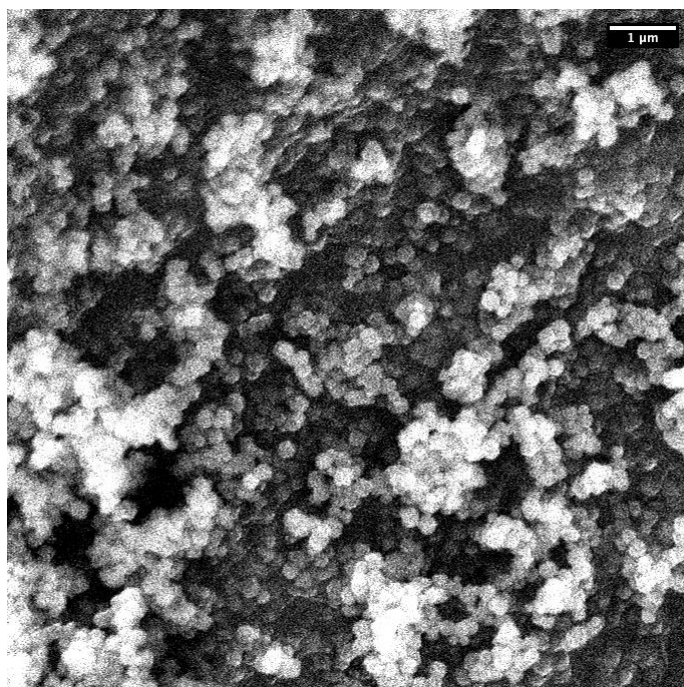
Figure A.6 SEM micrograph of MOF-808 (distilled DMF/ commercial acetone)
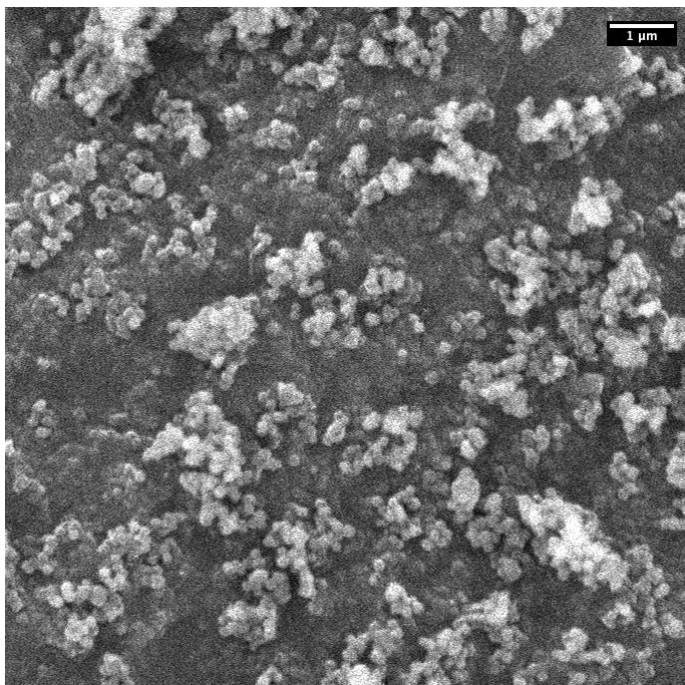
Figure A.8 SEM micrograph of MOF-808 (collected DMF/ commercial acetone)
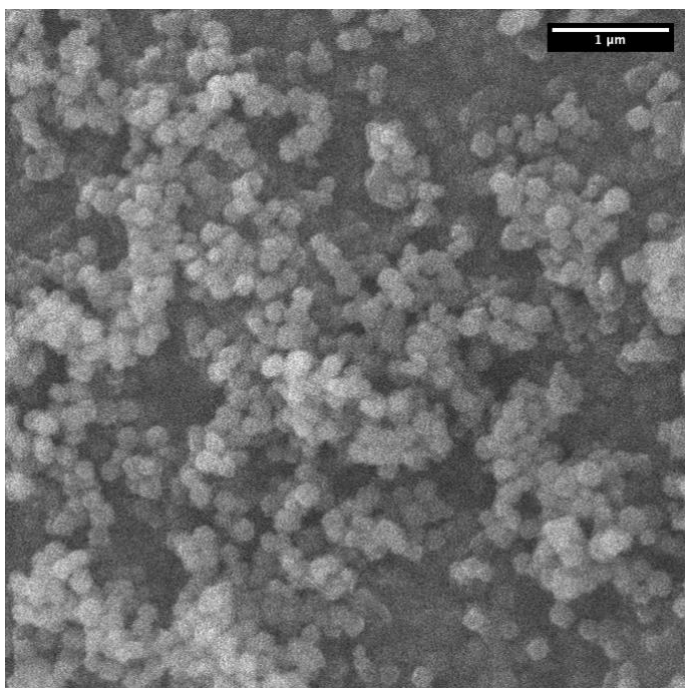
Figure A.9 SEM micrograph of MOF-808 (commercial DMF/ commercial acetone)
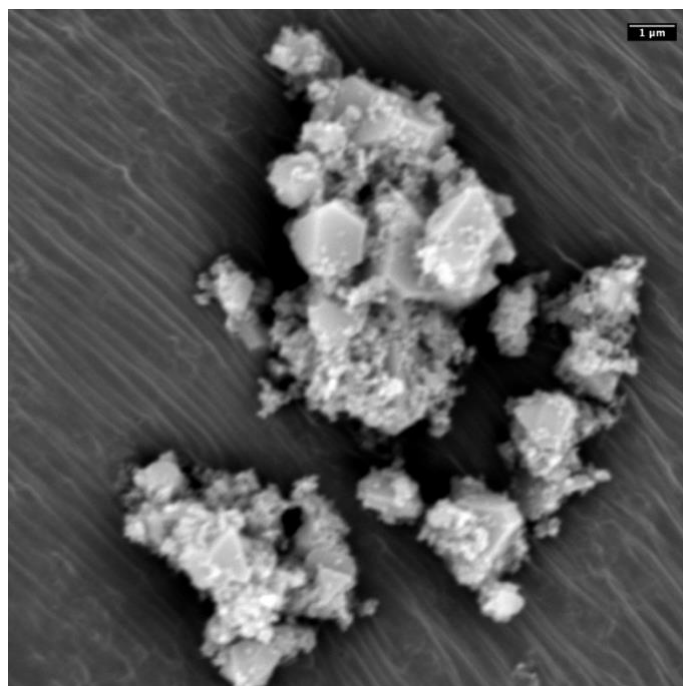
Figure A.10 SEM micrograph of HKUST-1 (distilled DMF/ distilled acetone)
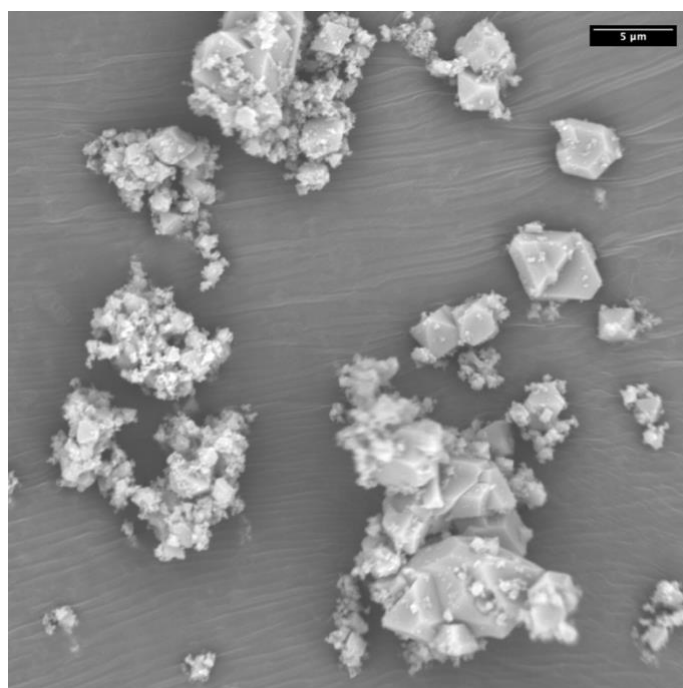
Figure A.11 SEM micrograph of HKUST-1 (distilled DMF/ commercial acetone)
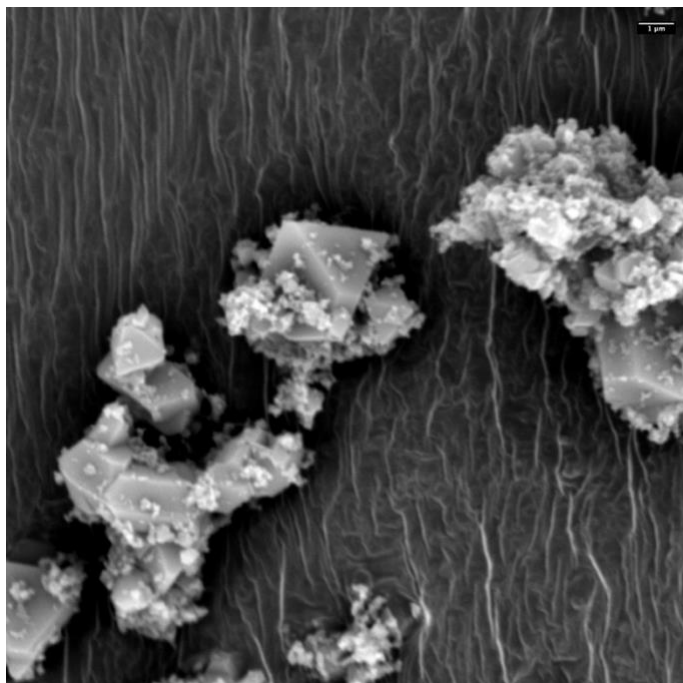
Figure A.12 SEM micrograph of HKUST-1 (collected DMF/ commercial acetone)
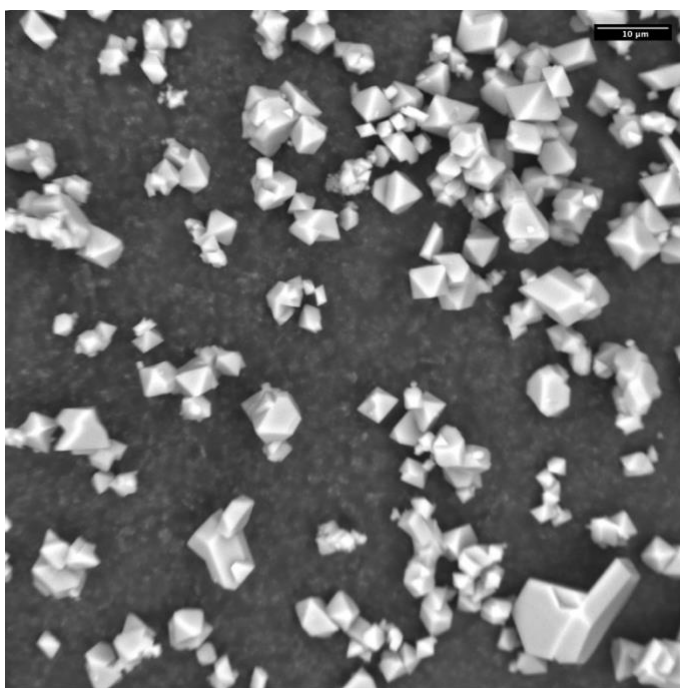
Figure A.13 SEM micrograph of HKUST-1 (commercial DMF/ commercial acetone)
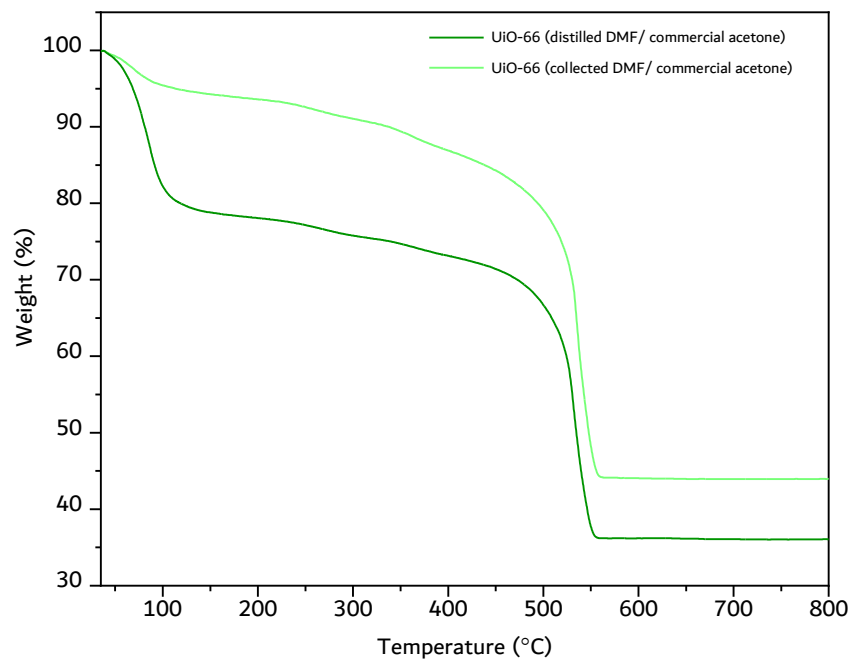
Figure A.14 TGA of UiO-66 samples
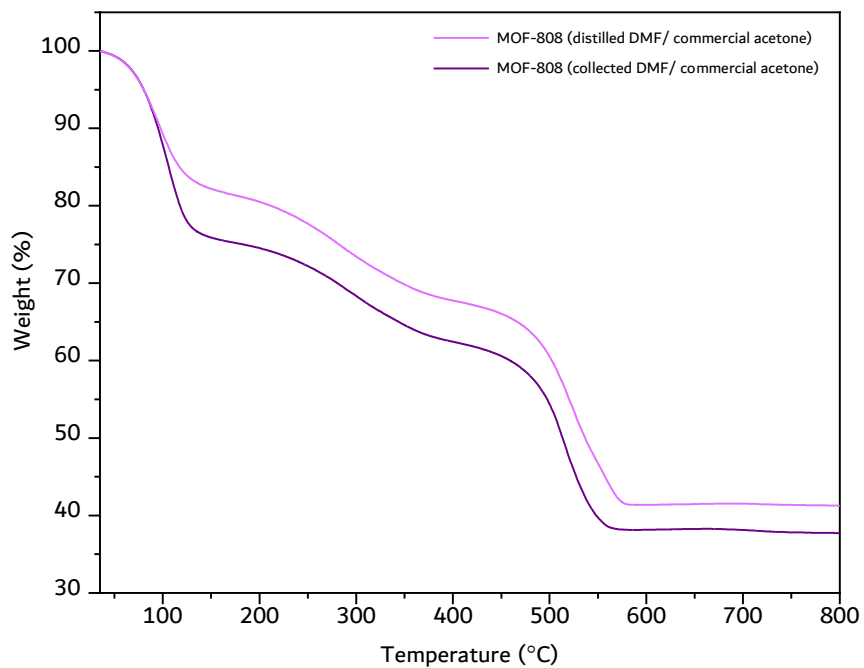
Figure A.15 TGA of MOF-808 samples
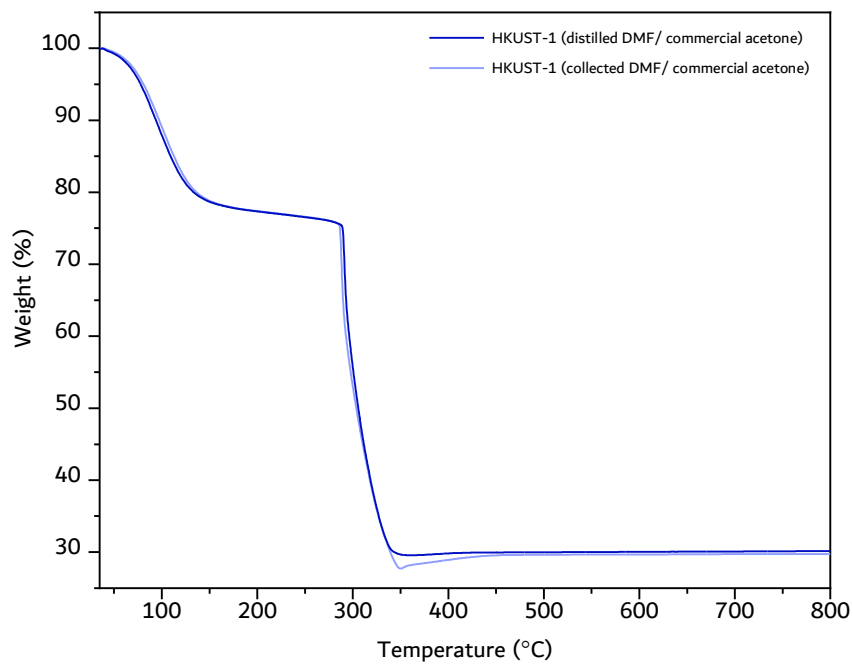
Figure A.16 TGA of HKUST-1 samples
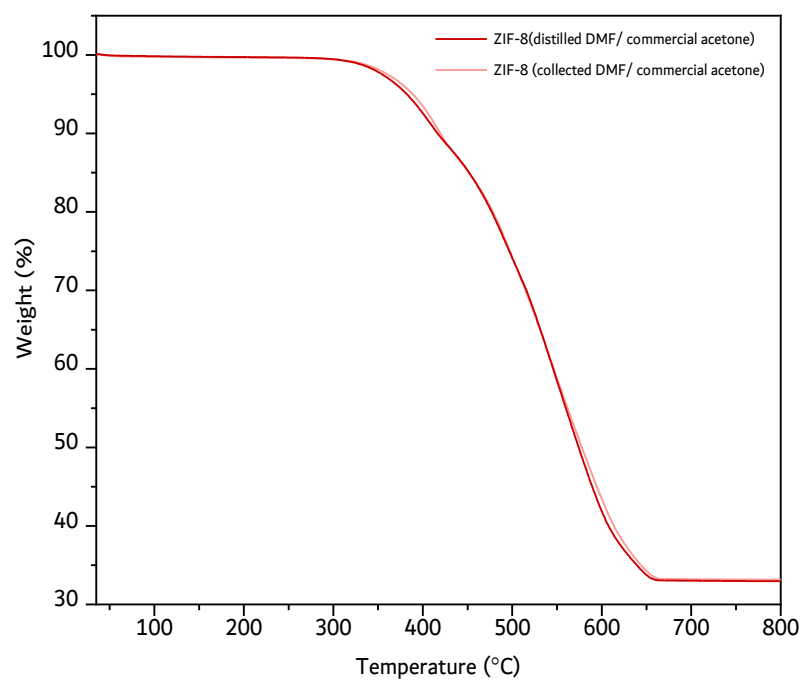
Figure A.17 TGA of ZIF-8 samples
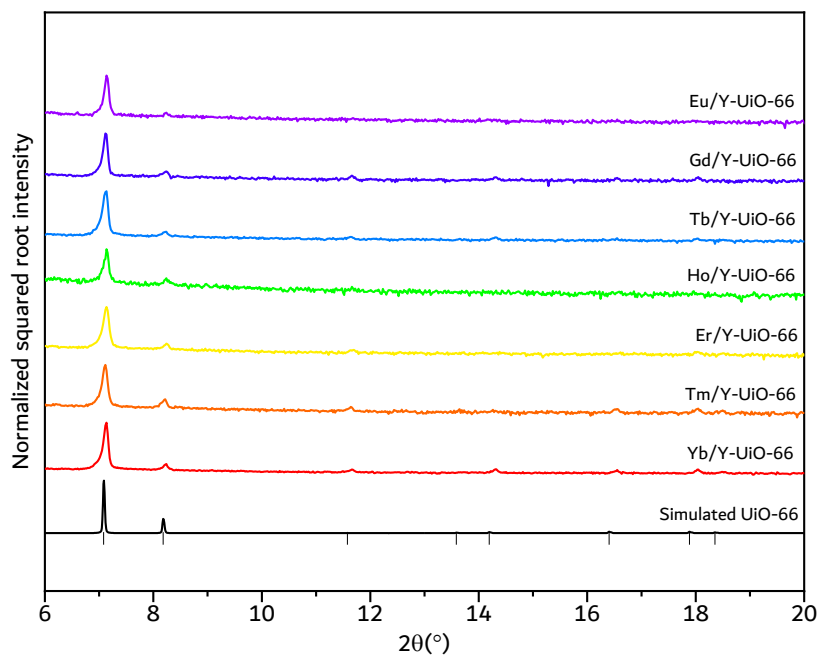
Figure A.18 PXRD pattern of samples after one round of transmetalation, with the square root of the normalized intensities
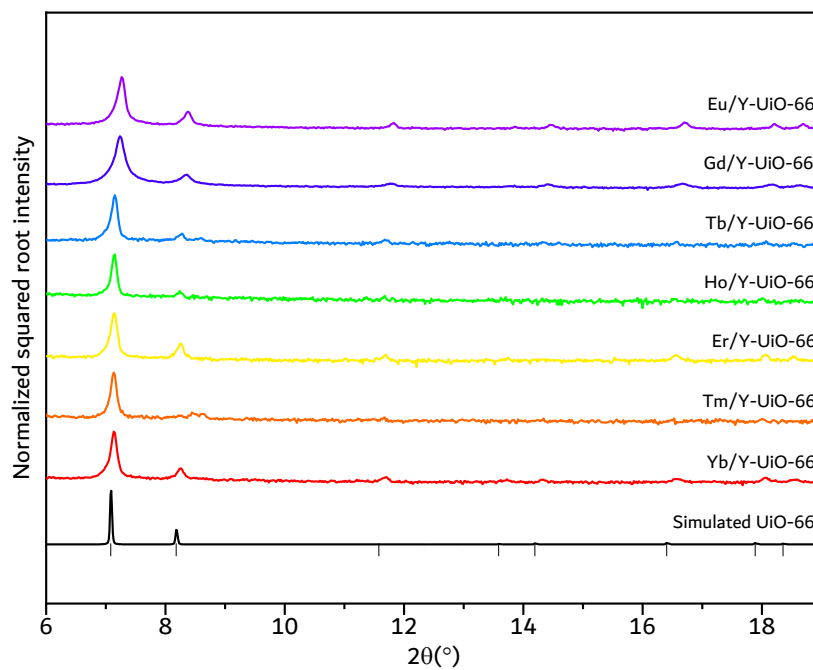
Figure A.19 PXRD pattern of samples after one round of transmetalation, with the square root of the normalized intensities

Table A.2 Summary of ICP-MS data for samples undergoing one round transmetalation

Metal	Rare-earth concentration (ppm)	Yttrium concentration (ppm)	Percent transmetalation (%)
Yb	17.09	26.72	24.73
Yb	27.5	22.89	38.17
Yb	36.4	21.89	46.07
Tm	26.54	12.89	52.01
Tm	26.28	11.46	54.69
Tm	21.31	10.47	51.72
Er	27.77	13.86	51.57
Er	20.3	18.3	37.09
Er	25.91	27.82	33.11
Ho	19.61	23.66	30.88
Ho	10.91	13.99	29.60
Ho	8.486	12.77	26.37
Tb	9.17	24.58	17.27
Tb	9.159	28.27	15.34
Tb	9.022	34.08	12.90
Gd	7.998	20.07	18.39
Gd	5.626	10.69	22.93
Gd	4.608	14.92	14.87
Eu	16.74	25.66	27.62
Eu	8.548	24.98	16.68
Eu	7.102	20.55	16.82

Table A.3 Summary of ICP-MS data for samples undergoing two rounds of transmetalation

Metal	Rare-earth concentration (ppm)	Yttrium concentration (ppm)	Percentage transmetalation (%)
Yb	46	16.91	58.29
Yb	33.85	12.17	58.83
Yb	40.67	14.51	59.02
Tm	19.06	9.458	51.47
Tm	44.66	19.15	55.10
Tm	37.81	17.22	53.61
Er	20.23	8.644	55.44
Er	23.15	10.45	54.08
Er	24.95	13.39	49.76
Ho	33.32	27.37	39.62
Ho	30.1	23.07	41.29
Ho	44.4	36	39.93
Tb	37.55	22.33	48.47
Tb	52.09	27.75	51.22
Tb	18.78	14.04	42.80
Gd	14.02	10.9	42.10
Gd	25.97	19.03	43.55
Gd	56.18	38.38	45.28
Eu	24.09	14.29	49.65
Eu	29.16	16.85	50.31
Eu	46.76	26.75	50.56